

AUG 26 1966

FRIE M64 0161

PETROFABRIC TECHNIQUES FOR THE DETERMINATION  
OF PRINCIPAL STRESS DIRECTIONS IN ROCKS

M. FRIEDMAN

1964

Reprint fr: "State of Stress in the Earth's Crust",  
p. 451-552, in W.R. Judd, editor.  
Amer. Elsevier Pub Co.,

PETROFABRIC TECHNIQUES FOR THE DETERMINATION  
OF PRINCIPAL STRESS DIRECTIONS IN ROCKS

Melvin Friedman\*

Introduction to Petrofabrics

PETROFABRICS (from Gefügekunde der Gesteine<sup>(1)</sup>) is an important geological discipline which can provide knowledge on the state of stress associated with naturally deformed rocks. According to Turner's interpretation (Ref. 2, p. 149) of "Gefüge" (fabric), petrofabrics is the study of all structural and textural features of a rock as manifested in every recognizable rock element from the configuration of the crystal lattices of the individual mineral grains up to and including large-scale features which require field investigation. The fabric of a rock, therefore, is extremely complex, is seldom completely specified, and is developed throughout the entire history of the rock. An undeformed sedimentary rock, for example, has a fabric which relates to its depositional and diagenetic histories. For instance, the long axes of detrital grains, flute casts on bedding planes, and cross beds are fabric elements related to current directions during sedimentation. Permanent deformation of this rock (Ref. 3, p. 3) modifies the initial fabric and introduces many new fabric elements. These may range in size over at least 15 orders of magnitude from changes in the crystal lattices ( $10^{-9}$  m =  $10^0$  Å) to deformation of the rock into great folds and faults of mountain ranges and basins ( $10^6$  m). Although many kinds of elements can be distinguished, in practice a few easily measured ones are chosen which are thought or are known to be critical to the problem at hand. Those recognized as criteria of deformation include a variety of crystallographic parameters, deformation lamellae, kink

---

\*Shell Development Company, Houston, Texas.

bands, lineations, fold axes, fractures, faults, and other planes of mechanical discontinuity. The spatial array of any one of these elements is called a "subfabric" (Ref. 4, p. 863), and the measurements that specify their orientation and distribution are termed "fabric data." Petrofabrics consists, therefore, of a descriptive phase in which the fabric elements are recognized, measured, and illustrated, and an interpretive phase in which the rock fabric serves as a basis for explaining the deformation history either kinematically or dynamically (Fig. 1).

Tectonically significant fabric elements have been recognized and the techniques for their study perfected primarily through the efforts of Professors Sander and Schmidt, their co-workers, and students in Germany and Austria, and Professors Knopf, Turner, Ingerson, Phillips, and Weiss, their co-workers, and students in the United States and England. The subject has evolved from the study of complexly deformed terrains for which normal field mapping methods did not provide structural resolution. In recent years several commonly occurring fabric

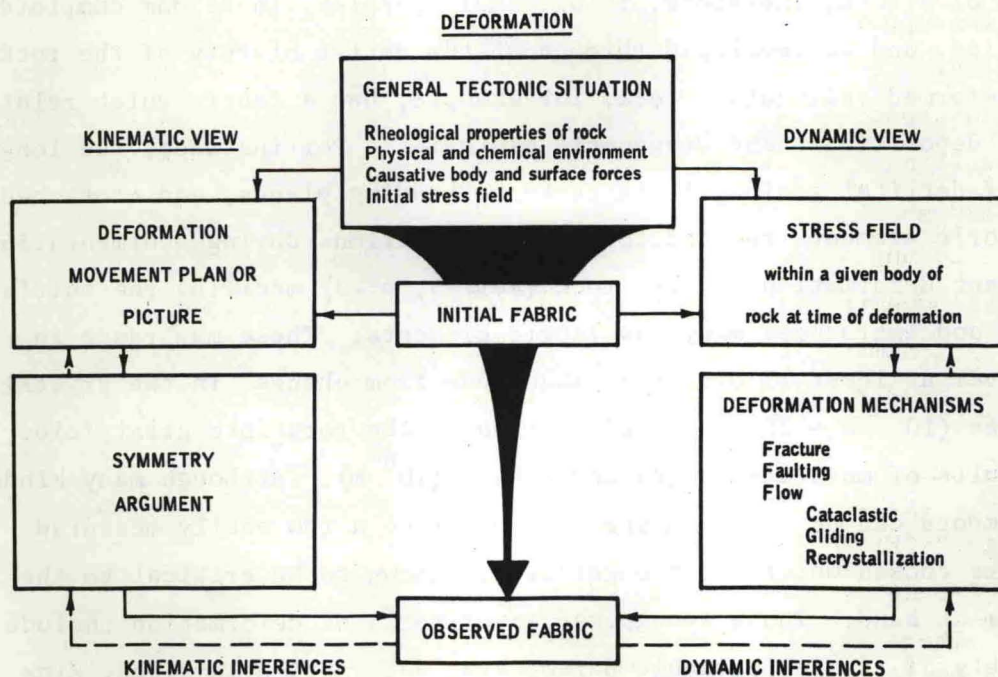


Fig. 1—Geologic deformation from the viewpoints of kinematic and dynamic petrofabrics.

elements have been given dynamic significance by comparisons between experimentally and naturally deformed rocks.

In the interpretive phase, the fabric elements are used to specify the nature of the deformation from two viewpoints, kinematic and dynamic (Fig. 1). Kinematic inferences concern the displacements that have transformed the initial fabric into the observed fabric. Dynamic inferences concern the nature of the stresses in the rocks at the time of deformation. In principle, all fabric elements that are significant criteria of deformation should lead to the same dynamic or kinematic interpretations even though they may be of different origin or scale.

The kinematic approach is favored by Sander and the Innsbruck school because "to correlate fabric with internal movements is less doubtful than is the more tenuous correlation with forces responsible for such movements" (Ref. 5, p. 2).<sup>\*</sup> Symmetry is the basic criterion for correlating fabric with movement.<sup>\*\*</sup> It is assumed that the symmetry of the rock fabric reflects the symmetry of the movement responsible for the evolution of that fabric. The principle is illustrated by the bending of wheat stalks and the rippling of the surface of water by wind. There is support for the validity of the principle in physics<sup>(4)</sup> and with regard to experimentally deformed rocks as discussed by Turner.<sup>(5)</sup> A second aspect of kinematic analysis involves unrolling ("Rückformungen") and levelling ("Horizontierung") proposed by Sander (Ref. 7, pp. 170-184) to derive an observed structure from an assumed earlier structure by the minimum amount and simplest possible kind of displacement consistent with the movement picture.

The kinematic viewpoint will not be considered further because it does not lead to the determination of the state of stress in rocks.<sup>\*\*\*</sup>

---

\* The forces referred to here are those of the "general tectonic situation" (Fig. 1).

\*\* See Refs. 1, 2, and 4-14.

\*\*\* There are vast amounts of excellent descriptive data on a variety of fabric elements, which to date have been only kinematically interpreted. These may eventually be amenable to dynamic analysis as the genetic relationships between the fabric elements and stresses in the rocks become known.

Moreover, usually only intensely deformed rocks exhibit fabrics with sufficiently clear symmetry for kinematic analysis. This excludes slightly and moderately deformed rocks from this form of petrofabric analysis.

The dynamic approach is an outgrowth of experimental and theoretical studies of deformation. The mechanisms by which common fabric elements are formed are systematically worked out by study of experimentally deformed single crystals, of monomineralic aggregates of these, and finally of polymineralic rocks. In addition, the relationships between these elements and the known stresses across the boundaries of the laboratory specimens are established. These specimens are then compared with their naturally deformed counterparts to determine statistically the orientation and relative magnitudes of the principal stresses in rocks at the time of deformation. This procedure is based on the assumption that the mechanisms of deformation observed in the laboratory are identical to those in nature. The dynamic approach is applicable to all deformed rocks irrespective of the intensity of deformation.

The limitations of the dynamic approach are as follows: (1) At present the mechanisms of deformation are known for only a relatively few fabric elements. (2) The orientations and relative magnitudes of the principal stresses can be determined statistically in a given volume of rock, but absolute magnitudes cannot be estimated from data of short-time laboratory experiments. (3) Although in principle it is possible to distinguish between two or more stress systems reflected in a given fabric, in practice it is difficult and often ambiguous.

Certain difficulties arise in petrofabric analysis because of the cumulative aspect of rock fabrics, the heterogeneity of stress and strain in rocks, and the scale on which a given fabric element may be sampled. Since the fabric develops throughout the history of a rock, distinction between the initial fabric and the modifications superposed by subsequent deformation(s) is a serious problem. For example, in deformed sedimentary rock it may be difficult to determine whether a given dimensional orientation of the grains is relict from the initial sedimentation or is a stable configuration in the strain field of the

deformed rock. The states of stress and strain within different parts of a rock are rarely homogeneous with respect to direction and/or magnitude. Although these tend to be statistically homogeneous, stress sensitive fabric elements sometimes show large variations in their orientations and/or frequency. Accordingly descriptions of orientation patterns of the elements are necessarily statistical, as are any inferences drawn from them. Finally, it is important to keep in balance the scale of the fabric element and that of the field on which it is sampled in order to correctly evaluate the fabric. It is helpful, here, to consider the penetrative nature of a fabric element. For a fabric element to be penetrative the feature must be repeated statistically so that it effectively pervades the body and is present in the same average orientation in every sample. If the body is sampled on a scale smaller than the average spacing of the element, or if it is sampled on a scale larger than that pervaded by the element, the element becomes nonpenetrative (Ref. 4, p. 861). Hence, the fabric can be correctly evaluated only if penetrative fabric elements for a given size domain are studied.

#### Scope of the Paper

The primary purpose of this paper is to review dynamic petrofabric techniques now available for mapping principal stress directions in naturally deformed rocks. It is necessary to begin with the descriptive methodology employed in petrofabric analysis. This is discussed in some detail for the convenience of those readers not familiar with this subject. Included are sections on sampling and measuring, stereographic and equal-area projection, and the construction and statistical evaluation of petrofabric diagrams. This is followed by discussions of five important processes: fracturing, faulting, gliding flow, rotation, and recrystallization. As each process is discussed, the associated fabric elements are described and the literature is cited to demonstrate their usefulness in dynamic analysis.

## Descriptive Methodology

### Sampling and Measuring

Generalizations from observations on samples of the whole are merely statistical inferences, and the confidence within which a given statement can be made is related to the representative significance of the observations.<sup>(15,16)</sup> Systems are designed to facilitate and ensure sampling that will be representative of the features to be examined. The systems include consideration of the number and location of stations where the rock is sampled, as well as the number of measurements and the manner in which they are made at each station. In petrofabrics, such schemes are a function of the type and scale of the fabric element under consideration, the degrees of homogeneity and development\* of the subfabric, and the purpose of the investigation. Sampling of macroscopic elements is obtained by standard field mapping techniques. Any microscopic petrofabric analysis begins with the collection of a geographically oriented specimen, i.e., one that is related to some fixed three-dimensional coordinate system. Oriented thin sections are cut from the hand specimen, so that the final results can be placed back into the geographic and geologic framework (Fig. 2). Various plans for sampling thin sections are discussed by Chayes.<sup>(17)</sup>

Poor sampling schemes can influence the observed orientation pattern for a fabric element. For example, one type of problem is the preferential sampling of a given fabric element because it is more easily measured in certain orientations than in others. If macrofractures are being measured along a road cut, for example, those fractures intersecting the long trend of the outcrop at high angles will tend to be preferentially sampled over fractures that trend more nearly parallel to the outcrop surface. Or on the microscopic level, a common bias in universal-stage work is to preferentially sample

---

\*The orientation pattern of any fabric element varies between two end points: randomness and total alignment. The relative strength of a fabric increases as the state of total alignment is approached; and, conversely, the relative weakness of a pattern increases as it approaches randomness.

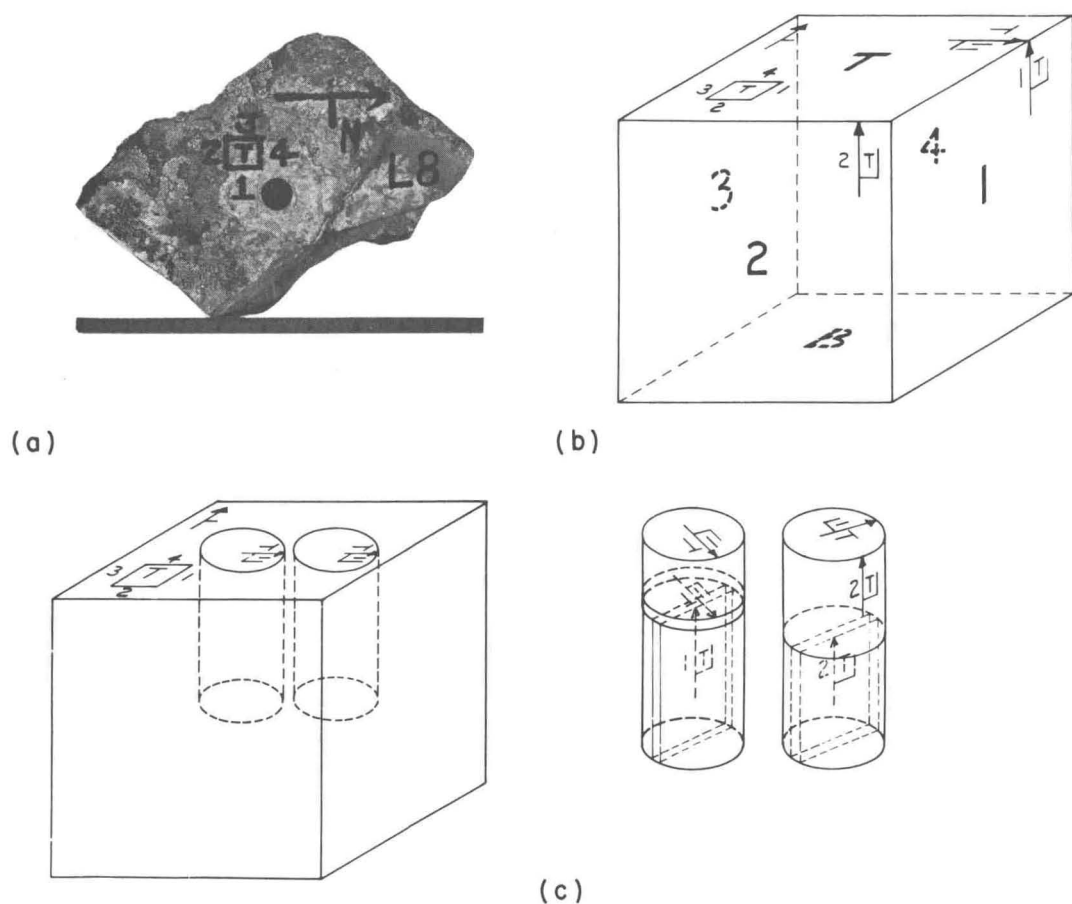


Fig. 2—Diagrams illustrating orientation convention commonly used to mark hand specimens and thin sections. (a) Hand specimen shows strike and dip directions marked on T (bedding) surface. Faces 1, 2, 3, and 4 are arranged in clockwise order with the 1 surface in the dip direction. (b) Cube shows relationships between different faces and the use of the orientation symbols. (c) Thin sections are taken from cylinders cored from the T surface of the block.

planar features inclined at high angles to the plane of a thin section at the expense of those inclined at lower angles. One can eliminate errors of this type by recognizing that they may exist and by designing a sampling plan that will eliminate or at least test for the effect.

Most measurements deal with the determination of the orientations of lines and planes in space. The choice of instrument one might use depends upon the scale of the fabric element, e.g., aerial photographs, a variety of telescopic instruments such as the theodolite and range finder, pocket transit (Brunton compass), petrographic microscope and

universal stage, or the X-ray diffractometer. Detailed discussion of microscopic and X-ray measurement techniques are found in Refs. 2, 7-13, and 18-20. The accuracy of strike and dip measurements on aerial photographs varies with the topography and the scale of the photographs, but, in general, azimuths of lines can be determined to  $\pm 3$  degrees and dip angles to  $\pm 5$  degrees for angles  $> 60$  degrees,  $\pm 3$  degrees for angles 45 to 60 degrees, and  $\pm 1.5$  degrees for angles  $< 45$  degrees. Linear and angular measurements from telescopic instruments are very reliable ( $\pm 0.1$  per cent and  $< \pm 0.1$  degree, respectively). Errors in the measurement of macroscopic fabric elements or in the marking of oriented specimens with the pocket transit can usually be held to  $\pm 3$  degrees. Universal-stage measurements of crystal optic axes are usually reliable to  $\pm 2$  degrees. Planar features can usually be located to  $\pm 1$  degree when they are inclined to the plane of the section at angles greater than 70 degrees. For inclinations of 30 to 70 degrees the error may be  $\pm 3$  degrees.\*

#### Stereographic and Equal-area Projection

Petrofabric analysis involves spacial relationships between lines and planes and their illustration. The stereographic projection represents the surface of a sphere on a plane surface and provides an effectual means for both analytical and illustrative purposes.\*\* Only those aspects needed to comprehend fabric orientation diagrams are reviewed here.

Consider a reference sphere cut by meridional or equatorial planes (Fig. 3), both passing through the center of the sphere. Either can serve as the reference plane of the projection, but the meridional is

---

\* Recently, Kamb<sup>(21)</sup> has discussed the nature of the corrections needed in universal-stage work to compensate for differences in index of refraction between the mineral under observation and the glass hemispheres of the stage. He points out that the true corrections are negligible for cases where the ratio of the mineral refractive index to that of the hemispheres is between 0.95 and 1.05. As this condition is usually obtained by use of suitable hemispheres, refraction corrections are seldom applied to fabric data.

\*\* See Refs. 11, 18, 22, and 23.

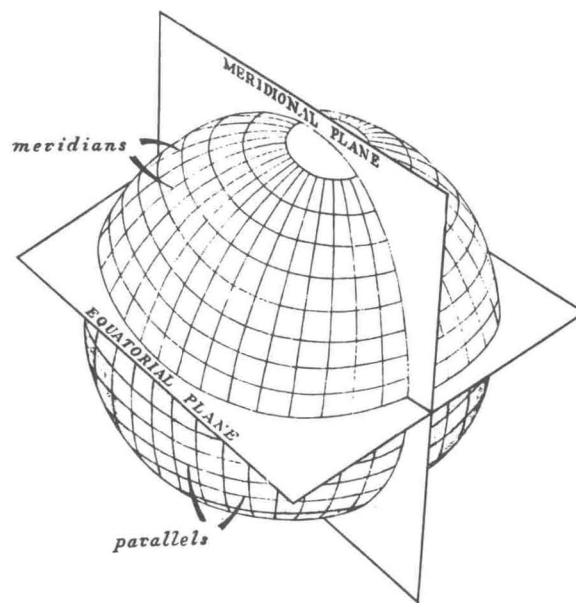


Fig. 3—A sphere or globe on which are drawn meridians or longitude circles separated by equal angles and parallels or latitude circles separated by equal angles (from Higgs and Tunell, Ref. 23, Fig. 2b).

used in petrofabrics. Next, consider any other plane of given attitude which is made to pass through the center of the sphere (Fig. 4(a)). A perpendicular to the plane is projected from the center of the reference sphere to the lower hemisphere of the sphere (P), in accord with petrofabric convention. From point P a line is projected to the zenith of the reference sphere. This line intersects the meridional plane at point  $P'$ , which is the lower hemisphere stereographic projection of point P--i.e., the normal to the shaded plane (Fig. 4(a)). If the viewpoint is changed such that the eye is at the zenith point and sights directly normal to the meridional plane, one sees the point  $P'$  as in Fig. 4(b). The plane itself rather than its normal can be drawn by tracing onto the meridional plane the line that marks the intersection of the shaded plane and the meridional plane, and the great circle which marks the intersection of the shaded plane and the lower hemisphere.

Similarly, the azimuth and plunge of a line can be plotted by passing the line through the center and surface of the reference sphere (a point comparable to P). Then projection of P to the zenith intersects the meridional surface at another point (comparable to  $P'$ ),

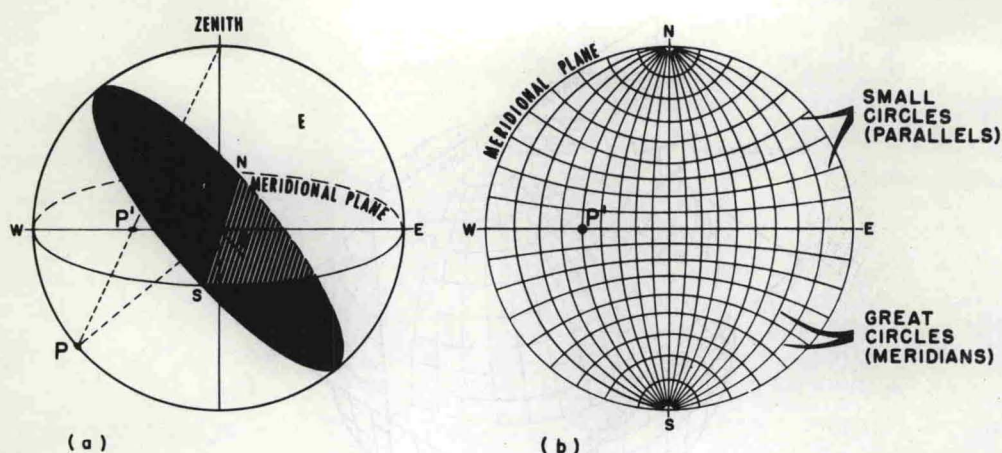


Fig. 4—Diagrams illustrating lower hemisphere stereographic projection. On the left is the reference sphere with a plane (strike N-S, dip  $50^{\circ}$ E) passing through center of sphere and intersecting the meridional plane along the N-S line. On the right, the normal to the plane ( $P'$ ) is plotted in lower hemisphere stereographic projection.

which is the lower hemisphere stereographic projection of the line. Clearly, if the meridional surface is considered to be horizontal, a horizontal line will be represented by a point at a given azimuth on the periphery of the meridional plane, and a vertical line will appear as a point at the center of the meridional plane. Similarly, the normal to a vertical plane will appear on the periphery, and the normal to a horizontal plane will fall at the center.

The stereographic plotting of lines and planes is facilitated by the construction of polar or meridional nets (Fig. 5(a)). These represent the stereographic projection of points of different azimuths and vertical angles (circles of longitude and latitude). On 10-cm- and 20-cm-diameter nets the meridians and parallels are drawn at 2-degree intervals and on 40-cm nets at 1-degree intervals. The general formula for projection of any point stereographically is  $r = R \tan \alpha/2$ , where  $r$  is the distance along the equator from the center,  $R$  is the radius of the reference sphere, and  $\alpha$  is the inclination from the zenith on the surface of the sphere. This generates a stereonet with true angular relationships (an equal-angle or Wulff net).

In plotting, a piece of tracing paper is usually pinned to the net so that it is free to rotate about the center of the net. A

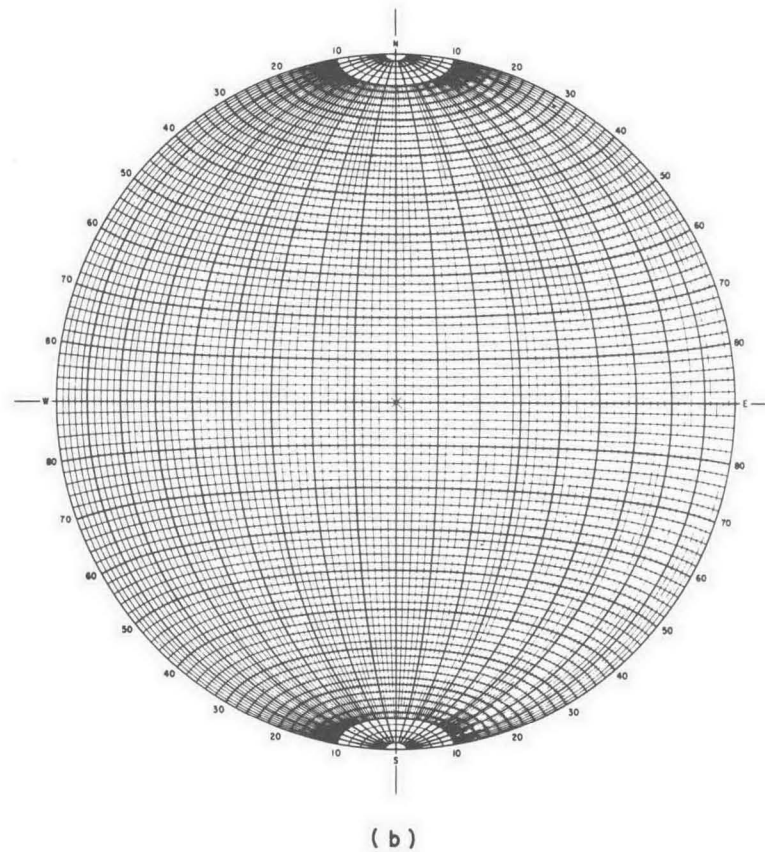
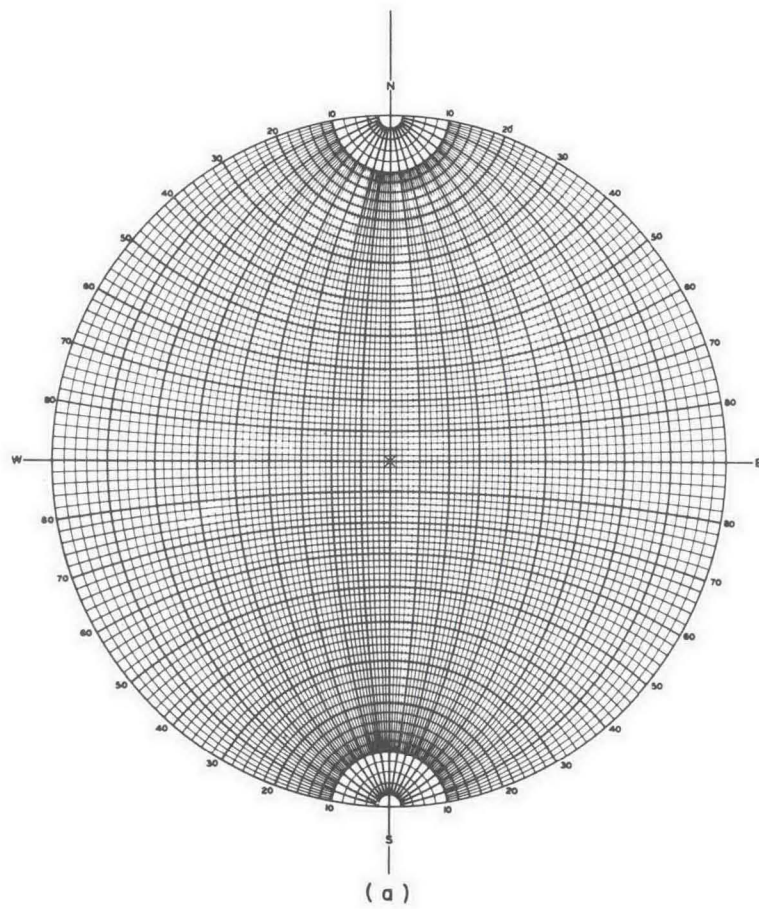


Fig. 5—Equal-angle or Wulff stereographic net on the left and an equal-area or Lambert-Schmidt net on the right.

reference point is marked on the paper over a corresponding point on the periphery of the net. Azimuths are read clockwise from north on the periphery, and angles from the vertical or horizontal are read along the equator. To plot the attitude of a line in space, the azimuth of the line is noted on the tracing paper. The paper is then rotated until the azimuth of the line coincides with the equator of the net. The plunge of the line from the horizontal or its deviation from the vertical is then marked off along the equator. Rotation of the paper back to its initial position permits one to visualize the attitude of the line in space. To plot the attitude of a plane, its strike line is noted on the tracing paper. The paper is rotated until the strike line coincides with the north-south diameter of the net. The dip is then plotted along the equator with respect to the lower hemisphere by either tracing the plane (a great circle) or plotting the normal to the plane. By working backward one can determine the azimuth and plunge of any line or the strike and dip of any planar element on a stereographic diagram.

Many other operations and graphical solutions are facilitated by use of the net--e.g., the determination of (1) the azimuth and plunge of the intersection of two planes, (2) the angle between two planes or two lines or a line and a plane (read along a great circle by rotating the tracing paper until the two corresponding points lie on the same great circle), and (3) the orientation patterns of many planes or lines that are plotted on the same diagram. Another important use of the net is to facilitate the rotation of fabric data from one plane of reference to another. <sup>(11)</sup>

Fabric orientation diagrams are amenable to statistical analysis only if the areal distribution of the data points at different locations on the diagram (different orientations) can be compared. The areal distortion inherent in the equal-angle or Wulff net is excessive. For example, a region bounded by 10 degrees of longitude and latitude near the center of the equal-angle net occupies a much smaller area than a 10-degree region near the periphery (Fig. 5(a)). To correct for this an equal-area or surface true net was devised by Lambert <sup>(24)</sup> for map projections and selected by Schmidt <sup>(25)</sup> for petrofabric analysis

(Fig. 5(b)). With this net, constructed from the formula  $r = \sqrt{2} R \sin \alpha/2$ , a unit area at any location on the projection corresponds to a unit area on the reference sphere, although somewhat distorted in shape. Equal subdivisions of the total area (e.g., 1 per cent area) can be chosen to illustrate concentrations of points projected onto the net from anywhere on the sphere.

The manipulation of the equal-area net in plotting lines or planes is identical to that previously described for the equal-angle net. Similarly, the equal-area net can be used to measure the angular relations between lines and planes. Moreover, rotation of data is more satisfactorily performed because the meridians are much more nearly equally spaced than on the equal-angle net. For these reasons the equal-area net is used almost exclusively in petrofabric work.

#### Petrofabric Diagrams

Petrofabric diagrams are the trademark of fabric studies. They illustrate as no other type of diagram can the three-dimensional orientations of fabric elements in a complete and concise manner. By convention these orientations are shown with respect to a specific plane of reference (the plane of the diagram) in lower hemisphere equal-area projection. Diagrams used in this review are of three types, as follows: (a) point or scatter diagrams (Fig. 6(a)) contain data from a number of measurements of a given fabric element, (b) contoured diagrams (Fig. 6(b)) show the same type of information as (a) except that the orientation pattern is emphasized by density contouring, and (c) stereograms (Fig. 6(c)) show the angular relations among relatively few lines and/or planes.

A partial petrofabric diagram illustrates data from one given field of observation or only part of the available data. Composite diagrams contain data from more than one field of observation on the same sample, e.g., elements measured in three mutually perpendicular thin sections cut from the same sample. Data from two of the sections are rotated into the plane of the third, or data from all three are rotated into some fourth plane of reference. Synoptic diagrams are summary in nature and show fabric data for a number of different

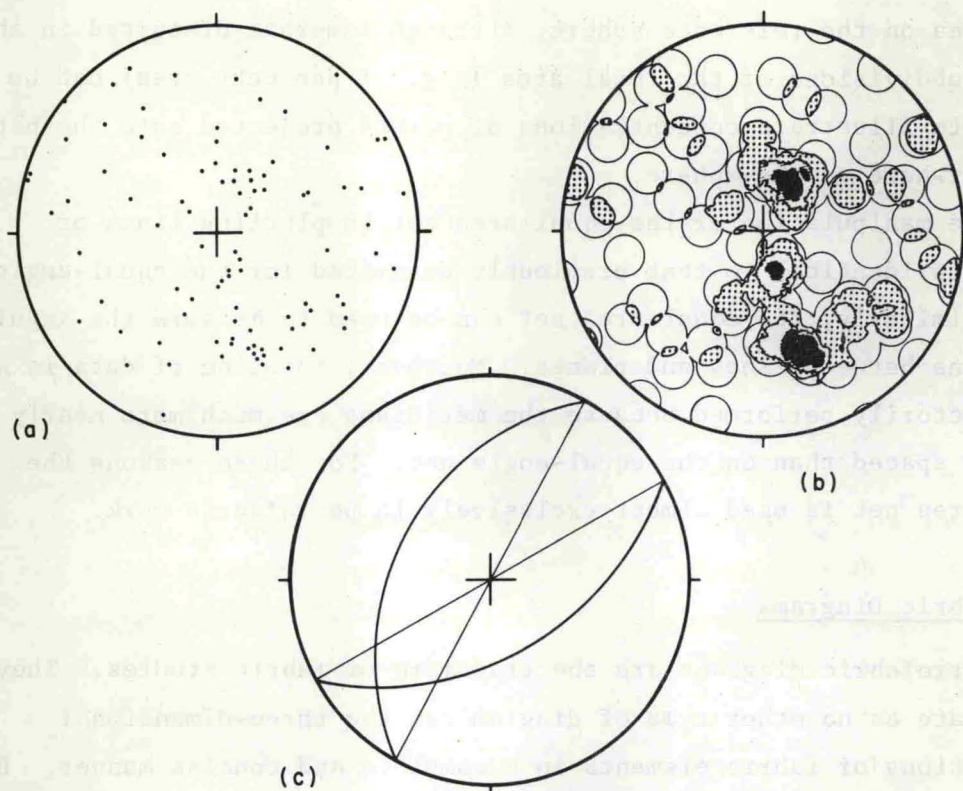


Fig. 6—Three types of petrofabric diagrams. (a) Point diagram illustrates the orientation of normals to 100 planar features or axes. (b) Contoured or density diagram of the points in (a); contours are at 1, 2, 4, and 6 per cent per 1 per cent area, 10 per cent maximum. (c) Stereogram shows two planes intersecting at 70 degrees. All diagrams are in lower hemisphere equal-area projection.

samples. In these, the data from the individual samples are rotated to a common plane of reference.

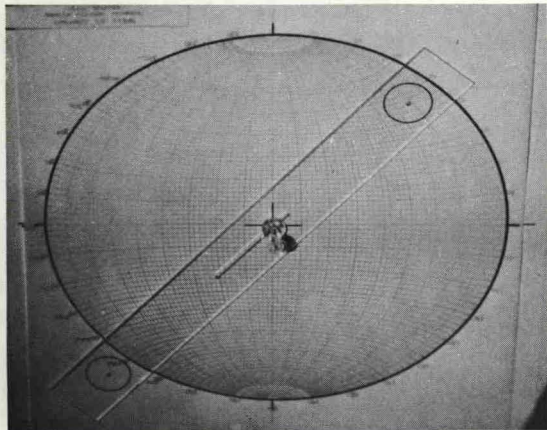
Petrofabric diagrams are easily read if the reader understands how lines and planes are plotted in lower hemisphere equal-area projection and if the writer has supplied a sufficiently informative caption. This should include at least the following: (a) sample designation, (b) type and number of data being illustrated, (c) orientation of the plane of the diagram, (d) location of geographic and/or geologic reference coordinates, and (e) nature of the contours and their values (if the diagram is contoured). The accuracy within which any point is located on a petrofabric diagram is a function of

errors arising from original measurement and, for microscopic elements, from the collection of the hand specimen and the preparation of oriented thin sections. Small plotting errors included, this may be as large as  $\pm 5$  degrees, is usually  $\pm 3$  degrees, and with extreme care can be held to  $\pm 1$  degree.

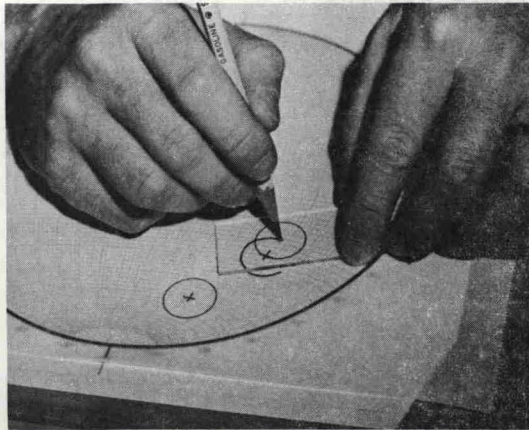
Several techniques are used to contour diagrams in order to emphasize the orientation pattern. In general the contour lines are based on the number of points per unit area of the net, and the contour levels are selected with respect to the concentrations exhibited by the population of data points. A sufficiently accurate and rapid method, particularly suited to diagrams containing less than 200 points, is used by the author (Fig. 7). A contouring tool (Fig. 7(a)) for a 20-cm diagram is constructed with two circles scribed 20 cm apart. Each circle has a diameter of 2 cm so that its area is 1 per cent of the area of the diagram. Tapered holes are drilled at the center of each circle to accommodate a pencil point, and a slit is milled along the central portion of the tool to permit free rotation and translation about a pin through the center of the diagram.

To generate a contour line based, for example, on 3 points per 1 per cent area, the 1 per cent circle of the tool is placed on the diagram such that 2 points are within and 1 point is on the circle (Fig. 7(d)). The tool is then moved (pencil in contact with the paper through the center hole) such that 1 point is always on the circle and 2 are within. As new points are encountered by the circle, old ones are left behind. This is continued until the contour line is closed. Thus wherever one places the 1 per cent circle on or within the closed 3-point contour line, the circle will always be observed to contain at least 3 points. Points at the periphery are handled as illustrated in Fig. 7(e). The contour is expressed in terms of the percentages of the total number of points per 1 per cent area.

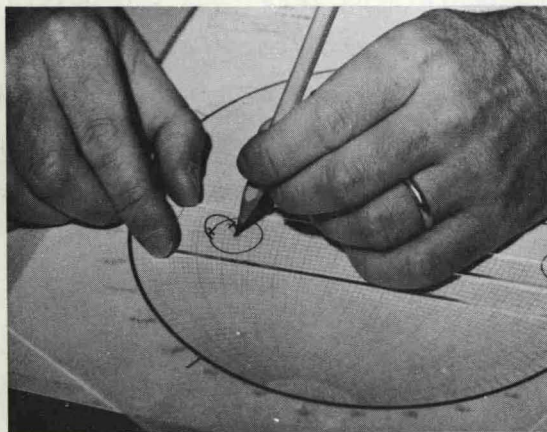
In practice, the contour line about 1 point is generated with a compass. In fact, the compass can be used throughout the procedure by drawing a 1 per cent circle about each point on the diagram and noting the areas of overlap.<sup>(26,27)</sup> Thus where two circles overlap, a 2 point per 1 per cent area is defined; and where three circles overlap, a 3



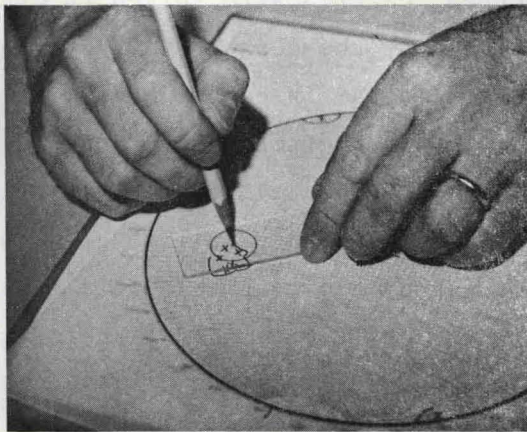
(a)



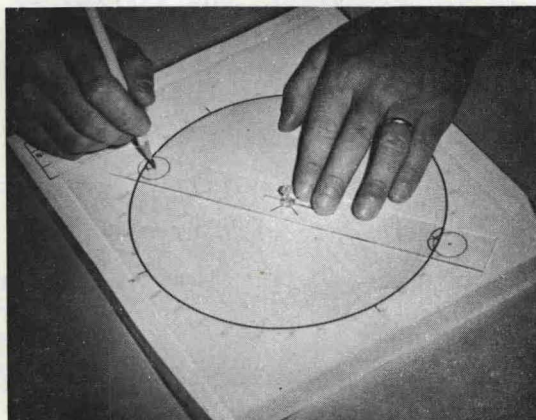
(b)



(c)



(d)



(e)

Fig. 7—Photographs illustrating a method for contouring points plotted in equal-area projection. Shown are (a) the contouring tool; (b, c, d) the method used to contour 1, 2, and 3 points per 1 per cent area, respectively; and (e) the procedure used to contour 2 points which lie on opposite sides of the diagram.

point per 1 per cent area is defined; etc. The author has found that searching for more than three overlaps consumes more time than contouring with the tool. The grid or Schmidt method is particularly useful in contouring large numbers of points. (11,18,25)

Kamb (Ref. 28, p. 1908) has prepared contoured diagrams by a novel procedure such that statistical inferences can be drawn directly from the diagrams. The area (A) of the contouring tool is so chosen that, if the population is randomly oriented, "the number of points (E) expected to fall within a given area (A) is three times the standard deviation of the number of points (n) that will actually fall within the area under random sampling of the population.... Observed densities that differ from E/A by more than two or three times the standard deviation  $\sigma$  (for random orientation) are then likely to be significant.... The observed densities are therefore contoured in intervals of  $2\sigma$  at values 0,  $2\sigma$ ,  $4\sigma$ , etc., the expected density = E/A for random orientation being  $3\sigma$ ."\*

For a random population in which the distribution of n values for random samples of size N is binomial,

$$\frac{\sigma}{E} = \sqrt{\frac{(1-A)}{NA}},$$

where  $E = NA$ , A is a given area expressed as its fraction of the total area of the diagram, and N is the total number of points on the scatter diagram. By setting  $\sigma/E = 1/3$ , one computes the appropriate area A of the counter to be used in preparing the diagram. Once A is obtained it is used to contour the point diagram by the Schmidt method. Kamb states that diagrams prepared in this way have a smoothed appearance in comparison with conventional contours because most of the irregular detail of the latter is of no statistical significance, the conventional  $A = 0.01$  being usually much too small.\*\*

---

\* Here  $\sigma$  is used to designate both the standard deviation and stresses in accordance with conventions in statistics and stress analysis, respectively.

\*\* All three contouring techniques contain a common source of error. Although the contoured points are plotted on an equal-area net,

## Statistics

The orientation of fabric elements as illustrated on petrofabric diagrams can be treated in a purely statistical manner to determine whether the observed distribution significantly deviates from one which is randomly oriented. This implies statistical, but not necessarily geological, significance. Pincus<sup>(29)</sup> fully discussed the application of statistical methods to the analysis of aggregates of orientation data. Little can be added to his treatment here. Flinn<sup>(27)</sup> re-examined several of the more popular tests of significance as applied to petrofabric diagrams and found them generally unsuitable. He suggested that fabric diagrams should be compared to artificially prepared "random" diagrams and significant differences attributed to the rock fabric.

The contouring method of Kamb<sup>(28)</sup> allows statistical inferences to be made directly, but one possible drawback may be that the contours based on areas considerably larger than 1 per cent could tend to average or mask two or more closely spaced concentrations which may be geologically significant.

Another means of utilizing a contoured diagram as the basis for statistical inference has been employed by the author with some success. The probability of obtaining concentrations on a point diagram which deviate from a random distribution is approximated by the Poisson exponential binomial limit.<sup>(30)</sup> This has been confirmed by the author from tests of goodness of fit between this distribution and apparently random diagrams of fabric elements in rocks. The probability of obtaining at least a given number of points in any 1 per cent area of a fabric diagram is given by the following equation:

---

there is an unavoidable, progressive distortion of the equal areas on this net from the center outward. Fully accurate contouring, therefore, would require continual changes in the shape of the contour from circular at the center to elliptical at the periphery as recognized by Mellis and Strand (in Flinn, Ref. 27, p. 532). This error is considered to be negligible in light of the accuracy with which any given point is plotted and the nature of the interpretation of contoured fabric diagrams.

$$P = \sum_{x=x'}^{x=\infty} \frac{e^{-Np} Np^x}{x!},$$

where  $P$  is the probability,  $N$  is the total number of points in the sample,  $p$  is the probability that 1 point will occur in a given 1 per cent area (here, 0.01), and  $x$  equals the number of points per 1 per cent area. When  $Np = 1$ , the probabilities of finding at least  $x$  points in any 1 per cent area are as follows: 0 points, 1.00; 1 point, 0.63; 2 points, 0.26; 3 points, 0.08; 4 points, 0.02; 5 points, 0.004; 6 points, 0.0006; and 7 points, 0.0001. Thus in a sample of 100 points ( $Np = 1$ ), the chances of obtaining a 6-point (6 per cent) concentration from a random distribution are 6 in 10,000, and a 7-point (7 per cent) concentration, 1 in 10,000.

Statistical tools should be used prudently--only to guide interpretations, not to dictate them. For example, none of the tests known to the author takes into account the locations (specific orientations) of the points on the diagram whose orientations are analyzed collectively. For instance, an orientation pattern may be characterized by points distributed within a band (girdle) along small or great circles. There is little doubt that this pattern would have geological significance, although statistical tests might show that the distribution was random. The role of statistics here should not be to dictate against reason that the pattern was random but rather to suggest that no significance should be attached to any concentrations within the girdle.

### Deformation Mechanisms and Criteria for Dynamic Interpretations

#### Fracturing and Faulting

General. Many classifications of fracturing, faulting, and related phenomena are found in the engineering and metallurgical literature,<sup>(31)</sup> but none is generally applicable to geological problems. The types of failure pertinent here are extension fracturing and faulting (including shear fracturing).<sup>(32,33)</sup> Brace<sup>(34)</sup> has recently found that these types may be gradational under certain states of stress.

Fracturing is regarded as a process involving separation into two or more parts after total loss of cohesion and resistance to load, and release of stored elastic strain energy. Extension fracturing is separation of a body across a surface oriented normal to the least principal stress ( $\sigma_3$ ).<sup>\*</sup> There is no offset parallel to this surface. Macroscopically the least principal stress may either be negative (tensile) or positive (compressive). Tensile fracture ( $\sigma_3$  negative) is regarded as a special case of extension fracture. Correlation between extension fractures (the feature) and the principal stresses follows from the criterion of no offset. The fracture surface is parallel to the plane of vanishing shear stress normal to  $\sigma_3$ , and contains  $\sigma_1$  and  $\sigma_2$  (Fig. 8(a)).

Faulting is defined as offset parallel to a more or less planar surface of nonvanishing shear stress. There is no restriction on the magnitude of offset. Faulting may or may not be accompanied by loss of cohesion and resistance to load, actual separation, or release of stored elastic strain energy. When these events do occur, it is proper to speak of shear fracturing. In the laboratory it is usually possible to distinguish between shear fracturing and faulting. In nature, however, it is rarely possible to observe the process and determine whether it is actually accompanied by a loss of cohesion, etc. Clearly, those features which have inherently maintained cohesion should be called faults. On the other hand, the fact that a feature exhibits no cohesion across its surface at present can not be used to infer that it formed as a result of shear fracturing. That is, the loss of cohesion may have occurred after the feature initially formed. Accordingly, there is a problem when dealing with naturally deformed rocks as to what to call the features that result from these processes. The usage adopted here is as follows: The term "shear fracture" will be used to designate features along which the shear displacement is less than an arbitrary amount (1 m), and the term "fault" will refer to features

---

<sup>\*</sup> By the convention often adopted in geology, compressive stresses are positive, tensile stresses are negative. The greatest principal compressive stress is designated  $\sigma_1$ , the intermediate principal stress is  $\sigma_2$ , and the least principal stress is  $\sigma_3$ .

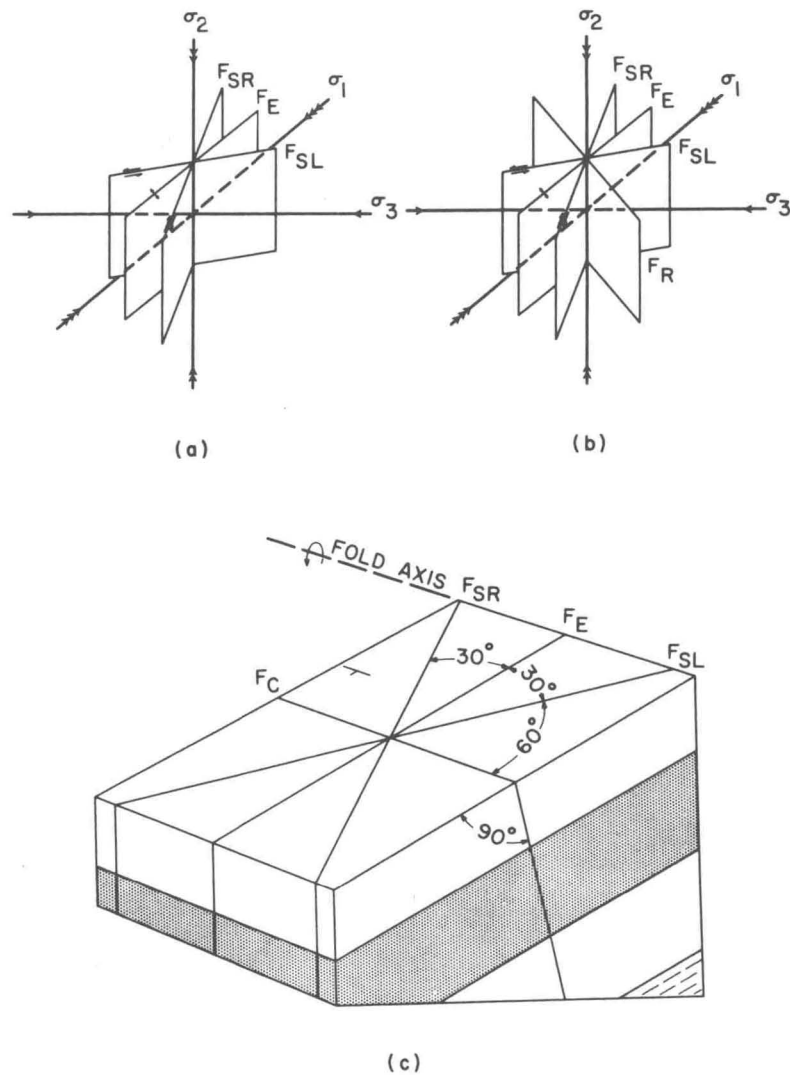


Fig. 8—Idealized geometric relationships between the principal stresses and fractures. (a) Two shear fractures ( $F_{SL}$  and  $F_{SR}$ ) are illustrated with the enclosed extension fracture ( $F_E$ ). (b) A relaxation fracture ( $F_R$ ) is added to the configuration in (a). (c) An additional extension fracture ( $F_C$ ) is added to the geometry in (a) in folded beds only.

along which the shear displacement is greater than about 1 m. These terms are then descriptive within the bounds of shear failure and do not necessarily imply distinction between the shear fracturing and the faulting processes.

The correlation between faults (including shear fractures) and the

principal stresses has been established by a wealth of empirical data. In homogeneous, isotropic materials in which  $\sigma_1 > \sigma_2 > \sigma_3$ , a fault may occur along one or both of two equipotential surfaces, each inclined from 45 degrees to a few degrees to the direction of  $\sigma_1$ . When faulting occurs along both surfaces,  $\sigma_1$  is the acute bisector;  $\sigma_2$  lies in the plane of the faults (parallel to their line of intersection); and  $\sigma_3$  is the obtuse bisector (Fig. 8(a)). For rocks that do not have pronounced planar anisotropy, the angle between  $\sigma_1$  and the fault ( $\theta$ ) varies within narrow limits. In 70 short-time triaxial compression tests on a variety of dry sedimentary rocks at room temperature and 0 to 2-kb confining pressure,  $\theta$  ranges from 25 to 35 degrees in 65 per cent of the cases and from 20 to 40 degrees in 95 per cent of the cases.<sup>(3)</sup> Subsequent work by Handin and Hager<sup>(35)</sup> at elevated temperatures and in the presence of pore water<sup>(36)</sup> has confirmed the earlier results. In fact, one of the outstandingly consistent observations from all properly designed short-time experiments on a wide variety of rock types is that faults tend to occur at less than 45 degrees to  $\sigma_1$ .<sup>(3,33-59)</sup> This holds also for sandstone, Solenhofen limestone, and diorite deformed at strain rates from  $10^{-1}$  to  $10^{-5}$  sec<sup>-1</sup>,<sup>(60)</sup> and for Solenhofen limestone, granite, diabase, dunite, and quartzite deformed at strain rates to  $10^{-7}$  sec<sup>-1</sup>.<sup>(61)</sup>

In rocks with strong planar anisotropy the value of  $\theta$  is dependent upon the orientation of the foliation, schistosity, or cleavage (s-planes) with respect to the load axis (Fig. 9).<sup>(62-64)</sup> For rocks experimentally deformed at room temperature and under confining pressures up to 2000 bars, faults tend to develop parallel to the s-planes for inclinations up to 60 degrees to the direction of maximum principal stress. When the s-planes are at 60 and at 75 degrees to the load axis,  $\theta$  tends to be between 40 and 60 degrees; and when the s-planes are at 90 degrees to the load axis,  $\theta$  is again at about 30 degrees. Moreover, in all except the 90-degree orientation the strike of the fault tends to parallel that of the s-planes in the test specimens.<sup>(63)</sup>

No entirely satisfactory theory of shear fracture or faulting is yet available. This is not to say, however, that there are no criteria which qualitatively describe shear failure in rocks. The Coulomb-Mohr

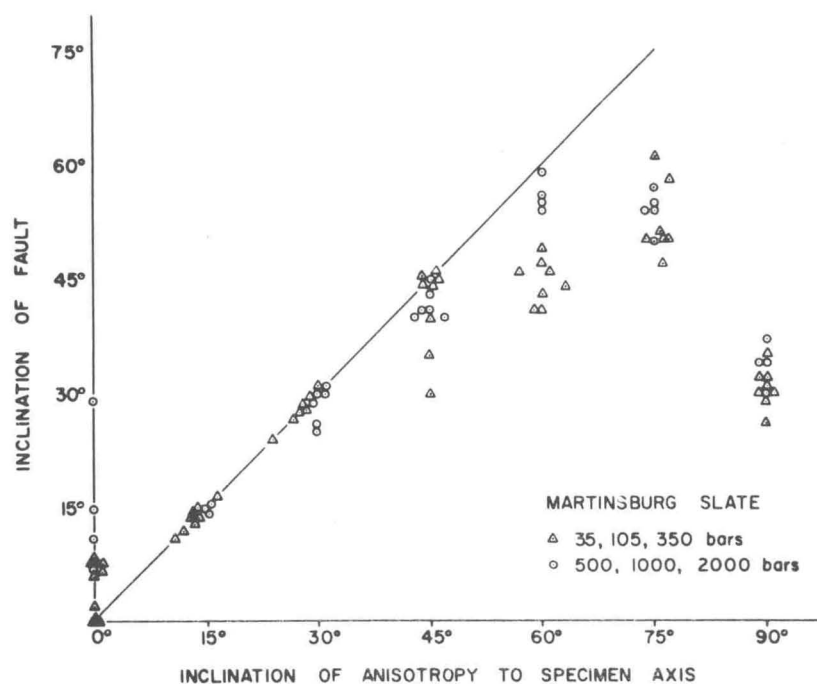


Fig. 9—Effect of cleavage on the angle of faulting, Martinsburg slate (Donath, Ref. 64).

and Griffith theories, for example, have been discussed by Brace earlier in these proceedings.<sup>(34)</sup> It is significant that all current theories and experimental observations show that  $\theta$  is less than 45 degrees, and the relationships shown in Fig. 8(a) are essentially valid.

That naturally deformed rocks fault at less than 45 degrees to  $\sigma_1$  is demonstrated by the attitude of normal faults in regions where it is logical to assume that  $\sigma_1$  was nearly vertical at the time of faulting. Hubbert<sup>(65)</sup> points out that in areas of relatively uncomplicated structure normal faults occur with dips consistently greater than 45 degrees. He cites Sax's<sup>(66)</sup> study of the dip of 2102 individual underground faults in the coal measures of the Netherlands, which shows that 1651 of these were normal faults and had a well-defined preference to dip 63 degrees (the remaining were reverse faults with dip preference at 22 degrees). Moreover, the average dip of normal faults (from United States Geological Survey Folios published to 1913) is 78 degrees.<sup>(67)</sup> Anderson<sup>(68)</sup> has generalized these relationships by calling attention to the orientation of the principal stresses with respect to normal, reverse, and wrench faults (Fig. 10).

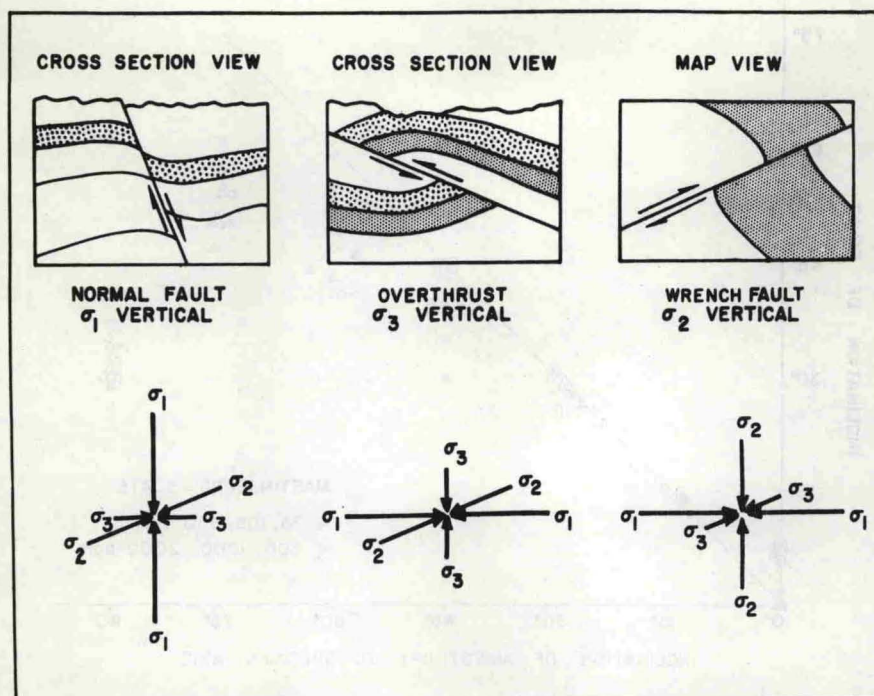


Fig. 10—The orientations of the principal stresses associated with the common fault types (after Anderson, Ref. 68).

Empirically the processes of faulting and of shear and extension fracturing are independent of scale down to at least the microscopic domain ( $10^{-5}$  m). Thus one may consider microfractures in individual grains of a rock as essentially identical genetically and geometrically to fractures and faults of outcrop scale and larger. This is a useful concept in petrofabrics as it leads to predictions of large-scale features from statistical inferences drawn from the study of smaller-scale features.

Dynamic Interpretation of Fractures and Faults. Suppose that a given domain contains extension and shear fractures which for the purpose of this discussion have no distinguishing characteristics other than their attitude in space. That is, extension fractures can not be distinguished by any physical feature from shear fractures. The fractures within a given size range are collectively regarded as a fabric element, their orientations are measured, and their subfabric is illustrated by the distribution of their normals on a petrofabric diagram.

This orientation pattern can be used to position the principal stresses if it is characterized by groups or concentrations of normals which define planes that can be related to patterns expected from previous experience.

For example, if  $\theta$  is 30 degrees, the geometric relationships between shear and extension fractures for the general state of stress are shown in Fig. 8(a). By comparison to this configuration all three principal stresses can be located from the observed subfabric orientation pattern (a) if it exhibits three planar sets intersecting in a nearly common line and inclined at 30 and/or 60 degrees to each other, or (b) if it shows two sets of features intersecting at about 60 degrees (two conjugate faults). Frequently, partial geometries are encountered, perhaps in part because all elements of the basic geometry (Fig. 8(a)) do not always form. Accordingly, the pattern observed at any one locality may consist of any or all parts of the basic configuration. Indeterminate cases occur if the pattern consists of two elements intersecting at about 30 degrees or if a single concentration results. In the former case, it is not clear whether one is dealing with two conjugate shear fractures of small dihedral angle<sup>(69)</sup> or a set of extension fractures and a set of one of the potentially conjugate faults. At best, one can state only the orientation of  $\sigma_2$  (parallel to the line of intersection) and, therefore, define the plane containing  $\sigma_1$  and  $\sigma_3$ . In the case of a single concentration, one can not determine whether the concentration is related to a set of shear fractures or to a set of extension fractures. Ambiguities in the subfabric for a single locality can frequently be resolved by comparison with fabric data from other neighboring localities in similar structural positions where the pattern is unambiguous. Similar comparisons of observed fracture orientation patterns with expected patterns for the states of stress  $\sigma_1 > \sigma_2 = \sigma_3$  and  $\sigma_1 = \sigma_2 > \sigma_3$  lead to determinations of the unique principal stress only.

Along with the orientation data, information is sometimes available on the sense of shear along faults or shear fractures. Shear criteria permit reliable determination of principal stress directions provided the observed offset occurred at the time of faulting, the slip direction

of the movement is known,\* and the value of  $\theta$  is known or can be determined experimentally. Given these facts one can determine (1) that  $\sigma_2$  lies in the plane of the fault at right angles to the slip direction, (2) that  $\sigma_1$  is inclined at  $\theta$  degrees to the fault in the direction appropriate for the observed sense of shear and lies in the plane that is normal to the fault surface and contains the slip direction, and (3) that  $\sigma_3$  lies in this same plane at 90 degrees to  $\sigma_1$ . Valid sense of shear criteria also permit resolution of the pattern consisting of two elements intersecting at a small dihedral angle. Observations of a consistent sense of shear displacement along one of the features and none along the other implies that the former is a fault and the latter an extension fracture set, provided the extension fracture set is disposed appropriately with respect to the observed sense of shear on the fault. Similarly, if consistent and opposite senses of shear are observed on each of two sets of features they can be recognized as two conjugate faults of low dihedral angle. Once the fractures and faults have been recognized, the derivation of the principal stresses follows from the basic relationship in Fig. 8(a).

Certain morphological features on the surfaces of macrofractures and faults have been investigated by a number of workers as possible criteria for the distinction between extension and shear failure. Three types of features have been recognized: slickensides, plumose structure, and conchoidal structure.<sup>(70-78)</sup> Unfortunately the genetic implications of these features are not well understood.

Clearly, slickensides (polished and striated surfaces) indicate offset parallel to the walls of the fracture or fault. They can not, however, be regarded as generally reliable criteria because they record only the last movement along the surface. Conceivably the surface of an extension fracture (initial movement normal to the fracture walls) may be slickensided as a result of later movements parallel to the walls. Plumose structure consists of grooves and ridges on a rock surface. There is a central axis into which barbs or plumes converge

---

\* Direction of slip along a fault is needed only if one fault or one set of faults is present. For those cases involving intersecting conjugate elements, the line of intersection is parallel to  $\sigma_2$  and normal to the slip direction.

in featherlike form. Conchoidal structure consists of concentric grooves and ridges which usually center about one or two points on the surface. It is not clear whether conchoidal structure is merely a part of a larger plumose structure or a separate phenomenon with distinct genetic implications. The only certain fact about these features is that where they occur there has been little shear movement along the surface in question. Hodgson (Ref. 77, p. 29) implies that plumose and conchoidal structure are not diagnostic criteria. On the other hand, Parker (Ref. 74, p. 397) and Roberts (Ref. 78, p. 486) find that plumose structures are apparently restricted to shear fractures or faults. This would imply at least some shear displacement at the time of formation. Further analysis of these features, perhaps experimentally, would seem justified as it might lead to diagnostic criteria.

Field Examples--Microfractures. To the writer's knowledge there are only a few published studies in which the subfabrics of microfractures have been used to derive the orientations of the principal stress in rocks at the time of deformation. On the microscopic scale, fractures occur in the individual grains or crystals of the rock. They may or may not cross grain contacts. Their size, therefore, is somewhat dependent upon grain size. Though they may be visible to the unaided eye, they are best studied in thin section with the aid of the petrographic microscope and universal stage. The microfractures are often essentially planar features such that their dip and strike can be measured by one setting of the universal stage. Commonly they are developed in sets of two or more parallel individual features. They are fresh clean breaks in all experimentally deformed rocks and are commonly healed or filled in naturally deformed rocks.

That microfractures can be valid dynamic fabric elements has been demonstrated by studies of experimentally deformed, dry, unconsolidated, quartz sand aggregates and calcite-cemented sandstones.<sup>(58,59)</sup> Results show statistically that the grains tend to fracture with respect to the principal stresses across the boundaries of the whole specimen rather than with respect to local stress concentrations at grain contacts (Fig. 11). That is, even though the stresses must be transmitted

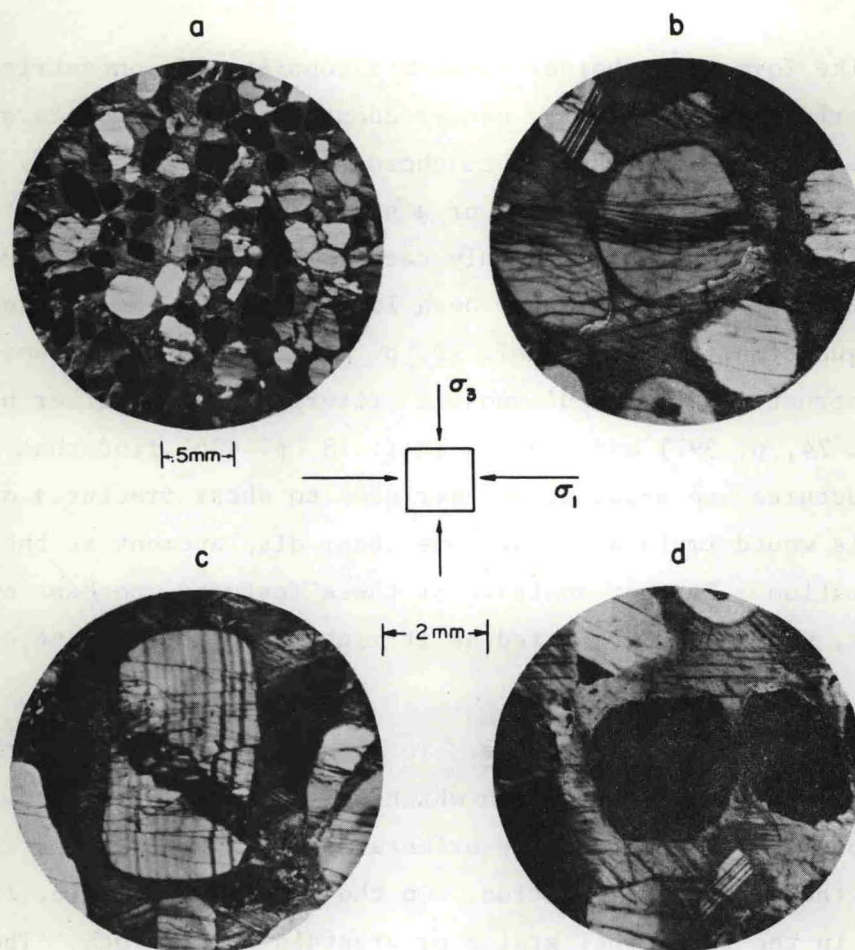


Fig. 11—Photomicrographs of microfractures in quartz and feldspar grains in an experimentally deformed calcite-sand crystal (from Friedman, Ref. 59, plate 2). The orientation of the principal stresses across the boundaries of the whole specimen is shown; extension fractures predominate.

through grain boundaries, the individual grains tend to fracture as if each grain were loaded in the same manner as the whole aggregate. This is a statistical statement, but reference to the photomicrographs in Fig. 11 shows that the phenomenon is quite pronounced. Moreover, the phenomenon in quartz grains is essentially independent of the crystal structure of quartz. <sup>\*(59)</sup>

\* This result for quartz sand aggregates is in marked contrast to recent data on quartz single crystals deformed at very high pressure. In such specimens the fracturing and faulting is controlled by the anisotropy of the crystal structure.

Bonham<sup>(79)</sup> studied both macrofabric and microfabric elements associated with the Pico anticline and syncline, which are located some 35 mi northwest of Los Angeles, California. The structure lies along the southern margin of the Ventura basin. Three Tertiary formations are encountered, the Modello (Miocene), the Pico (Pliocene), and the Saugus (Pliocene). These are composed of a poorly indurated turbidite sequence of interbedded arkose and graywacke sandstones, siltstones, and shales, with an aggregate thickness of nearly 15,000 ft. The anticline is 9 mi long and is folded tightly, showing an almost chevron cross section. The axial plane of the fold is nearly vertical and has a strike of about N-65°-W in the eastern and central parts and about N-75°-W in the western part. Dips on the flanks are commonly over 50 degrees with some overturning on the northern flank. The anticline plunges both east and west. Several normal faults, with as much as 500 ft of stratigraphic separation, cut the structure and tend to strike NE-SW and NW-SE. Bonham characterizes the anticline as a flexural slip fold with three mutually perpendicular axes of folding (Fig. 12).

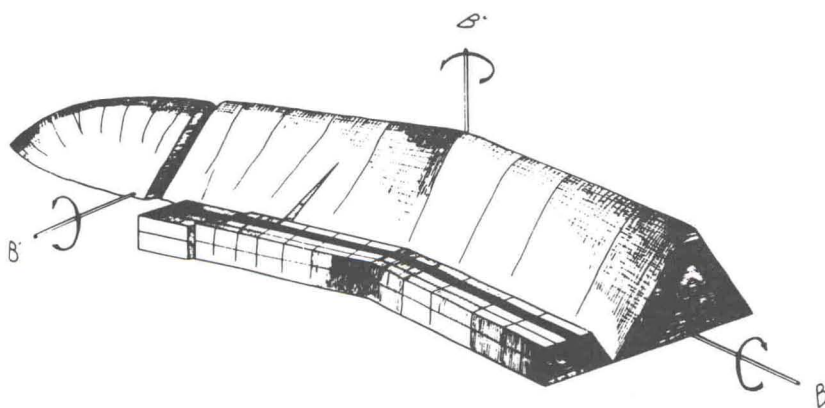


Fig. 12—Idealized block diagram of the Pico structure showing three axes of folding (from Bonham, Ref. 79, Fig. 3).

Bonham's data on orientation of microfractures and macrofractures (joints) are given in Fig. 13. For convenience, he refers his diagrams to three axes--a, b, and c. The b direction is parallel to the fold axis; the a axis lies in the bedding plane and is normal to the fold axis; and the c axis is normal to bedding. Accordingly, the

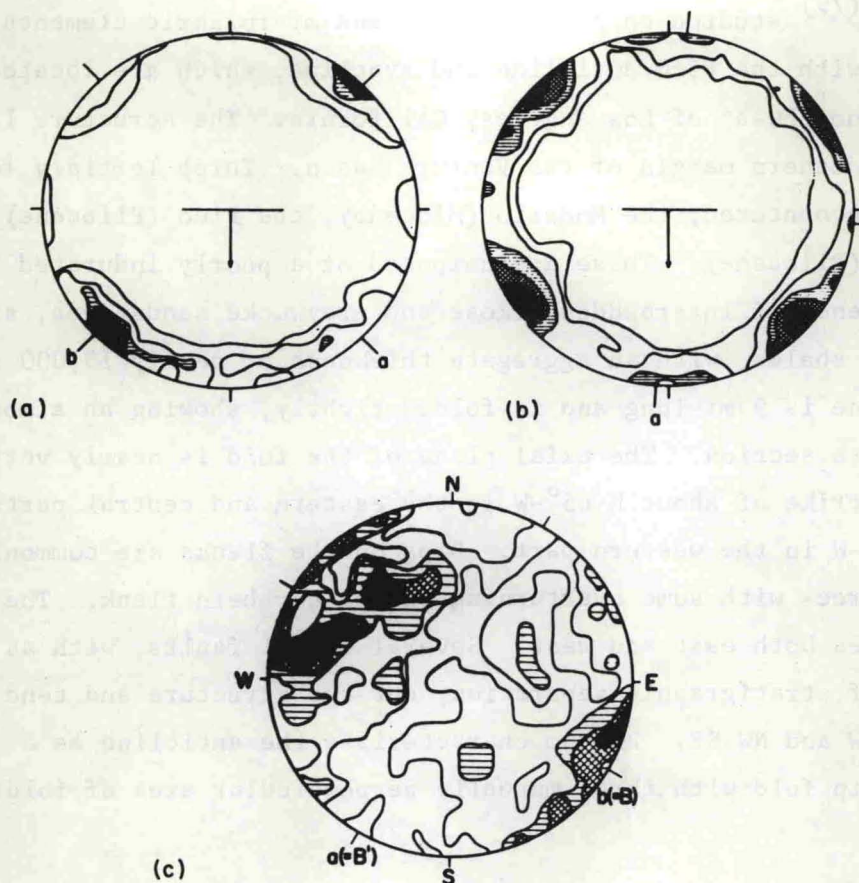


Fig. 13—Diagrams showing orientation of microfractures and macrofractures associated with the Pico structure (from Bonham, Ref. 79, Figs. 4 and 5). The plane of each diagram is parallel to bedding (ab). (a) Normals to 200 quartz microfractures. Contours are at >2, 4, 6, 8, and 10 per cent per 1 per cent area. (b) Normals to 200 quartz microfractures. Contours are at >1, 2, 4, 6, and 8 per cent per 1 per cent area. (c) Normals to 210 sets of macrofractures. Contours are at >1, 2, 3, and 4 per cent per 1 per cent area.

ab plane is parallel to the bedding plane, and the ac plane is normal to the fold axis ( $b = B$ ). In diagrams with a single concentration (Fig. 13(a)), the microfractures are preferentially oriented in the ac plane of the fold. In diagrams with two concentrations (Fig. 13(b)), the microfractures are oriented in two planes which intersect in a line normal to bedding. The acute angle between these planes is bisected by the ac fabric plane. Macrofractures (Fig. 13(c)) also tend to lie in the ac plane. Stereograms showing the major plane(s) defined by the microfractures at each of 28 stations on the fold (Fig. 14) indicate

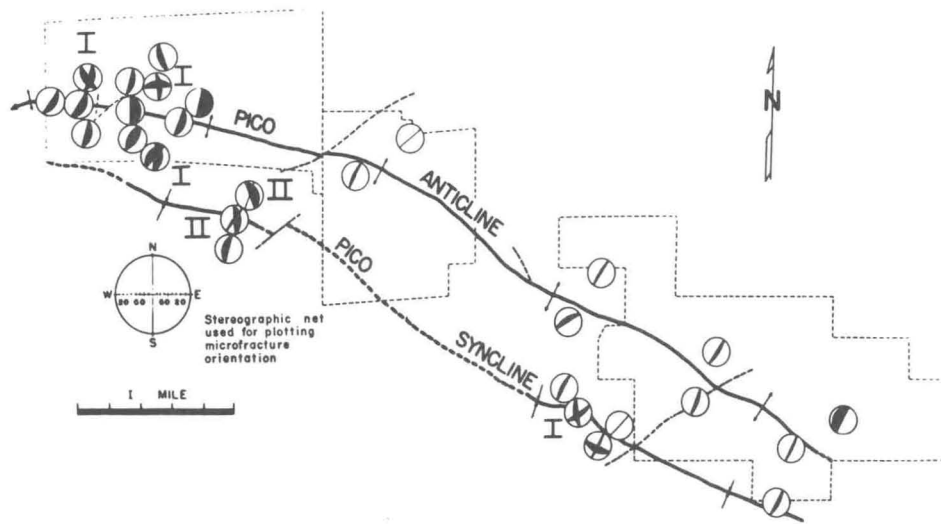


Fig. 14—Stereograms showing the orientation of major sets of microfractures associated with the Pico structure (from Bonham, Ref. 79, Fig. 7). The reference plane of each stereogram is horizontal.

that most are vertical and lie in the ac plane of the fold. Bonham points out that those near the western end of the structure reflect the westward plunge of the fold about the  $B'$ -axis.

Bonham does draw a dynamic inference from the ac fractures. He attributes them to tension parallel to the fold axis during deformation. Further inferences are possible from examination of the microfracture subfabrics. Consider first the diagram illustrating two concentrations (Fig. 12(b)). These define planes which intersect at about 75 degrees along a line nearly normal to the bedding plane. This configuration suggests that the fabric maxima define two sets of conjugate shear fractures ( $\theta = 38$  degrees) for which  $\sigma_1$  is parallel to the bedding plane and normal to the fold axis,  $\sigma_2$  is normal to the bedding plane, and  $\sigma_3$  is in the bedding plane and parallel to the fold axis. In Fig. 14, there are four stereograms (marked "I") that contain two sets of planar features intersecting at 50 to 80 degrees. By correlating the line of intersection of the two sets with the probable dip of the beds (see fold axes), one concludes that at each station, sets comprise a pair of conjugate shear fractures that intersect in a line normal to bedding. In each case the orientations of the derived stresses are as stated above. Next, consider the many stereograms in

Fig. 14 that contain a single set of features oriented in the ac plane of the fold. These not only parallel the ac macrofractures, but also tend to bisect the acute angle between the conjugate shear fractures at nearby stations. By reference to the basic configuration (Fig. 8(a)), the ac features are recognized as extension fractures. Finally, at two stations (marked "II" in Fig. 14), it appears as though one set of ac microfractures and one set of shear fractures occur in the grains of the rock. That is, the lines of intersection are at high angles to bedding, the shear fractures nearly parallel those at other stations, and the small dihedral angle between the ac set and the shear fracture set is in each case about 20 degrees.

Thus, Bonham has mapped microfractures and macrofractures that (1) exhibit consistent orientations throughout the fold, (2) are geometrically related to the fold in a meaningful way, and (3) can be interpreted as genetically related to the same state of stress. These principal stresses appear to be uniformly oriented with respect to the bedding planes and to be independent of the dip of the beds. Unfolding brings principal stresses mapped at each station throughout the structure into congruency. Accordingly, one can conclude that the fractures occurred either throughout the folding process or early in the history of folding in response to a horizontal greatest principal stress oriented roughly N-25°-E, a vertical intermediate principal stress, and a horizontal least principal stress trending roughly N-65°-W. The first alternative requires that  $\sigma_1$  remain nearly parallel to the bedding throughout folding.

Field Examples--Macrofractures and Faults. The literature is replete with purely geometric descriptions of macrofractures and faults. In most cases, the authors have referred to these features as joints ( $10^{-1}$  to  $10^3$  m in observed length) and related them to larger-scale folds and faults. Some workers have attempted to associate the joints genetically with the regional state of stress, but few have had an adequate understanding of the problem. Good examples of enlightened investigations are available, however. Several of these are reviewed by De Sitter (Ref. 80, pp. 122-142), and Schmidt (Ref. 81, pp. 10-17) gives a comprehensive review of the literature. Additional significant

dynamic interpretations of fracture and fault assemblages are to be found in Cloos,<sup>(82)</sup> Dawson-Grove,<sup>(83)</sup> Price,<sup>(84)</sup> Harris *et al.*,<sup>(85)</sup> Muehlberger,<sup>(69)</sup> and Donath.<sup>(86)</sup>

Melton's reconnaissance study of the fracture systems in the Ouachita Mountains and Central Plains of Oklahoma<sup>(87)</sup> can be used to illustrate how dynamic inferences are made from geometric data. The geology of the area is sketched in Fig. 15. In general the intensity of the deformation decreases northwestward from the Ouachita Mountains through the Open Fold zone to the nearly flat-lying strata of the Central Plains. Melton measured the attitudes of fracture sets in outcrops distributed throughout this region (Fig. 16). He concluded

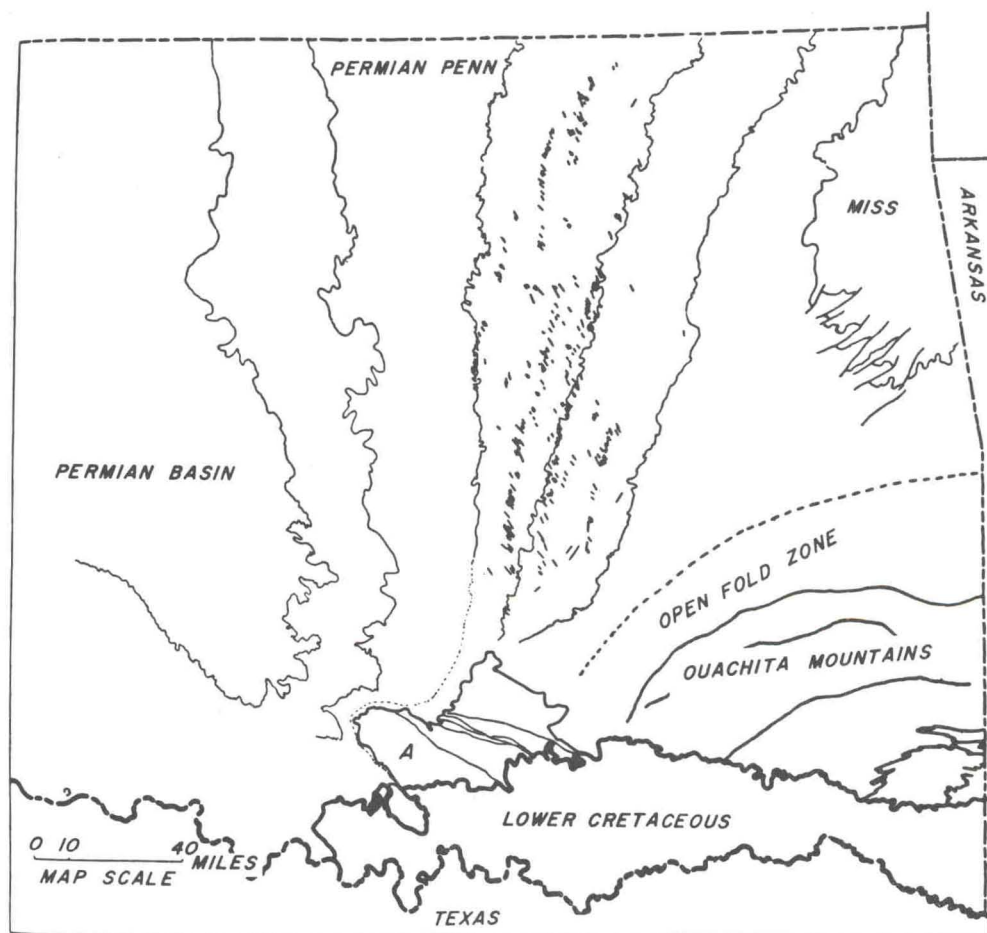


Fig. 15—The major structural units of Oklahoma. The Arbuckle Mountains (A), the Ouachita Mountains, the Permian (Anadarko) Basin, the Mississippian rocks of the southwestern part of the Ozark Dome, and the "belts" of *en échelon* faults in the Central Plains are shown (from Melton, Ref. 87, Fig. 1).

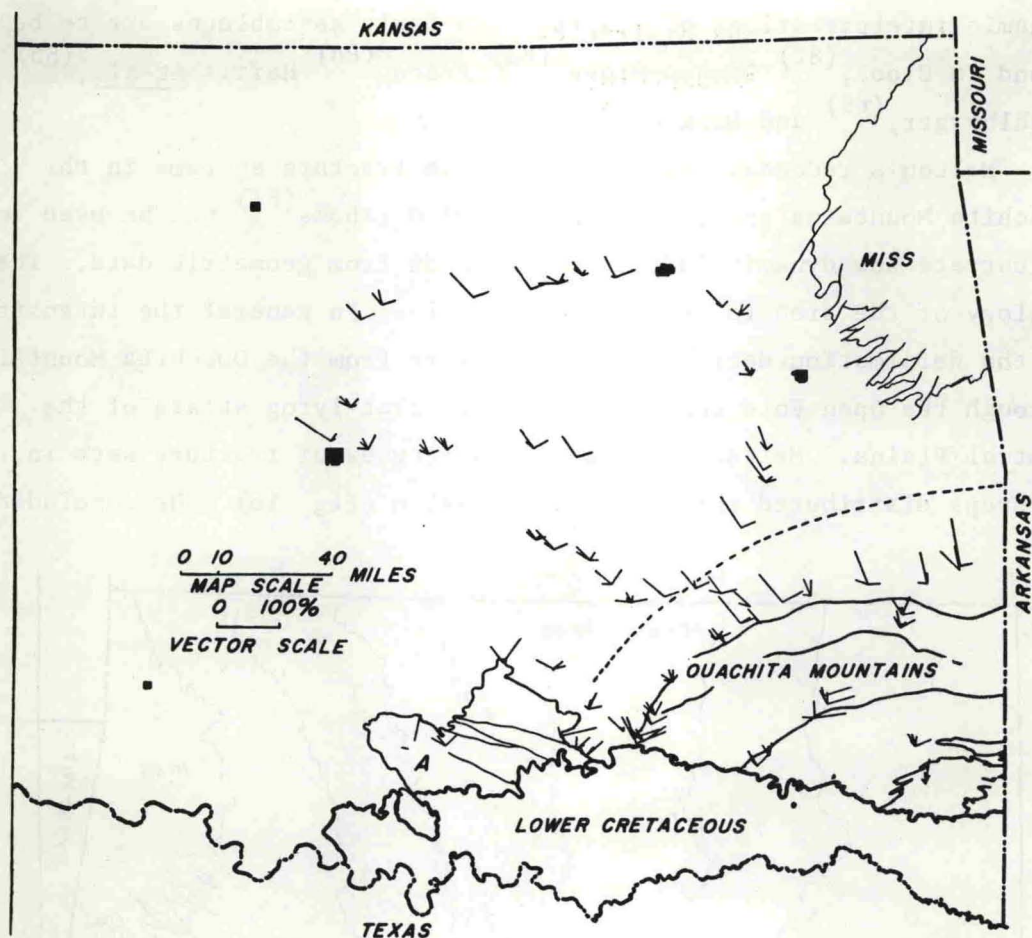


Fig. 16—Fracture trends in southeast Oklahoma shown with the bedding at each station unfolded to the horizontal position (from Melton, Ref. 87, Fig. 3). The length of each line is proportional to the number of fractures at that station with the indicated strike.

that (1) the prominent systems in the Central Plains radiated in a fan-like manner from the Ouachita Mountains and originated from the forces of the Ouachita orogeny, (2) the Ouachita Mountains were probably formed after the Middle Permian, and (3) the short faults of the en échelon belts east of Oklahoma City (Fig. 15) correlated closely in strike with the dominant fracture set in the Central Plains, thereby tying their genesis to the Ouachita Mountain orogeny more closely than was theretofore recognized.

If the fracture array at each station (Fig. 16) is examined closely, one can distinguish individual elements of a four-set pattern (Fig. 17). This pattern is repeated throughout the region, even though

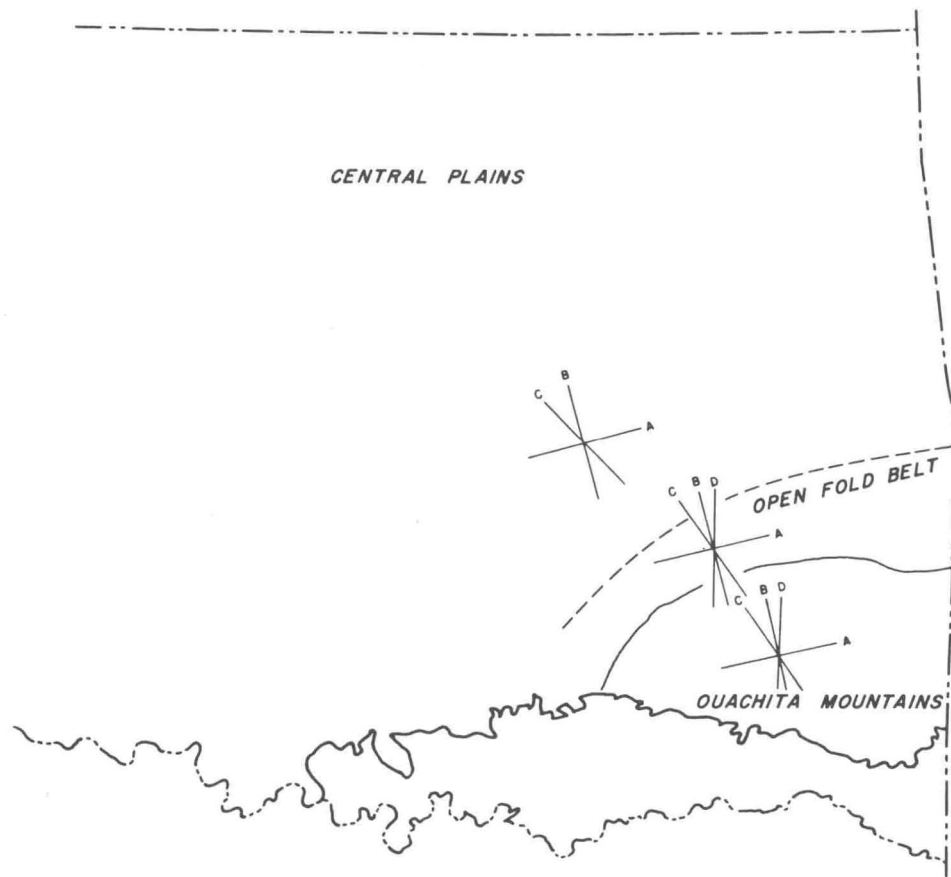


Fig. 17—The average fracture patterns in the Central Plains, Open Fold zone, and Ouachita Mountains (obtained from Melton, Ref. 87, Figs. 6, 8, and 10, respectively).

all four sets are rarely developed at any one station. Moreover, the pattern tends to rotate with the change in strike of the beds in the Ouachita Mountains and Open Fold zone. Each set is oriented normal to bedding. When beds in the Ouachita Mountains and Open Fold zone are unfolded, the fracture-fault sets become congruent with those in the Central Plains. Sets A and B (Fig. 17) intersect at 90 degrees. Sets C and D intersect at about 40 degrees and are about equally disposed on either side of set B. Set C is the best developed of the four. The configurations of sets B, C, and D suggest that they represent an extension fracture and two conjugate shear fractures, respectively. From this pattern,  $\sigma_1$  is placed horizontal and everywhere normal to the strike of the Ouachita Mountain trend,  $\sigma_2$  is vertical (normal to

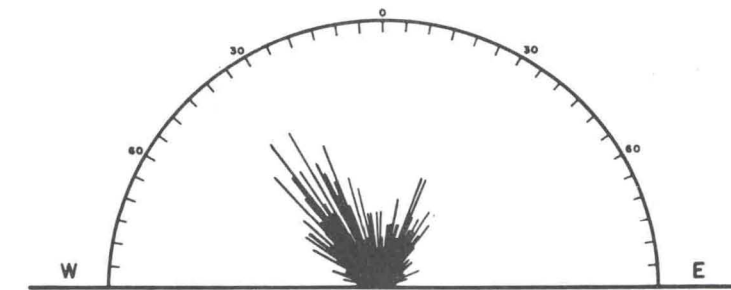
bedding), and  $\sigma_3$  is horizontal and normal to  $\sigma_1$ .<sup>\*</sup> The fourth element of the pattern (set A) needs further explanation. In the Ouachita Mountains and Open Fold zone it tends to parallel the strike of the beds (Ref. 87, p. 741) and therefore occupies an orientation similar to that of the often mentioned "tension" fractures that develop during folding (Fig. 8(c), and Ref. 80, p. 100; Ref. 82, p. 185; Ref. 88, p. 150; Ref. 89, p. 102; and Ref. 90, p. 118). It is unreasonable to extend this explanation for set A into the unfolded strata of the Central Plains. In the writer's view set A is there a relaxation fracture (Fig. 8(b)), i.e., an extension (or tensile) fracture formed upon release of stored elastic strain energy. Finally, the belts of en echelon faults (Fig. 15) are interpreted as near surface features related to wrench faults at depth, which would be left-lateral and would trend N-10-15°-E. The principal stress directions derived from these wrench faults are in good agreement with those derived from the regional joint pattern. It is significant that the fracture-fault pattern giving rise to these dynamic interpretations extends more than 100 mi into the Central Plains from the Ouachita Mountains.

An even-larger-scale example is afforded by the fault trends in the Great Basin of the western United States. Donath<sup>(86)</sup> compiled fault-strike frequency diagrams (Figs. 18(a) and 18(b)) for a 420-sq-mi area in south-central Oregon. The faults tend to strike in two main directions (N-35°-W and N-20°-E). The evidence indicates that the first movement on these faults was strike-slip and that this was followed by dip-slip displacement. Donath (Ref. 86, p. 1) states "... the intersection angle of approximately 55° and the nearly vertical dips indicate that the faults originally developed as conjugate strike-slip shears in a stress system characterized by a north-south maximum principal stress and an east-west minimum principal stress." The subsequent dip-slip movements on these planes reflect a redistribution of the surface forces acting on the individual fault blocks.

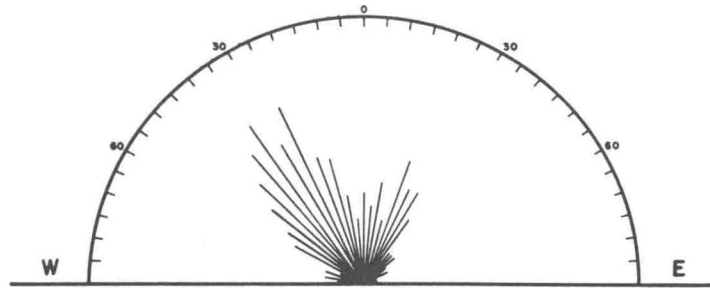
This same fabric is even more strikingly demonstrated by range-edge trends in a 50,000-sq-mi area in Nevada. On the assumption that

---

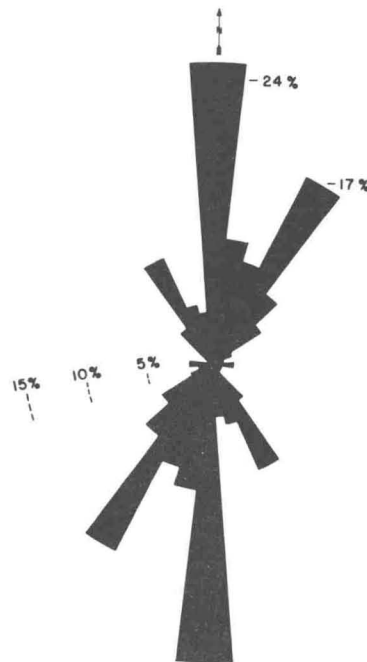
\* Dynamic inferences by Friedman.



(a)



(b)



(c)

Fig. 18—Fault-strike frequency diagrams for areas in the Great Basin of western United States. (a) Strikes of 625 faults or fault segments plotted at 1-degree intervals. Radius of diagram equals 18 faults or fault segments. (b) Same data replotted for 5-degree class intervals. Radius of diagram equals 62 faults or fault segments (from Donath, Ref. 86, Fig. 4). (c) Strikes of 410 range-edges in over 50,000 sq mi in Nevada, as measured from 1:250,000 USGS topographic sheets (from Conger, Ref. 91).

these are delineated by faults, Conger<sup>(91)</sup> compiled the trends of 410 segments (Fig. 18(c)). North-south, N-30°-E, and N-30°-W trends are prominent, and comparison with Fig. 8(a) suggests a north-south greatest principal stress and an east-west least principal stress. Donath's explanation would seem to apply to Conger's data, with the exception that the initial movement on Conger's north-south set would have to have been normal to the walls of the fracture. The same stress orientations derived from these faults are also appropriate for the right-lateral strike-slip movement associated with the San Andreas wrench fault system in California.

The consistent fracture fault patterns in Oklahoma and in the Great Basin serve to illustrate that macroscopically uniform states of stress can be transmitted through large portions of the earth's crust.

#### Intracrystalline Gliding

General. Intracrystalline gliding flow (the "plastic" flow of metallurgy) takes place by the relative displacement of atomic or ionic layers over one another. The true nature of gliding seems to have been first recognized by Reusch<sup>(92)</sup> in halite and calcite. During the late nineteenth and early twentieth centuries mineralogists worked out the morphology of most of the known gliding systems. Since then metallurgists have much improved our physical understanding of the gliding (= slip) process.

In gliding, the strain can be regarded as a simple shear with no volume change. Displacement is restricted to a gliding (or slip) plane (T), a definite gliding direction (t) within that plane, and sometimes to a particular sense of shear parallel to the gliding line. These constitute the gliding system, which is determined by the crystal structure and is independent of the loading condition. Gliding is initiated when the shear stress along t exceeds some critical value ( $\tau_c$ ), which is essentially independent of the normal stress across the gliding plane<sup>(93-95)</sup> and of the orientation of the load relative to the gliding system. Accordingly in an aggregate or in a single crystal, gliding takes place most readily for systems of low  $\tau_c$  and high resolved shear stress coefficient ( $S_0$ ). (See Fig. 19.)

Translation gliding involves displacement through an integral number of interionic distances so that after slip the configuration of the crystal lattice is unchanged across the slip plane (Fig. 20). The slip need not be equally distributed throughout the deformed crystal, and the shear strain is not fixed. Although no general theory relates the translation gliding system to a particular crystal structure, in metals the gliding plane is usually one of high atomic

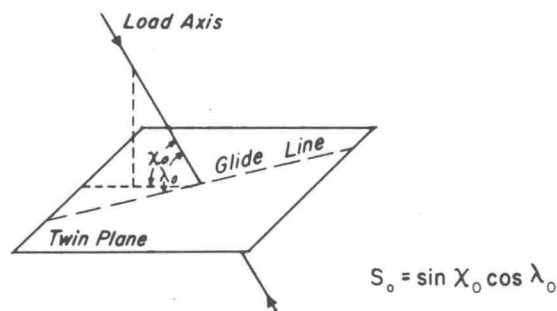


Fig. 19—Diagram showing nature of the resolved shear stress coefficient ( $S_o$ ).

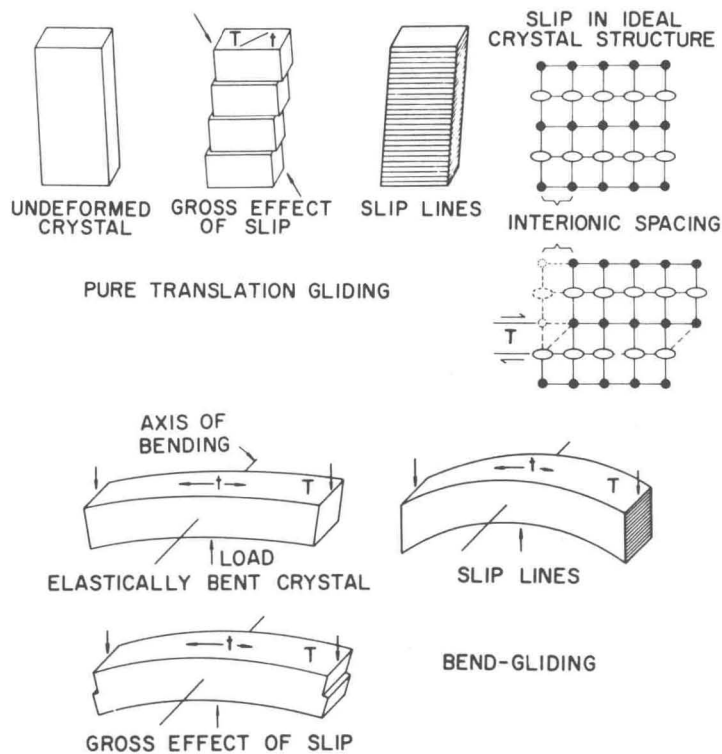


Fig. 20—Models of translation gliding.

or ionic density and of simple crystallographic index. The gliding direction is usually the densest atomic row (Ref. 93, p. 86). Bend gliding (Fig. 20) is a special form which occurs when planes are initially oriented parallel or normal to the load axes and are bent elastically before slip occurs. A compilation of translation gliding systems in 80 crystals is given by Handin.<sup>(96)</sup>

In mechanical twin gliding each ionic layer moves through a fixed fraction of the interionic distance so that the shear is fixed and the twinned portion of the crystal is in the proper symmetrical relationship to the original untwinned structure. The physical discontinuity between the twinned and untwinned portions of a crystal makes twin lamellae conspicuous in thin section (Figs. 21 and 22). The morphology of

### TWIN GLIDING

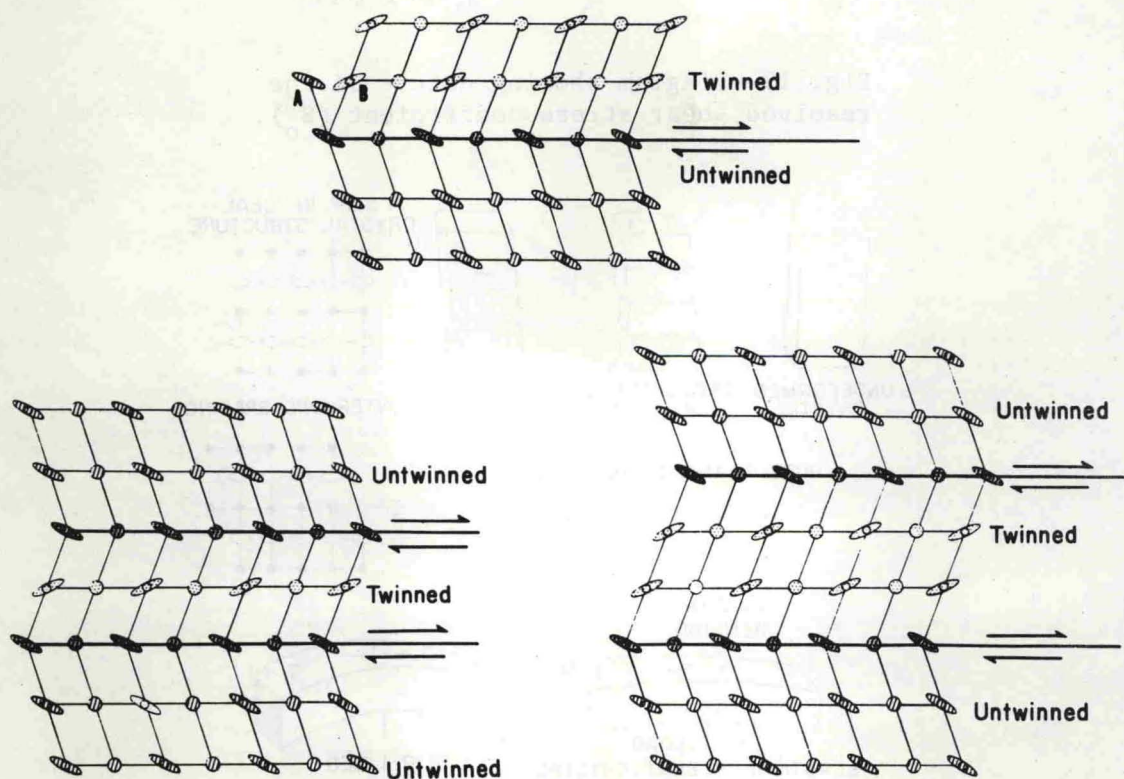


Fig. 21—Diagrammatic illustration of twin gliding and the development of a twin lamella. The movement along any one ionic layer (gliding plane) is a fixed fraction of the unit interionic distance, e.g., ion at A moves to B. As a result, a symmetrical relationship exists across the twin plane. A twin lamella is formed if twinned material is bounded on both sides by untwinned structure.

twinning has been discussed by Bell<sup>(97)</sup> and Pabst<sup>(98)</sup> and the metallurgical literature includes reviews by Cahn<sup>(99)</sup> and Hall.<sup>(100)</sup>

It is adequate for our present purpose to consider the model of twin gliding illustrated by the hypothetical structure shown in Fig. 23. If the relative displacement (sense of shear) of the upper layers is

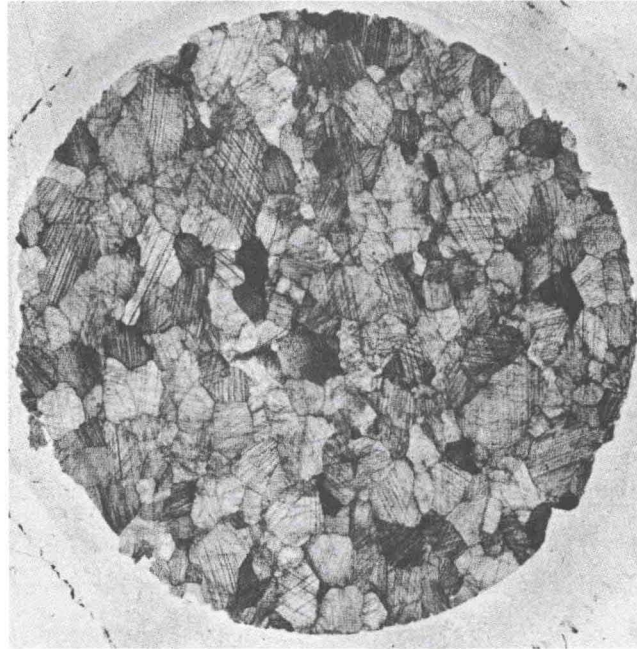


Fig. 22—Photomicrograph of  $e\{01\bar{1}2\}$  twin lamellae in calcite grains of a Pre-Cambrian (?) marble, Schell Creek Mountains, near Ely, Nevada. Diameter of the specimen is 1/2 in.

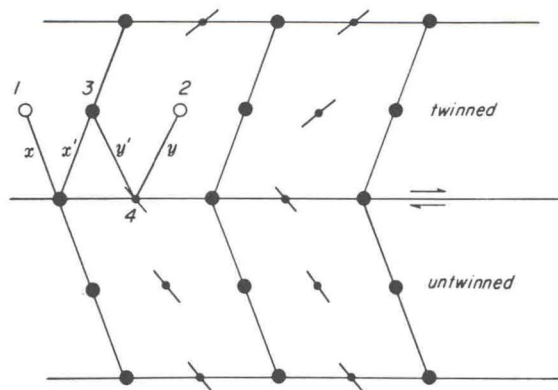


Fig. 23—Section through a hypothetical lattice illustrating different movements of the ions for different senses of shear in twin gliding (after Higgs and Handin, Ref. 55, Fig. 4). The plane of the paper is normal to the gliding plane and contains the gliding direction.

from left to right, the ion at position 1 (initial position) moves to position 3. The angle between lines  $x$  and  $x'$  is the angle of shear ( $\psi$ ), and the shear ( $s$ ) is given by

$$s = 2 \tan \frac{\psi}{2} .$$

If the displacement of the upper layers is from right to left, the ion at position 2 (initial position) moves to position 3 and the angle of shear  $\psi'$  is between  $y$  and  $y'$ . Actually, twin gliding on a particular gliding plane is restricted to movement in only one direction, presumably that requiring the least energy. The proper sense of shear is indicated by the arrows. This qualitative picture of twin gliding involving only initial and final states of the ions is useful even though the actual paths of the ions may be unknown. Twin gliding systems for some 70 minerals have been compiled by Higgs. <sup>(96)</sup>

Dynamic Inferences from Gliding Systems. Twin and translation gliding is initiated for a given system when the resolved shear stress along the gliding direction and in the correct sense of shear exceeds a critical value  $\tau_c$ . As gliding is largely independent of the normal stress,  $\tau_c$  is reached most effectively when the resolved shear stress coefficient ( $S_o$ ) is maximum (0.5). Accordingly, the most favorable state of stress in the crystal is characterized as follows: (1)  $\sigma_2$  is parallel to the gliding plane (T) and normal to the gliding direction (t); (2)  $\sigma_1$  is inclined at 45 degrees to T in the plane normal to T that contains t and is oriented so as to produce the correct sense of shear; and (3)  $\sigma_3$  is inclined at 45 degrees to T in the plane containing t and  $\sigma_1$ . Clearly, if the gliding system(s) for a given crystal is known and if T and t can be recognized and measured, then one can derive the orientations of the principal stresses within the crystal that would best produce gliding. Petrofabric techniques are employed to locate these stresses in a number of individual crystals in polycrystalline aggregates, to plot them in fabric diagrams, and then to evaluate the average local state of stress in the rock at the time of gliding.

Dynamic Interpretation of Twin Lamellae in Calcite and Dolomite.

Although in principle it is possible to make dynamic inferences from any known gliding system, in nature only a few common rock-forming minerals show the diagnostic features required in practice. Twinning in calcite and dolomite has received most attention in the laboratory and in the field. Knowledge of the deformation mechanisms in calcite has evolved from Brewster's observations<sup>(101)</sup> of mechanical twins in 1826 to the comprehensive experimental studies of deformed calcite single crystals and marbles, together with their petrofabric analyses.\* As a result, gliding flow in calcite can be adequately accounted for by three gliding systems (Fig. 24):

(1) Twin gliding parallel to  $e\{01\bar{1}2\}$  with  $[e_1:r_2]$  as the gliding direction, and with a positive sense of shear,\*\* effective throughout the temperature range of 20° to 800°C.

(2) Translation gliding on  $r\{10\bar{1}1\}$  with  $[r_1:f_2]$  as the gliding direction, sense of shear negative, effective over the temperature range 20° to 800°C.\*\*\*

(3) Translation gliding on  $f\{02\bar{2}1\}$  with  $[f_1:r_3]$  as the glide direction, sense of shear negative, effective at 20°C and at 500° to 800°C, where it predominates over r translation.

Turner<sup>(111)</sup> has developed a technique for dynamic interpretations of twin lamellae in naturally deformed rocks by locating the mutually perpendicular directions of compression and extension that most favored development of the observed twin lamellae. The geometry of these relationships was initially set forth by Handin and Griggs (Ref. 105, pp. 866-869). If a maximum  $S_0$  value (0.5) for twinning is assumed,

---

\* See Refs. 43, 95, and 102-110.

\*\* Arbitrarily, relative displacement of the upper layers of the lattice upward toward the optic axis (or c axis, or  $c_v$  as used here) is called gliding in the positive sense; relative displacement of the upper layers downward from the upper end of the  $c_v$  is called gliding in the negative sense.

\*\*\* Direct visual evidence of translation (e.g., slip lines) is rare. Accordingly, translation gliding systems will not be utilized here, but will be discussed in the section on intragranular rotation phenomena.

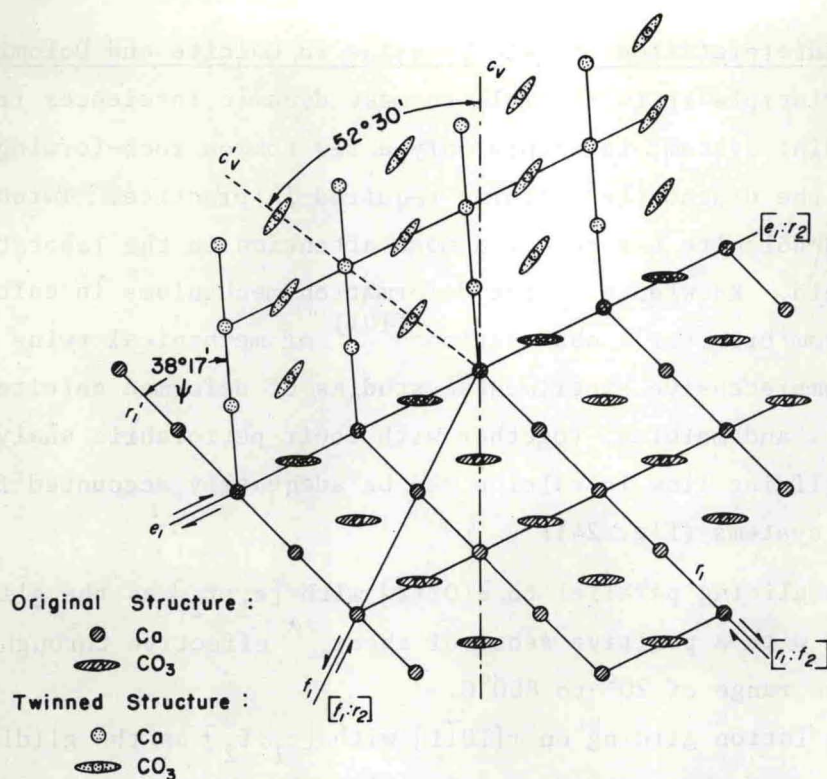


Fig. 24—Diagrammatic representation of the calcite structure. Section is drawn normal to the  $a_2$  axis. The structure is twinned on  $e_1$ , with the gliding direction and sense of shear for the twin gliding indicated. Translation gliding systems along  $r_1$  and  $f_1$  are also shown.

the position of the load axis can be uniquely defined, because  $\chi_0$  and  $\lambda_0$  must be 45 degrees (Fig. 19). Accordingly,  $\sigma'_1$  and  $\sigma'_3$  are fixed for twin gliding when  $S_0 = 0.5$  (Fig. 25(a)).\* The compression axis  $\sigma'_1$  is inclined 45 degrees to  $e_1$  or to the normal to  $e_1$ , and 71 degrees to  $c_v$  (the  $c$  axis).\*\* The extension axis  $\sigma'_3$  is inclined 45 degrees to  $e_1$  or the normal to  $e_1$ , and 19 degrees to  $c_v$ . For any calcite grain,

\* Primes are used to denote principal stress axes derived from any one crystal.

\*\* By convention, the three twin planes in each calcite crystal are designated as  $e_1$ ,  $e_2$ , and  $e_3$ ;  $e_1$  is identified as the plane along which the twin lamellae are best developed, i.e., most densely spaced or widest, and  $e_3$  is identified as the plane along which they are the most poorly developed. In a calcite crystal in which at least one set of twin lamellae is developed ( $e_1$ ), the positions of the other potential sets can be determined from the crystallography of calcite.

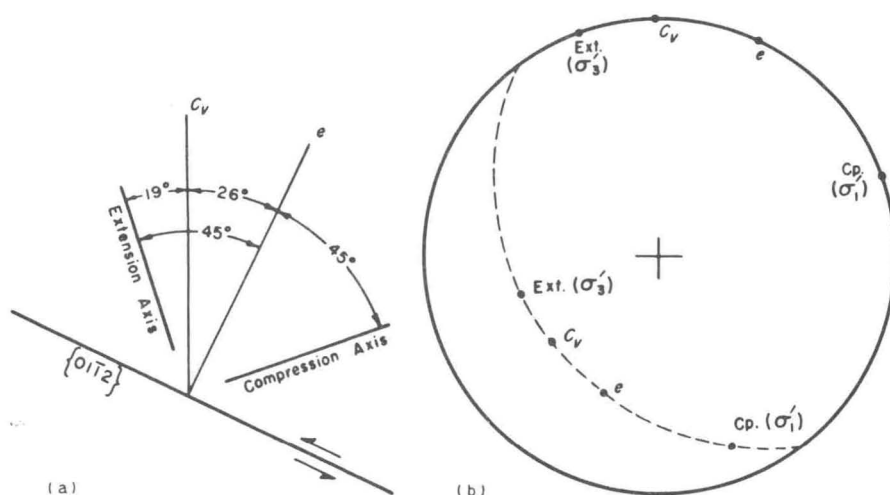


Fig. 25—Diagrams illustrating the orientation of the axes of compression ( $\sigma_1'$ ) and extension ( $\sigma_3'$ ) that would be most effective in causing twin gliding on  $e\{0112\}$  in calcite. (a) The plane of the diagram is perpendicular to the gliding plane and contains the gliding direction, the  $c_v$ , and the normal to the gliding plane ( $e$ ). (b) Lower hemisphere, equal-area projection of the relationships in (a) are shown for two differently oriented cases.

therefore, the positions of  $\sigma_1'$  and  $\sigma_3'$  for  $S_o = 0.5$  can be determined (Fig. 25(b)) by measuring and plotting  $e_1$  and  $c_v$ .

Twinning can, of course, be initiated for  $S_o$  values less than 0.5 as long as  $\tau_c$  is exceeded and the correct sense is maintained. For example, the average  $S_o$  value is 0.27 for the twinned calcite cement of an experimentally deformed sandstone.<sup>(59)</sup> Turner's technique utilizes  $S_o = 0.5$ , however, because this value allows unique location of the principal stresses. (There are an infinite number of possible orientations for the stress axes for  $S_o < 0.5$ .) Moreover, there is a good empirical relationship between the amount of twinning and  $S_o$  values. In experimentally deformed Yule marble and Hasmark dolomite, the greatest amount of twinning occurs on that set of twin gliding planes for which the resolved shear-stress coefficient was highest (Fig. 26).<sup>(52,106)</sup>

The technique using calcite twin lamellae to derive the orientations of the principal stresses in a rock consists of the following steps. (1) The orientation of the best developed set of twin lamellae and the host  $c_v$  in each grain are determined by universal-stage

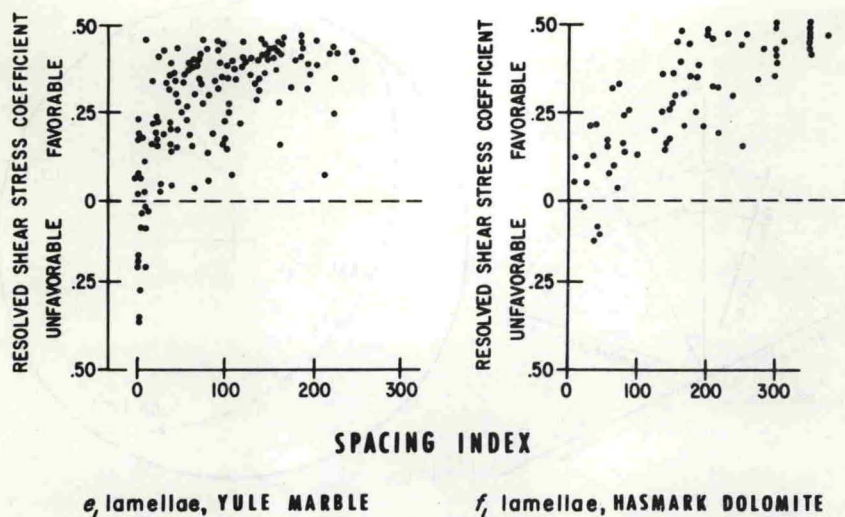


Fig. 26—Plots illustrating the relationship between  $e_1$  and  $f_1$  twin-lamellae spacing indices and  $S_0$  values for these planes as calculated from the known stress orientations in experimentally deformed Yule marble and Hasmark dolomite, respectively (from Turner and Ch'ih, Ref. 106, Fig. 6; and Handin and Fairbairn, Ref. 52, Fig. 6, respectively). Twin-lamellae spacing index is defined as the number of lamellae per millimeter when viewed on edge.

measurements. (2) These data are plotted in equal-area projection, and the compression and extension axes are located for each grain as outlined above. (3) The data measured in two or more mutually perpendicular thin sections are combined into a composite diagram, and the resulting orientation pattern is interpreted as reflecting the average orientation of  $\sigma_1$  and  $\sigma_3$  in the rock at the time twinning took place. Friedman<sup>(59)</sup> has found good agreement between the derived position of  $\sigma_1$  and the known orientation of  $\sigma_1$  in experimentally deformed calcite-cemented sandstones (Fig. 27).

A readily visible example of this technique is described by Friedman and Conger.<sup>(112)</sup> Calcite crystals within the walls of a naturally deformed fossil shell (Fig. 28) exhibit in thin section a systematic development of  $e$  twin lamellae. In transverse section the walls are elliptical and the crystals along two opposite sides of the ellipse (each encompassing 120 degrees of arc) are profusely twinned, whereas those along the two remaining 60-degree arcs are sparsely twinned. Calcite  $c_v$  are oriented radially. Fig. 29(a) shows that the preferential development of twin lamellae probably depends on favorable

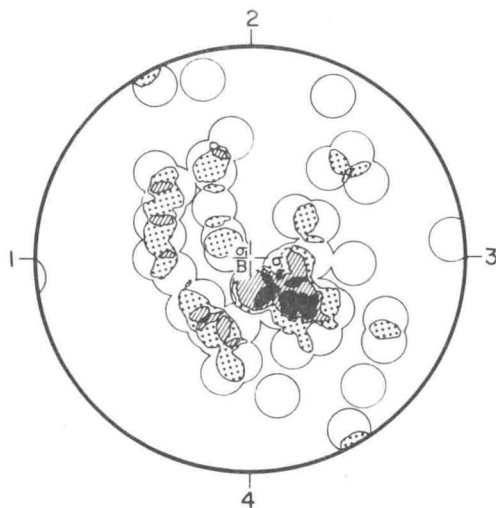


Fig. 27—Diagram of 50 compression axes derived from sets of  $e_1$  twin lamellae in 50 calcite-cement crystals from an experimentally deformed calcite-cemented sandstone (from Friedman, Ref. 59, Fig. 16c). Specimen was shortened 9.2 per cent under 2-kb confining pressure at 300°C. Plane of the diagram is normal to the long axis of the deformed cylinder with the known position of  $\sigma_1$  at the center of the diagram. Contours are at 2, 4, 6, and 8 per cent per 1 per cent area. The derived position of  $\sigma_1$  is 10 to 15 degrees SE of the center.

or unfavorable orientation for twinning of a given crystal with respect to an assumed east-west  $\sigma_1$ . Moreover, compression and extension axes derived from  $c_v$  and  $e_1$  lamellae in each grain are strongly oriented parallel to bedding and trend N-75°-W and N-15°-E, respectively, when the beds are unfolded (Figs. 29(b) and 29(c)). These results are in good agreement with the geologic framework because these directions are within 15 degrees of being perpendicular and parallel, respectively, to a series of nearly parallel north-south fold axes located where the sample was collected some 7 mi south of Drummond, Montana.

Twin lamellae in complexly deformed metamorphic rocks have been studied in considerable detail. Turner<sup>(111)</sup> applied his technique to the study of three marbles and concluded that the visibly twinned  $e$  lamellae developed during the last stages of deformation. McIntyre and Turner<sup>(113)</sup> employed the same methods in a study of three different marbles from Scotland and also concluded that twinning in calcite was the expression of minor postcrystallization deformation, probably compression transverse to the regional fold axis. Gilmour and

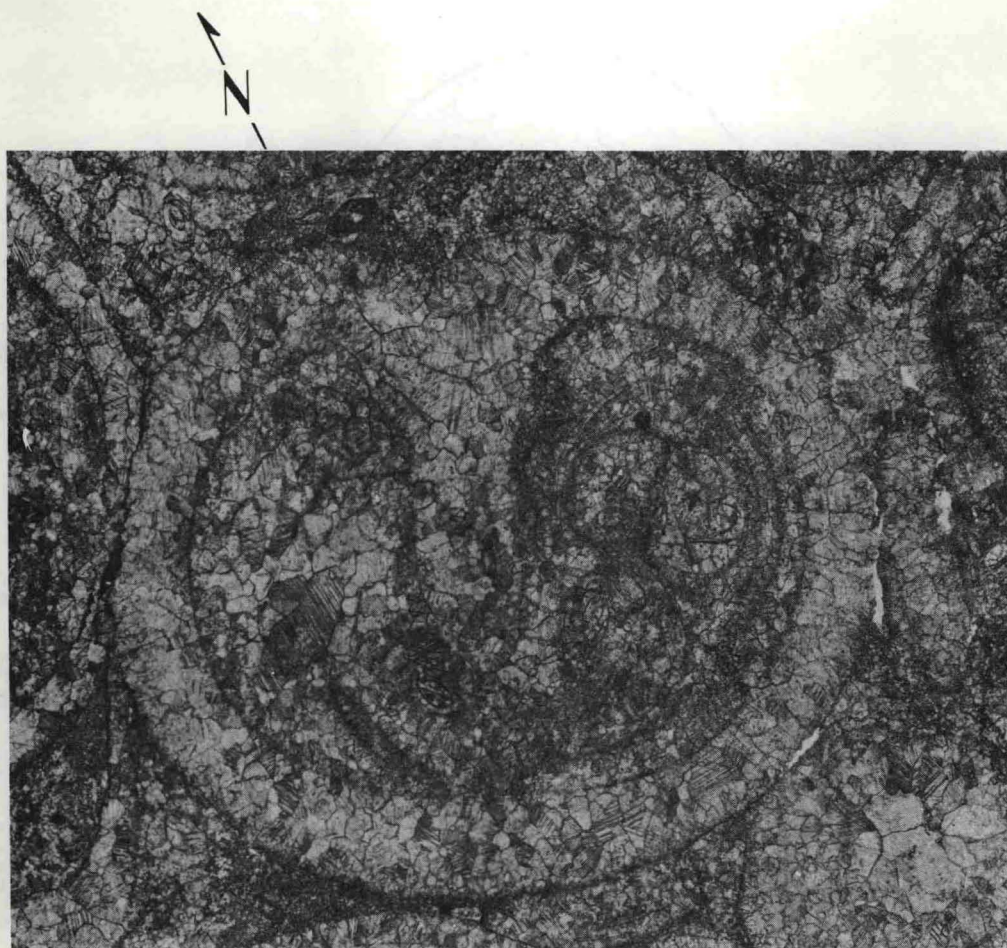


Fig. 28—Photomicrograph of a transverse section through a gastropod. Plane of the photomicrograph is also parallel to bedding. North is as indicated after the bedding is rotated to the horizontal. East-west diameter of the gastropod is approximately 4 mm (from Friedman and Conger, Ref. 112, Plate 1).

Carman,<sup>(114)</sup> taking the same approach, found that the compression axis deduced from postcrystallization e twin lamellae confirmed the direction of movement deduced from megascopic structures. Clark<sup>(115)</sup> studied the calcite twinning in still other marbles from the Scottish Highlands and found a consistent stress pattern over the 5 sq mi investigated. He concluded that the calcite twinning could best be explained by a compression oriented normal to the trend of the regional fold axis, followed by a mild "squeeze" at right angles. Weiss<sup>(116)</sup> investigated the dynamic significance of visibly twinned e lamellae in a marble-quartzite complex in southern California. He found that only

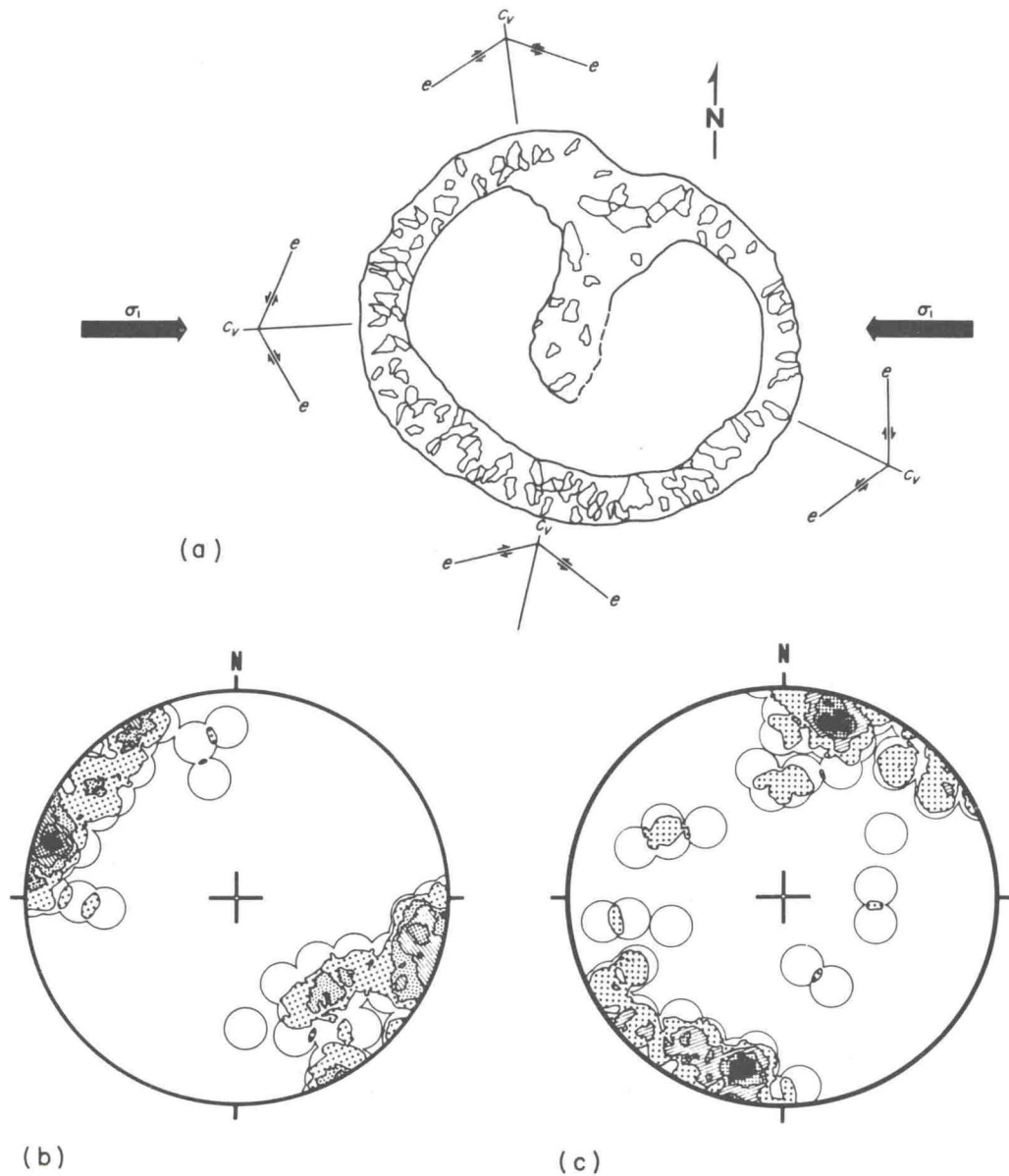


Fig. 29—Petrofabric analysis of calcite twin lamellae in the gastropod shell. (a) Approximate orientations of two  $e$  twin planes and the  $c_v$  in calcite crystals at four points within the gastropod shell. With respect to an assumed east-west greatest principal compression, the grains along the north and south sides of the shell are favorably oriented for twinning because of the sense of shear on the twin planes, whereas those on the east and west sides are unfavorably oriented (from Friedman and Conger, Ref. 112, Fig. 4). (b) Diagram illustrating the orientation of 70 compression axes derived from grains with high  $e_1$  lamellae spacing. Plane of the diagram is parallel to bedding with north as indicated for bedding unfolded. Contours are at 1.4, 2.9, 5.7, 8.6, 11.4, and 14.3 per cent per 1 per cent area, 15.7 per cent maximum (from Friedman and Conger, Ref. 112, Fig. 8b). (c) Diagram illustrating the orientations of 70 extension axes derived from same grains as in (b). Diagram oriented same as in (b). Contours are at 1.4, 2.9, 5.7, 8.6, and 11.4 per cent per 1 per cent area, 14.3 per cent maximum (from Friedman and Conger, Ref. 112, Fig. 9b).

those twin lamellae formed during the last stages of deformation yielded consistent results, and that the lamellae formed earlier were disturbed by later differential movement of the grains and so gave inconclusive, nearly random stress patterns.

This brief review emphasizes at least two difficulties encountered in applying this technique to metamorphic rocks. (1) The rocks have probably undergone recrystallization during deformation such that the observed twin lamellae relate only to the latest phase in the deformation history. Clearly, this limits the usefulness of highly deformed calcite. (2) In marbles the  $c_v$  of the grains are typically strongly oriented at high angles to the foliation. As a result the orientations of the derived compression and extension axes are restricted by the  $c_v$  subfabric. Only when the grains in a rock are randomly or diffusely oriented can one equate the derived compression and extension axes to the principal stresses  $\sigma_1$  and  $\sigma_3$ .<sup>(117)</sup>

The study of calcite twin lamellae in slightly and moderately deformed rocks (which are relatively free of the recrystallization and the strong  $c_v$  orientation effects) has only recently been initiated. Nickelsen and Gross<sup>(118)</sup> extended the technique to study two low-grade metamorphic, sandy textured, carbonate rocks from the Ordovician Conestoga formation in Pennsylvania. They found concentrations of compression axes in a broad zone whose center was approximately normal to a slaty cleavage. According to the authors this agreed very well with the observation that grains, pebbles, and boulders were flattened parallel to the cleavage. In addition, the authors positioned the axes that corresponded to the bisectors of the acute angles between the two gliding lines for grains in which two sets of lamellae were developed. This gave a similar compression axis orientation pattern.

Conel<sup>(119)</sup> determined compression and extension axes in two specimens within a single bed of folded limestone (Fig. 30). His specimens were collected from the trough portion of a syncline--one near the top of the bed and the other near the bottom. In the former, compression axes are strongly grouped normal to the fold axis, whereas in the latter, the compression axes are strongly grouped normal to bedding. Conel concluded that these orientations were analogous to those expected from elastic analyses of bent plates.

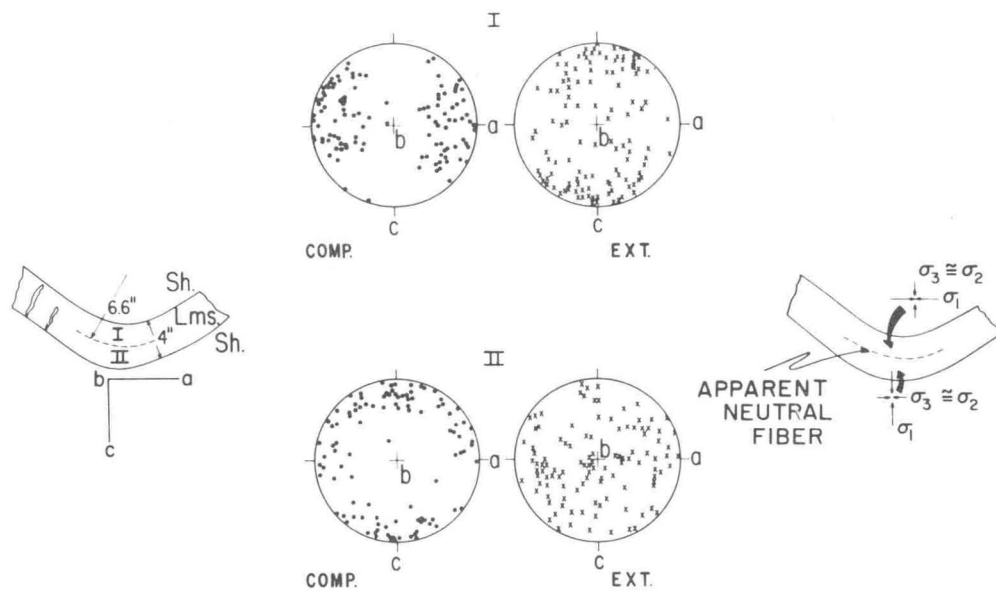


Fig. 30—Diagrams of compression and extension axes determined from calcite twin lamellae in regions I and II of a folded limestone bed in the Silurian McKenzie Creek formation of western Maryland (Conel, Ref. 119, Figs. 10a and 14). In region I, 114 compression axes are grouped about the a reference axis, and the 117 extension axes form a wide bc girdle with a tendency to be grouped about the c reference axis. In region II, 105 compression axes tend to be grouped about the c reference axis, while the 112 extension axes are diffusely oriented but show a tendency to lie in an ab girdle. Dynamic interpretation of these patterns is idealized at the right.

Hansen and Borg<sup>(120)</sup> studied deformed calcite cement in three specimens of folded Oriskany sandstone from eastern Pennsylvania. They found that the derived compression axes are oriented parallel to bedding and normal to the fold axis, while the extension axes are concentrated normal to bedding. This study will be discussed in more detail later in connection with quartz deformation lamellae.

Nissen<sup>(121)</sup> recently described a naturally deformed crinoidal limestone in which many of the individual calcite (crinoid) crystals exhibit two equally well developed sets of e twin lamellae. Nissen modified the Turner technique to locate the compression and extension axes that would produce equal  $S_0$  values on each of the two sets of twin planes. Thus, his compression axis is parallel to the crystallographic a axis cozoal with  $e_1$  and  $e_2$ , and his extension axis is normal to the undeveloped or poorly developed third set of twin planes ( $e_3$ ) in

each grain. In Nissen's specimens these gave essentially the same stress pattern as that derived through use of the Turner technique.

Gliding mechanisms in dolomite have been determined from studies of experimentally deformed dolomite single crystals and rocks.\* Only two gliding systems are known (Fig. 31):

(1) Translation gliding on  $c\{0001\}$  parallel to an  $a$  axis in either sense is the dominant flow mechanism below  $400^\circ\text{C}$ .

(2) Twin gliding on  $f\{02\bar{2}1\}$  in a negative sense along a line of the type  $[f_2:a_3]$  begins to occur at  $400^\circ\text{C}$  and is the major flow mechanism at  $500^\circ\text{C}$ .<sup>(55)</sup>

The writer is aware of only two studies in which dolomite twin lamellae have been dynamically interpreted by the Turner technique. This is in part due to the fact that twin gliding in dolomite is

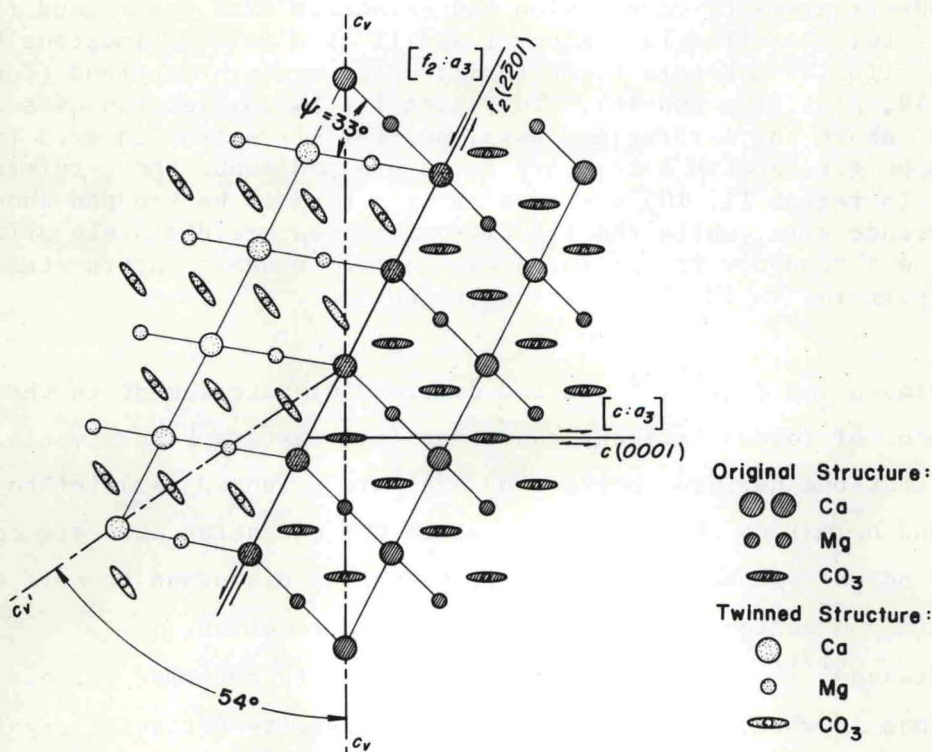


Fig. 31—Diagrammatic representation of the dolomite structure. Plane of the section is parallel to  $a_3(11\bar{2}0)$ . Gliding direction for translation on  $\{0001\}$  is not in the plane of the section, but is parallel to any of the three  $a$  axes. The system for twin gliding parallel to  $f$  is also illustrated.

\* See Refs. 52, 55, 122, and 123.

restricted to deformation at high temperatures, which is relatively rare in all but intensely deformed metamorphic rocks. Crampton<sup>(124)</sup> studied Cambro-Ordovician dolomite and calcite marbles from the north-west Highlands of Scotland. He determined compression and extension axes from f twin lamellae in dolomite as well as from e twin lamellae in calcite. Both gave similar results--compression axes oriented at high angles to the foliation. Christie<sup>(125)</sup> studied deformed dolomite from the Moine thrust zone. He concluded that the compression and extension axes inferred from twinned f lamellae reflect the final stage of deformation. He found the derived compression axes to be oriented at high angles to the foliation in the Moine thrust block.

In general, there are certain inherent limitations in the use of twin lamellae to derive principal stress directions. (1) Derived compression and extension axes are fixed by the crystallographic orientation of the grains in the rock. Accordingly, only when the grains are nearly randomly oriented can one equate the derived stress axes to the principal stresses  $\sigma_1$  and  $\sigma_3$ .<sup>(117)</sup> (2) Some of the spread in the fabric diagrams of derived compression and extension axes results from the assumption that  $S_o$  is always 0.5. In reality twinning can occur when the load axes are inclined at angles far from 45 degrees to the gliding plane and direction, provided  $\tau_c$  is exceeded in the proper sense. The scatter in these patterns can be reduced by constructing partial diagrams containing compression and extension axes from only the best developed  $e_1$  lamellae.<sup>(112)</sup> (3) Designation of host and twinned lattices (characterized by  $c_v$  and  $c'_v$ , respectively) is difficult in intensely deformed grains. By necessity the host is defined as the dominant lattice of the crystal. As twinning on  $e_1$  progresses, however, the host lattice gives way to the twinned lattice as the predominant structure. In grains which are in reality more than half twinned, an observer must select the now dominant lattice as the host.\* Compression and extension axes located with respect to  $e_1$  and this new "host" ( $c'_v$ ) will depart 90 degrees from the true axes associated with the twinning (Fig. 32). (4) Use of false  $e_1$  lamellae to

---

\* Crystals more than half twinned are usually elongated by the shear strain of twinning. The dominant lattice of nearly equidimensional grains, therefore, is very probably the "true" host.

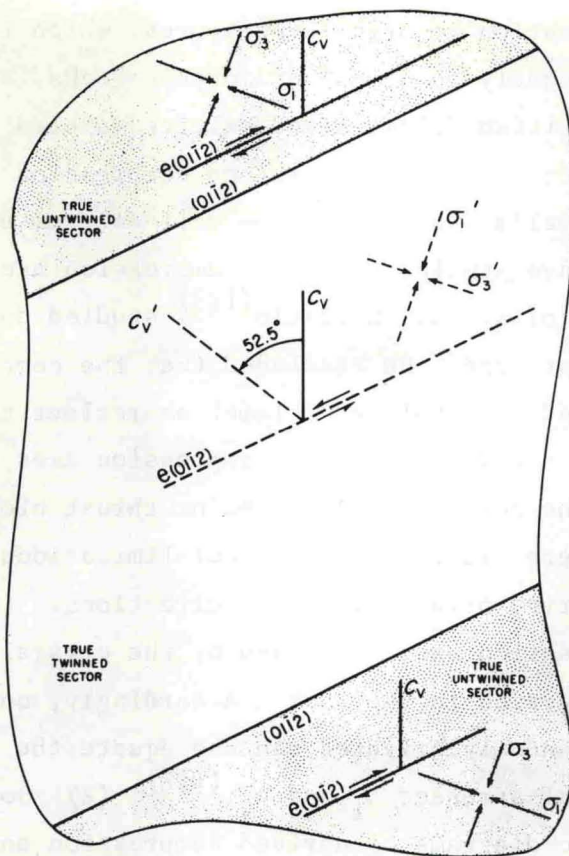


Fig. 32—Diagrammatic section through a calcite grain which is more than half twinned by gliding on  $e(01\bar{1}2)$ . Plane of the section is normal to the twin plane and contains the gliding direction.  $(01\bar{1}2)$  is common to both the twinned and untwinned structures, which are designated by  $c'_v$  and  $c_v$ , respectively. Orientations of  $\sigma_1$  and  $\sigma_3$  that would best cause the twin gliding are shown at the top and bottom of the grain with respect to the true host structure. An observer, however, would mistake the dominant portion of the grain (the real twinned portion) to be the "untwinned host." That is, he would measure  $c'_v$  and the observed twin lamellae  $(01\bar{1}2)$ , and from these measurements would position  $\sigma'_1$  and  $\sigma'_3$  as indicated in the center of the grain. These orientations for the principal stresses are 90 degrees out of phase with those actually best oriented to produce the twinning.

position compression and extension axes results in misleading interpretations. For example, as twinning nears completion on  $e_1$ , the "true"  $e_2$  lamellae may appear to be the best developed set in the grain and incorrectly designated  $e_1$ ;  $e_2$  or  $e_3$  sets may appear to be the best developed in a grain because the true  $e_1$  lamellae are inclined at too low an angle to the plane of the thin section to be correctly evaluated;

or in highly twinned grains one can easily mistake well developed  $e_2$  lamellae for  $e_1$  lamellae. The angle between compression axes derived from  $e_1$  and  $e_2$  lamellae, respectively, is 70 degrees, while that for the extension axes is 32 degrees. Clearly, Turner's technique can be expected to give the most meaningful results when applied to slightly and moderately deformed rocks (strain less than about 20 per cent), for in such rocks, the effects of limitations 1, 3, and 4 are usually negligible.

### Rotation Phenomena

Intragranular Rotations. Gliding in a constrained crystal is accompanied by an external rotation of the gliding planes toward the axis of extension and away from the axis of compression. Turner<sup>(95)</sup> recognized that this would cause an internal rotation of any intersecting pre-existing plane to an irrational position within the lattice.\* He was then able to develop an important new technique to identify gliding systems and to compute shear strain (e.g., for calcite, Ref. 95; for dolomite, see Ref. 55) and to utilize translation gliding systems for dynamic analysis.<sup>(125)</sup>

Consider, for example, a lamella P in existence prior to deformation (Fig. 33). This will be rotated to a new position by gliding on the set of parallel planes T. In an unconstrained crystal, the lamella P has been rotated internally to the position L in the deformed sector. In a constrained crystal the gliding plane T and the lamella P in the deformed sector have both been rotated externally relative to the load axis to  $T'$  and  $P'$ , and  $P'$  has also been internally rotated to L. Internal rotation is always opposite in sense to that of external rotation.

The concept of intragranular rotation is applicable to any crystal that can be examined in thin section with the petrographic microscope

---

\* External rotation is defined as rotation of crystallographic elements relative to external coordinates (e.g., rotation of the optic axis relative to the load axis). Internal rotation is defined as rotation of visible elements relative to internal coordinates (e.g., rotation of twin lamellae relative to the  $c_v$  of the crystal in the immediate vicinity of the lamellae).

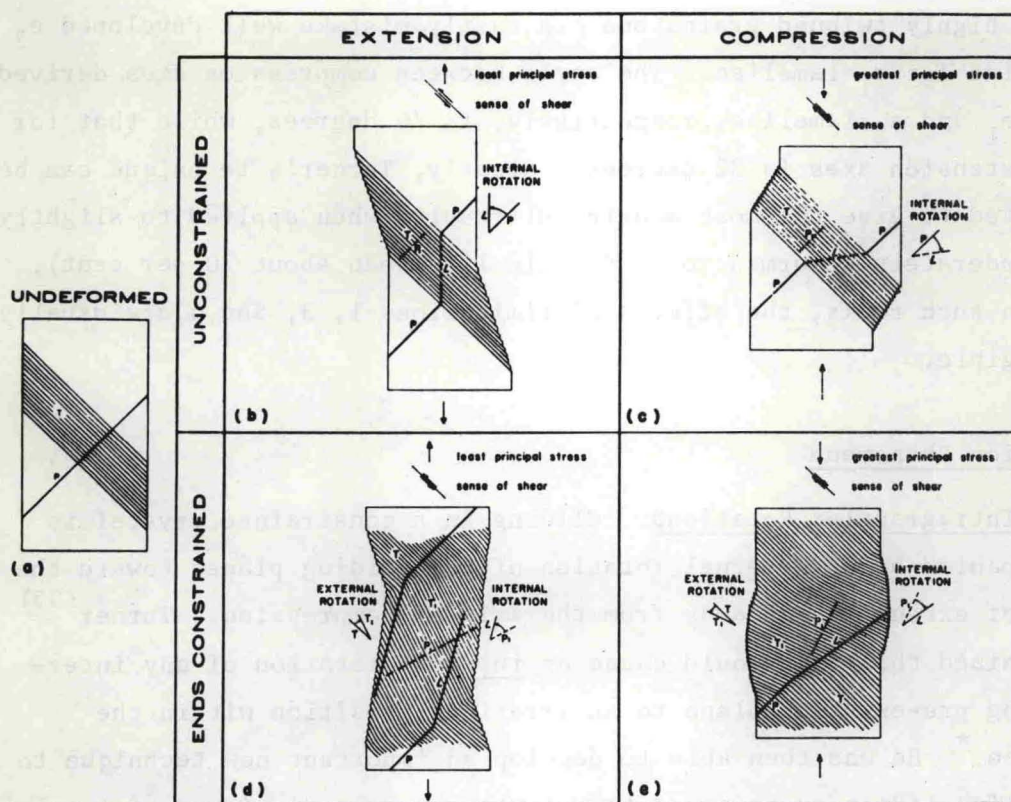


Fig. 33—Schematic illustration of internal and external rotations (from Higgs and Handin, Ref. 55, Fig. 1).

and universal stage. Visible rotations (Fig. 34) can be utilized even though the mechanism by which a pre-existing lamella is rotated through a crystal structure is not yet understood. Of importance here is that internal rotation of a visible feature is evidence that translation gliding has occurred even though there may be no visible trace parallel to the translation gliding plane itself. Once the translation gliding system is established, the directions of compression and extension that would best cause the gliding can then be determined in a manner similar to that employed for twin gliding. Christie<sup>(125)</sup> has utilized this approach and found good agreement between the principal stresses derived from internal rotation phenomena and those derived from f twin lamellae in dolomite.

Intragranular rotation phenomena in an experimentally deformed dolomite single crystal<sup>(55)</sup> serve to illustrate how a translation gliding system can be recognized and how the stresses that would most favorably produce the translation can be derived. A specimen was

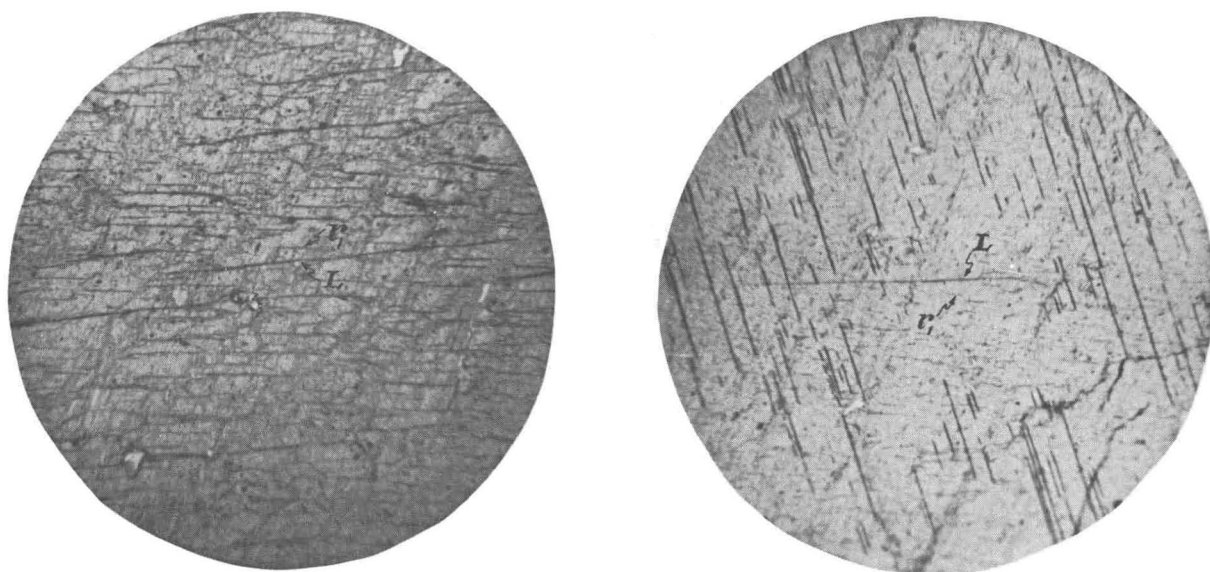


Fig. 34—Photomicrographs illustrating features characteristic of internal rotation in an experimentally deformed dolomite single crystal. The internally rotated lamellae (L) are typically coarse and dark, and occasionally serrated. The rational lamellae (r) are straight, narrow, and sharply defined lines. X 175.

extended 12 per cent under 5-kb confining pressure, 24°C, at a constant strain rate of 1 per cent per minute. The specimen was extended normal to  $r_1$  (cleavage plane), an orientation favorable for basal ( $c\{0001\}$ ) translation. In thin section, the specimen is characterized by a central deformed sector bounded on either side by relatively undeformed sectors. The orientations of the  $c_v$  and cleavage are measured in the undeformed areas ( $c_v$  and  $r_1$ ) and in the deformed sector ( $c'_v$  and  $r'_1$ ). These are plotted in lower hemisphere equal-area projection (Fig. 35). It is apparent from their positions that there has been a clockwise external rotation of 12 degrees between the undeformed and deformed sectors. Detailed examination of the deformed sector reveals a coarse dark set of planar features ( $L_{r'_1}^{c'_v}$ ) that make a small angle with  $r'_1$ . The normals to  $r'_1$  and  $L_{r'_1}^{c'_v}$  lie on the same great circle as  $c'_v$ , which indicates that  $c'\{0001\}$  is the active gliding plane.\* Moreover, the

\*The active gliding plane and a rotated plane in all positions of rotation must be cozoal, i.e., share a common axis of intersection or rotation. Hence, the normals to these planes must lie on the same great circle.

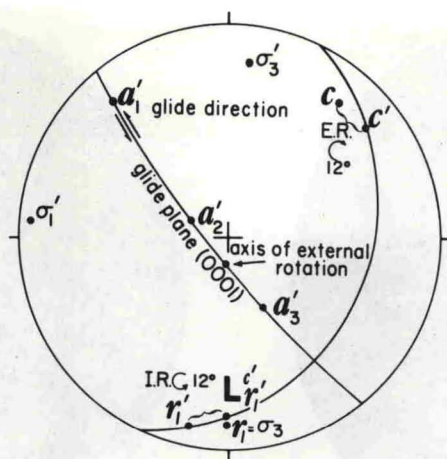


Fig. 35—Stereogram showing the internal and external rotation phenomena in experimentally deformed dolomite single crystal specimen No. 161 (from Higgs and Handin, Ref. 55). The specimen was extended 7.5 per cent under 5-kb confining pressure at 24°C. The least principal stress of the experiment ( $\sigma_3$ ) was oriented normal to  $r_1$  as indicated. External rotation of  $c$  to  $c'$  and  $r_1$  to  $r_1'$  and the internal rotation of  $r_1'$  to  $L_{r_1}^{c'}/r_1'$  are shown.  $\sigma_1$  and  $\sigma_3$  are the stresses derived from translation gliding on  $c'$  along the  $a_1'$  gliding direction in the sense indicated. The angle between  $\sigma_3$  and  $\sigma_3'$  is 31 degrees.

angle between  $r_1'$  and  $L_{r_1}^{c'}$  indicates that a counterclockwise internal rotation of 12 degrees has occurred. Although  $c'$  is established as the active gliding plane, dynamic inferences still require identification of the direction and sense of shear. Basal translation can occur along any one of the three crystallographic  $a$  axes in either sense. As a first step, draw the great circle representing  $c'$ , i.e., the great circle normal to  $c'_v$  (Fig. 35). Because the rational position of  $r_1'$  is known, we can locate  $a_1'$ ,  $a_2'$ , and  $a_3'$  along the active gliding plane. One of these must be the gliding direction. This direction can be established from the axis of external rotation which must lie in the gliding plane and perpendicular to the gliding direction. Accordingly, the normal to the great circle through  $c_v$  and  $c'_v$  and to that through  $r_1$  and  $r_1'$  defines the axis of external rotation. Since this lies on the active gliding plane midway between  $a_2'$  and  $a_3'$ ,  $a_1'$  at 90 degrees to the axis of external rotation must be the gliding direction. Finally, the sense of shear is fixed by the sense of internal rotation. To bring  $r_1'$  to  $L_{r_1}^{c'}$  requires a left-lateral sense of shear along  $c'$  (Fig. 35).

The complete gliding system is now established, the gliding plane is  $c'$ , the gliding direction is parallel to  $a_1'$ , and the sense of shear is consistent with the known principal stress directions. The compression and extension axes that would best cause this gliding ( $S_0 = 0.5$ ) are in good agreement with the known stresses across the boundaries of the specimen during the experiment (Fig. 35).

Kink Bands. Kink bands are deformation features in crystals (Fig. 36) and in aggregates with pronounced planar anisotropy (Fig. 37). They were first recognized by Orowan<sup>(126)</sup> in compressed cadmium crystals, and have since become well known in metallurgy.\* Current understanding

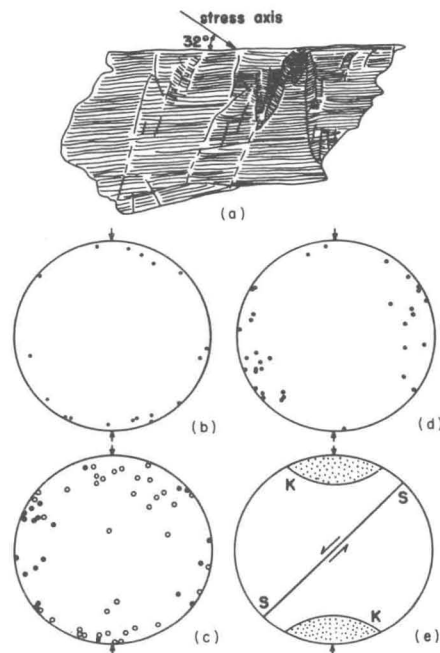


Fig. 36—Kink band development in biotite grains in experimentally deformed Westerly granite (from Griggs, Turner, and Heard, Ref. 43, Fig. 11). (a) Sketch of kink bands in a single grain of deformed biotite. Arrow shows orientation of compression axis. (b) Normals to kink band boundaries in 11 biotite grains. Arrows show axis of compression. (c) Normals to (001) in biotite grains with kink bands (solid circles) and lacking kink bands (open circles). Arrows show axis of compression. (d) Distribution of normals to (001) in 42 biotite grains with kink bands, as measured in 5 thin sections. Arrows show the axis of compression, which is also the common axis of reference for the 5 sections. (e) Relation of macroscopic surfaces of shear (SS), maximum concentration of normals to kink band boundaries in biotite (K), and sense of shear (arrows).

\* See Refs. 93, 94, and 127-129.

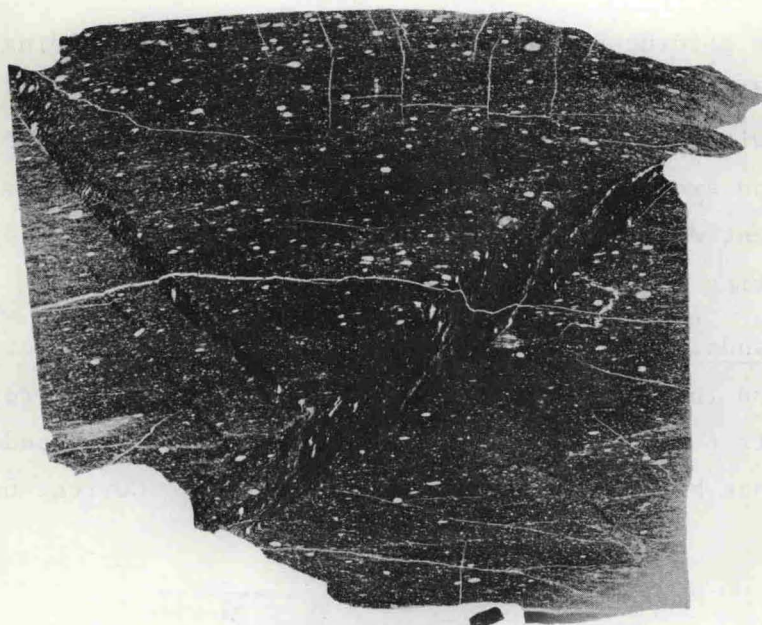


Fig. 37—Photomicrograph of kink bands in an experimentally deformed specimen of slate (from Handin and Borg, Ref. 53). Specimen was shortened 27 per cent under 5-kb confining pressure at 500°C. Slate cleavage (east-west) was initially oriented parallel to  $\sigma_1$ .

of their formation suggests that some kink bands may be dynamically significant petrofabric elements.

Kink bands characteristically form as a result of gliding flow along a set of closely spaced parallel planes. The boundaries of the bands are nearly planar features formed by an abrupt change in attitude of the active gliding plane. Flow is concentrated within the band where the structure is externally rotated with respect to the host about an axis in the gliding plane and normal to the gliding direction.<sup>(94)</sup> Kink band formation in a single crystal differs from that in an aggregate in that the gliding direction is fixed in the active gliding plane of the crystal but is apparently unrestricted in the s-plane of the aggregate.

Kink banding can result from pure translation gliding in a constrained crystal (e.g., for calcite, see Ref. 95, Plate 3, and Figs. 33(d) and 33(e) of this paper). However, kink bands are best developed in those crystals or aggregates whose active gliding plane is oriented subparallel to the axis of compression (Ref. 126, p. 644; Ref. 127, p. 192)--i.e., initially parallel to the plane of vanishing shear stress.

Bend gliding (Fig. 20) is presumably initiated after some elastic distortion, and the kink band is formed as the material buckles. According to Barrett (Ref. 94, p. 375), the kink band boundaries are initially planes that are normal to the gliding direction and the gliding plane. It follows, therefore, that well-developed kink band boundaries are initially oriented at high angles to the greatest principal stress.

Kink bands developed in biotite crystals of experimentally deformed Westerly granite<sup>(43)</sup> demonstrate their potential usefulness as a dynamic petrofabric element. Cylinders of the granite were compressed 15 to 23 per cent under 5-kb confining pressure at 500°C. Most of the shortening was achieved by faulting, localized along a zone of mylonitization. Biotite crystals near the shear zone were deformed by kink banding. The individual kink bands are described as being narrow and sharply bounded by nearly planar surfaces trending at high angles to the basal cleavage (001). They are conspicuous because the cleavage is sharply deflected through angles of 20 to 50 degrees. Opposite boundaries of a kink band typically are nonparallel, so that the band is wedge- or lens-shaped. In some grains several subparallel kink bands are present. In others there are two sets, symmetrically inclined to (001) of the host grain, giving a chevronlike pattern (Fig. 36(a)). Normals to the kink band boundaries tend to group around the known compression axis,  $\sigma_1$  (Fig. 36(b)). Moreover, kink bands tend to develop preferentially in grains whose [001] axes (normals to (001)) are steeply inclined to  $\sigma_1$  (Figs. 36(c) and 36(d)). That is, the (001) cleavages (the active gliding plane) are subparallel to  $\sigma_1$ . Subsequent work by Handin and Borg<sup>(53)</sup> on Fordham gneiss has substantiated these findings.

Accordingly, if biotite crystals in a naturally deformed rock are nearly randomly oriented, it is reasonable to conclude that the center of concentration of normals to kink band boundaries can be equated to  $\sigma_1$  in the rock at the time of deformation. On the other hand, as biotite in most rocks exhibits a nonrandom orientation, this technique can position the greatest compression axis only somewhere within the s-plane defined by the basal cleavages.

### Quartz Deformation Lamellae

General. Quartz deformation lamellae are here treated independently of any one mode of origin because the process by which they are formed in naturally deformed rocks is still somewhat in doubt. Sufficient information is available, however, to utilize these features in dynamic analyses. They occur in deformed quartz in a variety of rock types. Usually grains with deformation lamellae also show undulatory extinction. Their physical appearance is variable (Fig. 38 and Fig. 42 on p. 521). Most workers agree, however, that their tendency to lie at low angles to the {0001} plane in the quartz host is diagnostic (Fig. 39).

Origin. The origin of quartz deformation lamellae has been the subject of much speculation since they were first reported 85 years ago. According to Griggs and Bell<sup>(42)</sup> and Ingerson and Tuttle,<sup>(130)</sup> Kalkowsky<sup>(131)</sup> first described the lamellae; Boehm<sup>(132)</sup> identified them as planes of liquid inclusions; Judd<sup>(133)</sup> thought they were secondary twin lamellae; and Becke<sup>(134)</sup> identified them as healed fractures. Mügge,<sup>(135)</sup> Sander,<sup>(1)</sup> Hietanen,<sup>(136)</sup> Fairbairn,<sup>(137,138)</sup>

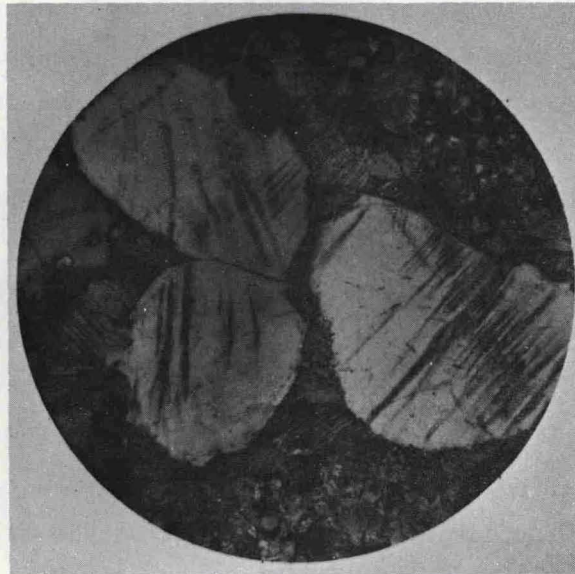
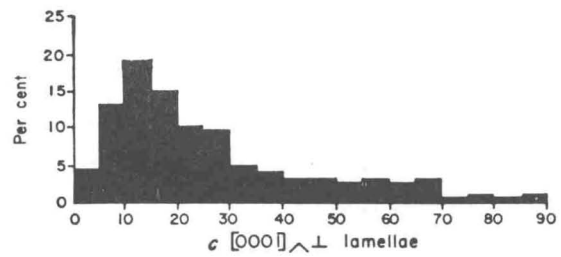


Fig. 38—Photomicrographs of quartz deformation lamellae in grains of a naturally deformed calcite-cemented sandstone from the Jurassic Piper formation, Park County, Montana. Note two sets of lamellae in one grain. Crossed Nicols, X 100.



(a) COMPOSITE DIAGRAM FOR 2471 LAMELLAE

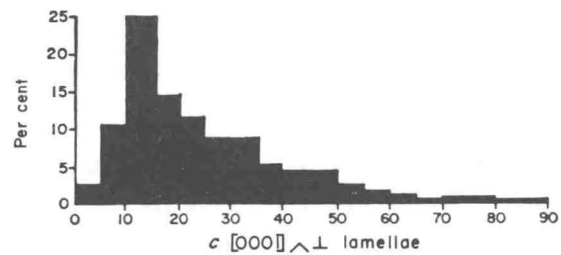
(b) COMPOSITE DIAGRAM FOR 457 LAMELLAE  
IN SIX SECTIONS  
ORISKANY SANDSTONE

Fig. 39—Histograms showing the orientation of quartz deformation lamellae with respect to the  $c_v$  in host grains (from Hansen and Borg, Ref. 120, Fig. 1). (a) Composite histogram compiled from previous literature: 775, Christie and Raleigh (1959); 885, De (1958); 102, Saha (1955); 373, Ingerson and Tuttle (1945); 336, Fairbairn (1941). Sources cited by Hansen and Borg, Ref. 120. (b) Histogram for the Oriskany sandstone studied by Hansen and Borg.

Brace,<sup>(139)</sup> and Christie and Raleigh<sup>(140)</sup> have suggested that the lamellae are a result of gliding mechanisms. Ingerson and Tuttle (Ref. 130, p. 105), on the other hand, concluded that the lamellae are not controlled by definite crystallographic planes or zones in the quartz structure and that they are "apparently controlled almost entirely by the stress pattern which determined the fabric of the quartz in the rocks." Riley,<sup>(141)</sup> Turner,<sup>(2)</sup> and Weiss<sup>(116)</sup> suggested that the lamellae are only partially controlled by the structure of quartz and that they are formed late in the deformation history. Bailey et al.<sup>(142)</sup> found that grains with deformation lamellae have Laue photograph patterns that are somewhat more disturbed than those from grains with no lamellae, but they found no evidence to establish whether or not the lamellae represent gliding planes. The controversy

seems to center mainly on whether the lamellae are caused by intracrystalline gliding or by fracture.

Attempts to produce this feature experimentally have only recently been successful. Work on quartz sand and on quartz single crystals<sup>(143-146)</sup> has produced deformation lamellae and provided a better understanding of their genesis. The sand specimens, compressed at confining pressures from 12 to 50 kb and temperatures from 25° to 700°C, contain abundant undulatory extinction, deformation bands, and deformation lamellae. Lamellae occur in over half the grains and at low angles to {0001}. Their inclination to the load axis indicates that they formed in planes of high shear stress with about as many inclined at < 45 degrees to  $\sigma$ , as at > 45 degrees to  $\sigma$ .<sup>(146)</sup> All the single crystals deformed at confining pressures of about 15 kb and at temperatures between 300° and 1500°C contain deformation lamellae. The lamellae are almost parallel to {0001} in those crystals compressed so that there was a high shear stress on {0001}. In crystals compressed along a line parallel or perpendicular to {0001}, the lamellae developed at angles from 30 to 60 degrees to {0001}, but always in planes of high resolved shear stress. Subsequent studies show conclusively that these artificial deformation lamellae result from translation gliding on {0001} with an a axis as the glide direction.<sup>(145)</sup>

Dynamic Interpretation of Quartz Deformation Lamellae. Even if natural deformation lamellae result from translation gliding, they can not be dynamically interpreted as, for example, calcite twin lamellae because the gliding direction (an a axis) cannot be located optically in quartz. Also there would be difficulties in establishing the sense of shear.\* It is possible, however, to draw dynamic inferences from their orientation pattern in naturally deformed rocks based on their experimentally determined formation in planes of high shear stress

---

\* Recently, Carter, Christie, and Griggs<sup>(146)</sup> have shown experimentally that the more deformed parts of kink bands and zones of undulatory extinction in quartz contain more abundant and closely spaced near-basal lamellae (the active slip plane) than the less deformed parts. They point out that a sense of shear can be established for the lamellae from consideration of the sense of external rotation within the kink bands or within zones of undulatory extinction.

provided that (a) for situations in which  $\sigma_1 > \sigma_2 > \sigma_3$ , one dihedral angle between two conjugate sets of lamellae is less than 90 degrees, and  $\sigma_1$  is unambiguously the acute bisector; or (b) for cases in which  $\sigma_1 > \sigma_2 = \sigma_3$  or  $\sigma_1 = \sigma_2 > \sigma_3$ , the lamellae lie along conical surfaces with half-angles of less than 45 degrees and greater than 45 degrees, respectively. In this hypothesis they are interpreted in the same manner as shear fractures or faults. Some examples of the angle between sets of quartz deformation lamellae and the attitude of the acute bisector for these sets in discrete samples are listed in the table on page 516. This compilation shows that the sets of lamellae intersect at an average acute dihedral angle of 74 degrees, and that they, therefore, probably formed in planes of high resolved shear stress. Moreover, the compilation indicates that in most cases the acute bisector, which the writer has equated to  $\sigma_1$  as a working hypothesis, is related meaningfully to geologic reference lines and planes. These relationships, however, do not by any means establish unambiguously that the acute bisector parallels  $\sigma_1$  in the rock at the time of lamellae formation. The hypothesis is strengthened, however, when other fabric elements are studied along with the deformation lamellae.

From studies of the Baraboo quartzite, Riley<sup>(141)</sup> showed that the character and orientation of lamellae could be used as a qualitative measure of the intensity of deformation. In addition he differentiated between microfractures and deformation lamellae, and found both strongly oriented and geometrically related to the major structure. It is instructive to examine Riley's Figs. 11(a) and 11(b) (see Fig. 40) which show the orientation of these features in his specimen. Two sets of deformation lamellae are defined which intersect at 60-80 degrees, and the normals to the microfractures define a single concentration. If the orientation diagrams for microfractures and lamellae are superimposed, it is apparent that the microfractures bisect the angle between the two sets of deformation lamellae. This geometrical relationship is identical with that of two sets of shear fractures and the enclosed extension fracture, i.e., two sets of lamellae are bisected by  $\sigma_1$ . In this case,  $\sigma_1$  is oriented normal to bedding and to the fold axis (Figs. 40(c) and 40(d)).\*

---

\*Dynamic inferences by Friedman.

SOME EXAMPLES OF THE ANGLE BETWEEN SETS OF QUARTZ DEFORMATION LAMELLAE AND  
THE ATTITUDE OF THE ACUTE BISECTOR BETWEEN THE LAMELLAE PLANES

Reference	Rock Type	Approximate Angle <sup>a</sup> between Best Developed Sets of Lamellae (degrees)	Orientation of Acute Bisector <sup>b</sup> ( $\sigma_1$ )
Fairbairn, Ref. 138	Ajibik quartzite	80	Normal to s-plane
Ingerson and Tuttle, Ref. 130	Ajibik quartzite	76	Normal to s-plane
	Biotite-gneiss	80	Parallel to s-plane
Riley, Ref. 141	Baraboo quartzite		
	Specimen No. 9	60	Horizontal and at high angles to regional fold axis
	Specimen No. 18	75	Nearly horizontal and sub- parallel to axial plane foliation and regional fold axis
	Specimen No. 38	65	Nearly horizontal, normal to bedding, and at high angles to regional fold axis
	Specimen No. 47	75	Nearly horizontal, subparal- lel to bedding, and sub- parallel to regional fold axis
	Specimen No. 55	85	Horizontal, subparallel to bedding, and at high angles to regional fold axis
	Specimen No. 58	65	Horizontal, at high angles to bedding and to regional fold axis
Mackie, Ref. 147	Quartz-piedmontite schist	60	Normal to fold axis and to s-plane

Preston, Ref. 148	Kinahmi and Kuopio quartzites (3 specimens)	67 76 81	High angles to s-planes
Naha, Ref. 149	Quartz-mica schist	78	Microfractures in garnet grains bisect acute angle between sets of deformation lamellae
Christie and Raleigh, Ref. 140	Quartzites (Orocopia Mts., southern California)		
	Specimen No. 1	90	.....
	Specimen No. 2	88	Subnormal to first generation fold axis and axial plane
	Specimen No. 3	76	Parallel to first generation fold axis
	Quartzite (Moine thrust zone, Scotland)	76	High angles to foliation
Hara, Ref. 150	Calcite-quartz vein (Sangun formation, western Japan)	72	Subparallel to c fabric axis and normal to $\sigma_1$ derived from calcite twin lamellae
Hara, Ref. 151	Quartz vein (Sangun formation, western Japan)	67	Subparallel to c fabric axis
Hansen and Borg, Ref. 120	Calcite-cemented sandstone		
	Specimen E2	74	Parallel to bedding, normal to fold axis, and subparallel to $\sigma_1$ derived from calcite twin lamellae
	Specimen E4	76	Subparallel to bedding, normal to fold axis, and subparallel to $\sigma_1$ derived from calcite twin lamellae

[continued on following page]

Reference	Rock Type	Approximate Angle <sup>a</sup> between Best Developed Sets of Lamellae (degrees)	Orientation of Acute Bisector <sup>b</sup> ( $\sigma_1$ )
Hansen and Borg (continued)	Specimen E6	60	Parallel to bedding, subnormal to fold axis, and parallel to $\sigma_1$ derived from calcite twin lamellae

<sup>a</sup>Determined by Friedman if not provided by the author.

<sup>b</sup>Attitude of acute bisector was determined by Friedman if not provided by the author. This bisector is equated to  $\sigma_1$  by Friedman as a working hypothesis.

The writer disregards the influence of pre-existing preferred orientations of quartz  $c_v$  on the deformation lamellae pattern. He agrees with Turner and Weiss (Ref. 13, pp. 433-434), who find that the quartz lamellae pattern, with its characteristic orthorhombic symmetry pattern, can be used to reconstruct the stress system (also commonly orthorhombic in symmetry) "because [even] in tectonites there is a wide range of orientation of  $c$  axes, and because crystallographic control of lamellae in any crystal is not rigorous, the influence of the initial orientation pattern of quartz axes upon the lamellae pattern is commonly negligible."

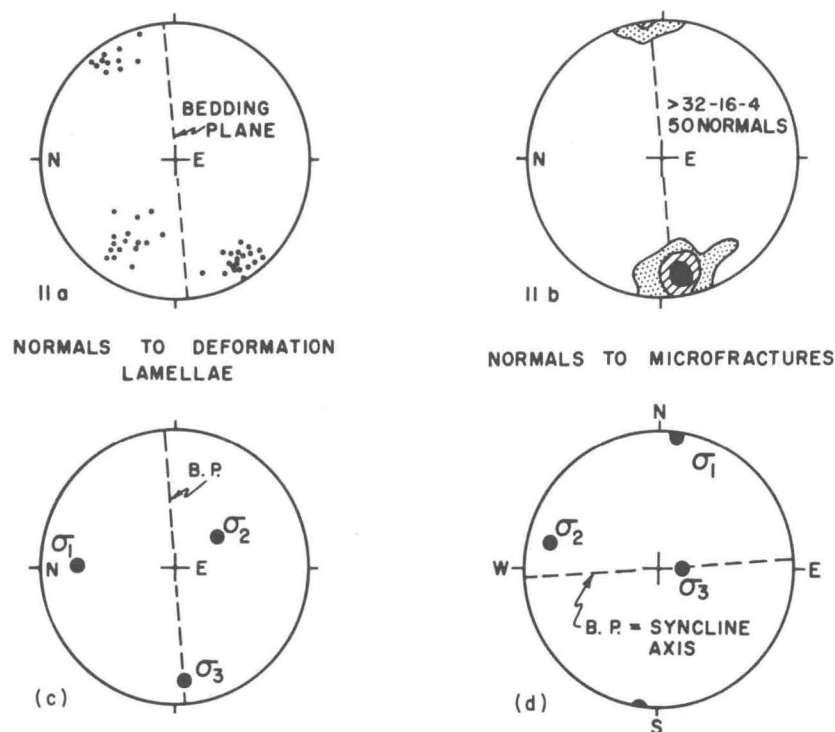


Fig. 40—Diagrams (11a and 11b) illustrating the orientation of 50 sets of quartz deformation lamellae and of microfractures, respectively, in a Baraboo quartzite specimen (from Riley, Ref. 141, Fig. 11). (c) Stereogram shows the orientation of the principal stresses deduced from the deformation lamellae and the microfractures, assuming the latter are extension fractures and the former are in planes of high shear stress and inclined at  $< 45$  degrees to  $\sigma_1$ . (d) Stereogram shows same data rotated to horizontal plane, with north as indicated.  $\sigma_1$  is nearly perpendicular to both the synclinal axis and the bedding plane.

From his studies of quartz deformation lamellae and microfractures in garnet grains of a quartz-mica schist, Naha (Ref. 149, p. 120) concluded that the normals to "deformation lamellae in quartz ... show two maxima in an incomplete girdle normal to the fold axis [i.e., the lamellae intersect in the fold axis] and are symmetrically situated with reference to late tension cracks in garnet." Thus the lamellae "have formed parallel to the two planes of maximum shearing strain...." His diagrams (see Fig. 41) show that the two sets of lamellae intersect at 78 degrees and that the set of microfractures acutely bisects this angle. This combined geometry is similar to that obtained by Riley. Here the derived  $\sigma_1$  and  $\sigma_3$  axes are oriented normal to the fold axis.

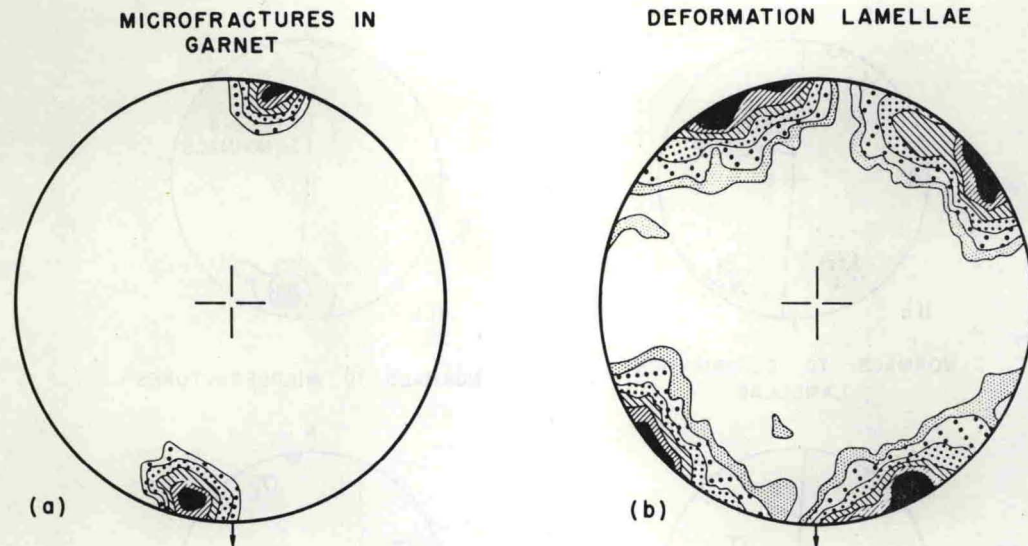


Fig. 41—Diagrams illustrating the orientation of microfractures in garnet (a) and deformation lamellae in quartz (b) (from Naha, Ref. 149, Fig. 2). Plane of each diagram is parallel to the  $ac$  plane of a fold, i.e., the fold axis is at the center. (a) Normals to 54 microfractures in 14 garnet grains. Contours are at 5, 10, 20, 30, 40, and 45 per cent per 1 per cent area, 52 per cent maximum. (b) Normals to 158 deformation lamellae in quartz. Contours are at 0.66, 1.3, 3.5, 7, 9, and 11 per cent per 1 per cent area, 13.7 per cent maximum.

Additional confirmation of these interpretations is afforded by Hansen and Borg<sup>(120)</sup> who studied both quartz deformation lamellae (Fig. 42) and calcite twin lamellae in three oriented samples of Devonian Oriskany calcite-cemented sandstone from an Appalachian fold in eastern Pennsylvania. Compression and extension axes derived from the deformed calcite cement are shown in Figs. 43(a), 43(b), 44(a), 44(b), 45(a), and 45(b). In each case the derived  $\sigma_1$  is within 10 degrees of the bedding and is normal to the fold axis, and  $\sigma_3$  is normal to the bedding,\* so that  $\sigma_2$  is subparallel to the bedding and to the fold axis. The orientation patterns of normals to the quartz deformation lamellae (Figs. 43(c), 44(c), and 45(c)) correspondingly show two distinct concentrations connected by an incomplete small circle girdle of 52 to 60 degrees half-angle, i.e., the lamellae lie along the surfaces of cones with half-angles of 30 to 38 degrees.

\*The girdle of extension axes in specimen E2 is an exception. It indicates that  $\sigma_2 \cong \sigma_3$  in magnitude for this specimen.

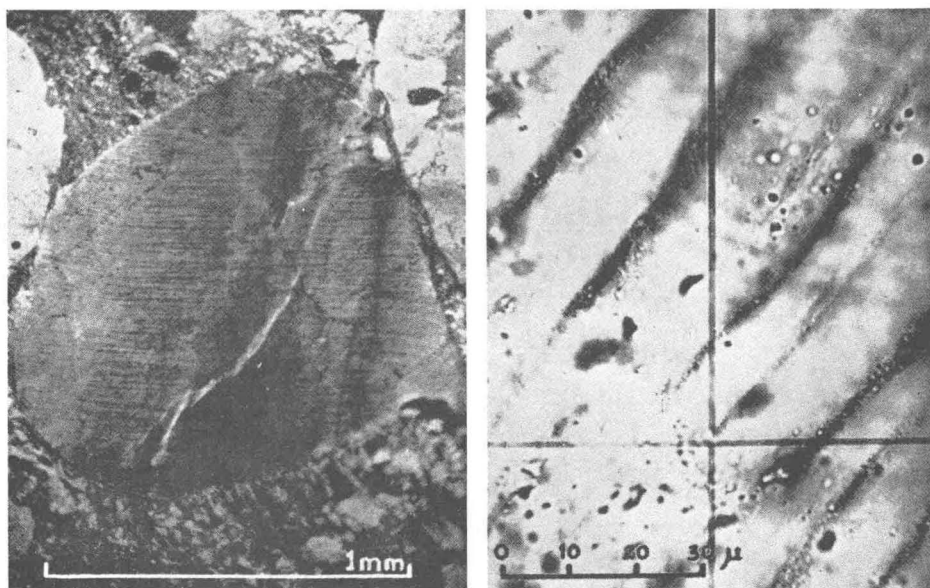


Fig. 42—Photomicrographs of quartz deformation lamellae in grains of Oriskany sandstone (from Hansen and Borg, Ref. 120, Plate 1). On the left is a grain with well-developed lamellae subnormal to zones of undulatory extinction. Crossed Nicols. On the right are lamellae at high magnification inclined at 75 to 80 degrees to the plane of the paper. Crossed Nicols.

Those corresponding to the major concentrations intersect at 60 to 76 degrees in lines parallel to the fold axis. The small circle girdle is best developed in specimen E2, in which the calcite extension axes also fall in a girdle. The acute bisector between the two major sets of deformation lamellae is within 10 degrees of the position of the corresponding derived  $\sigma_1$  from the twinned calcite; the obtuse bisector also agrees with  $\sigma_3$  from the calcite. This supports the conclusions that the deformation lamellae form in planes of high shear stress at less than 45 degrees to  $\sigma_1$  and so are the significant dynamic criteria.

A different view of the dynamic interpretation of quartz deformation lamellae is presented by Christie and Raleigh.<sup>(140)</sup> They

showed that the poles of lamellae in four quartzite specimens are distributed along small circles containing maxima. Three of these rocks are from a metamorphic terrain with a complex tectonic history, in which two major deformations are recognizable [Christie, personal communication]. The axes of the small-circles ( $A_1$  in Fig. 46) are almost parallel in the three specimens and are interpreted as the axes of maximum principal (compressive) stress in the deformation

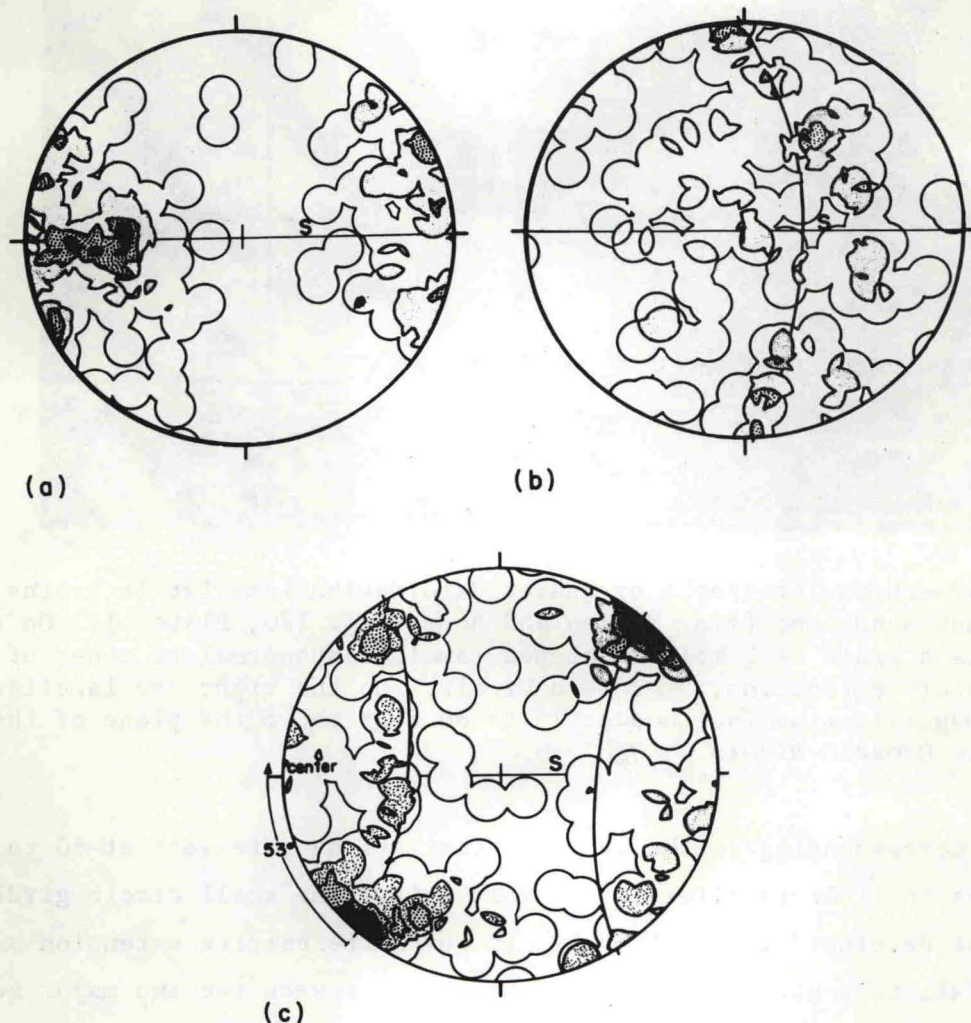


Fig. 43—Diagrams showing orientations of compression and extension axes (a and b) derived from calcite-cement twin lamellae and of quartz deformation lamellae (c) in Oriskany sandstone specimen E2 (from Hansen and Borg, Ref. 120, Figs. 4 and 5). The plane of each diagram is parallel to the *ac* plane of the fold with the fold axis near the center; *s* is the bedding plane. (a) 118 compression axes derived from well-developed sets of *e* twin lamellae in 200 grains. Contours are at 0.9, 2.6, 4.3, and 6.0 per cent per 1 per cent area, 6.8 per cent maximum. (b) 118 extension axes. Contours are at 0.9, 2.6, 4.3, and 6.0 per cent per 1 per cent area. Great circle indicates the trend of the plane containing the extension axes. (c) Normals to 147 deformation lamellae in 400 grains. Contours are at 0.7, 2.1, 3.5, 4.9, and 6.3 per cent per 1 per cent area, 8.4 per cent maximum. The center of the small circle defined by the normals to the lamellae is marked by a dot.

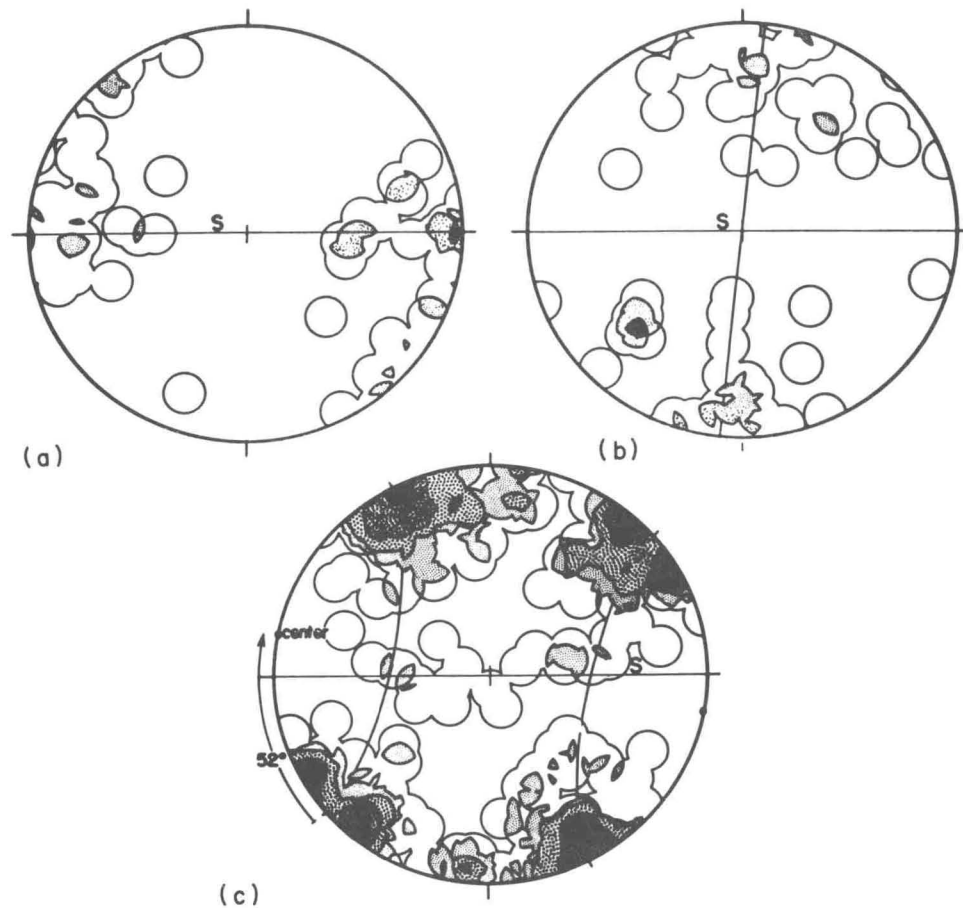


Fig. 44—Diagrams showing orientations of compression and extension axes (a and b) derived from calcite-cement twin lamellae and of quartz deformation lamellae (c) in Oriskany sandstone specimen E4 (from Hansen and Borg, Ref. 120, Figs. 6 and 7). Diagrams are oriented similar to those in Fig. 43. (a) 49 compression axes derived from the well-developed sets of e twin lamellae in 100 grains. Contours are at 2, 6, and 10 per cent per 1 per cent area. (b) 49 extension axes. Contours are at 2, 6, and 10 per cent per 1 per cent area. The great circle defines the plane normal to the major concentration of compression axes. (c) Normals to 220 deformation lamellae in 412 grains. Contours are at 0.5, 1.4, 2.3, 3.6, and 5.0 per cent per 1 per cent area, 7.3 per cent maximum. The center of the small circle defined by the normals to the lamellae is marked by a dot.

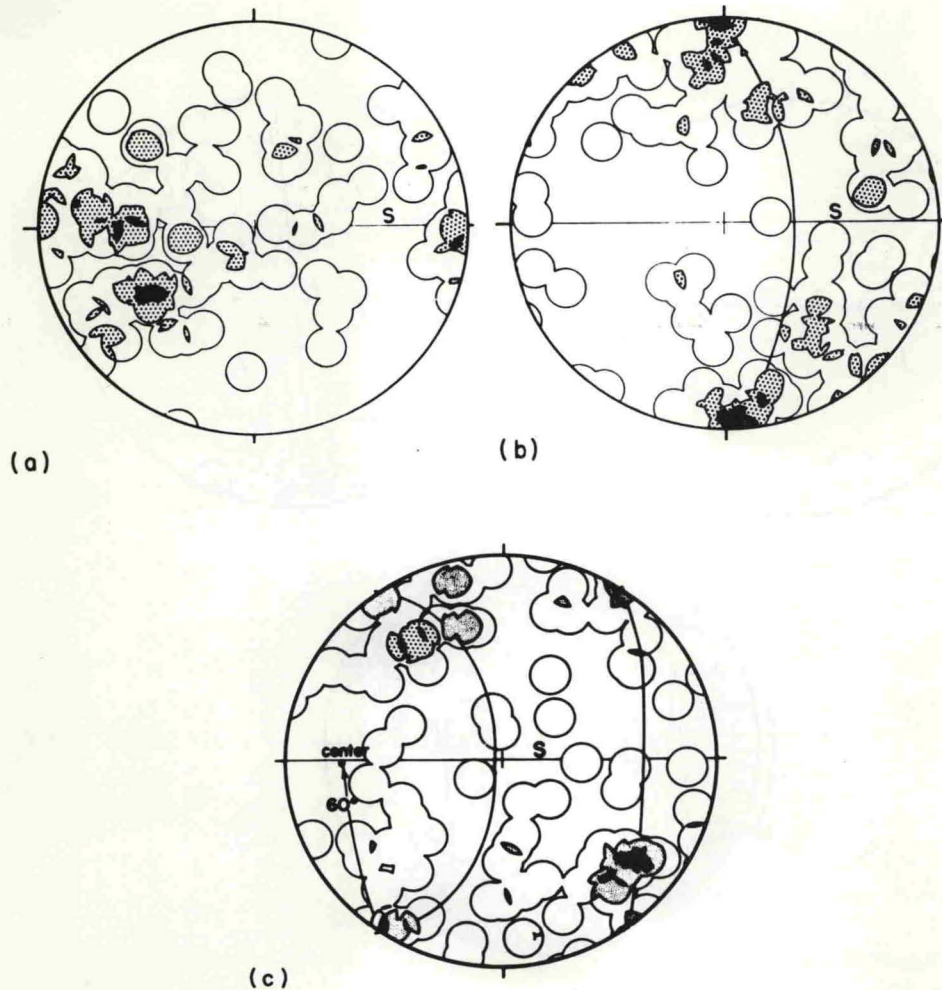


Fig. 45—Diagrams showing orientations of compression and extension axes (a and b) derived from calcite-cement twin lamellae and of quartz deformation lamellae (c) in Oriskany sandstone specimen E6 (from Hansen and Borg, Ref. 120, Figs. 8 and 9). Diagrams are oriented similar to those in Figs. 43 and 44. (a) 92 compression axes derived from the well-developed sets of e twin lamellae in 134 grains. Contours are at 1.1, 3.3, 5.5 per cent per 1 per cent area, 7.6 per cent maximum. (b) 92 extension axes. Contours are at 1.1, 3.3, and 5.5 per cent per 1 per cent area, 8.7 per cent maximum. Great circle defines the plane normal to the major concentration of compression axes. (c) Normals to 92 deformation lamellae in 210 grains. Contours are 1.1, 3.3, and 5.5 per cent per 1 per cent area, 5.9 per cent maximum. The center of the small circle is marked by a dot.

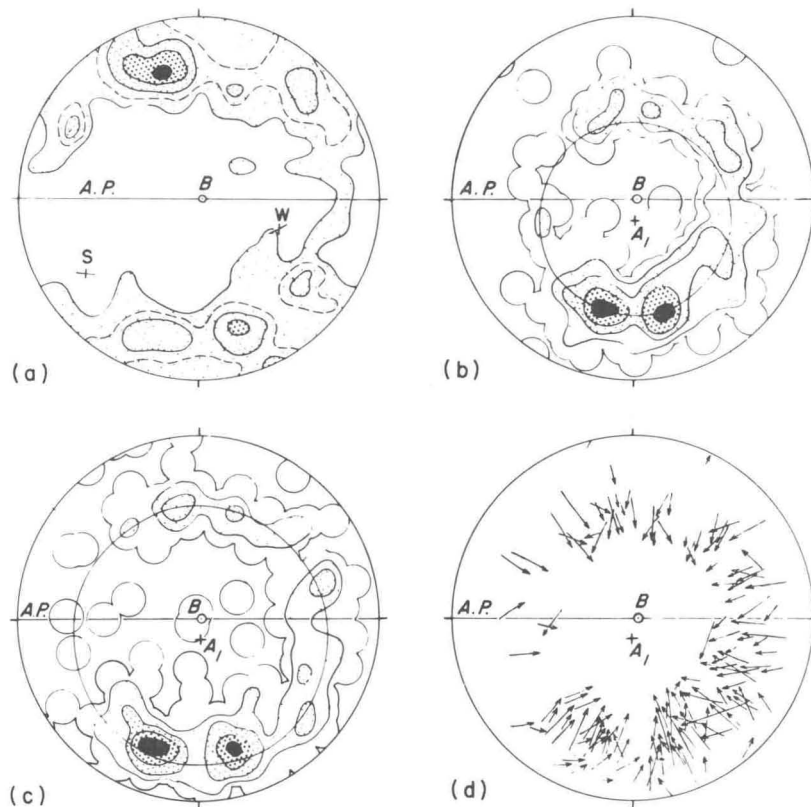


Fig. 46—Orientation diagrams for  $c_v$  and deformation lamellae in quartz of Specimen I, a quartzite from the Orocochia Mountains in southern California (from Christie and Raleigh, Ref. 140, Fig. 2). (a) 817 quartz  $c_v$ ; contours at 1, 1.5, 2, 3, and 4 per cent per 1 per cent area. (b) Normals to deformation lamellae in 195 grains (195 sets of lamellae); contours at 1, 1.5, 3, 5, and 8 per cent per 1 per cent area. (c)  $c_v$  in same 195 grains containing deformation lamellae; contours at 0.5, 1.5, 3, 5, and 7 per cent per 1 per cent area. (d) Normals to deformation lamellae (point of arrow) and  $c_v$  (end of arrow) in a representative number of grains from each section. B is the first generation fold axis and A.P. is the axial plane of the first generation fold.  $A_1$  is the axis of the small circle defined by the normals of the lamellae and  $c_v$  in grains containing lamellae. All four diagrams have the same orientation, shown by south (S) and west (W) directions in (a), and are plotted in lower hemisphere equal-area projection.

which produced the lamellae. This is consistent with the stress-field during the second deformation, as inferred from macroscopic folds and conjugate shear-surfaces. It is worth noting that in these specimens the radius of the small-circles of poles of lamellae are  $44^\circ$ ,  $45^\circ$ , and  $52^\circ$ , a fact inconsistent with the claim that the lamellae in any sample should be inclined, on the average, at less than  $45^\circ$  to  $\sigma_1$ . The rocks have moderate preferred orientations of quartz dating from the first deformation and this anisotropy appears to affect the orientation of the lamellae.

Carter, Christie, and Griggs [Ref. 146] find no support in their experimental work for the hypothesis that the lamellae are consistently inclined at less than  $45^\circ$  to  $\sigma_1$ . In sand samples deformed in a simple squeezer the lamellae are inclined at angles from  $0^\circ$  to  $85^\circ$  to the compression axis and in quartzite samples at angles from  $15^\circ$  to  $85^\circ$  to the compression axis [Ref. 146, Fig. 10]; in both types of samples most lamellae are inclined at slightly more or less than  $45^\circ$  to the compression axis. In some of their samples the poles of the lamellae lie consistently closer to the compression axis than the c-axes of the grains in which they occur [Ref. 146, Figs. 7 and 9] and it is suggested that this criterion might be used to distinguish between  $\sigma_1$  and  $\sigma_3$  in fabrics consisting of two planes of lamellae. Carter *et al.* also suggest that a study of the rotations in kink bands and undulatory zones might resolve the ambiguity, since lamellae are better developed in more deformed zones and the c-axes in such zones are rotated towards  $\sigma_1$ .\*

Clearly, a unique resolution to the dynamic interpretation of quartz deformation lamellae is not as yet established. Support for the experimental findings of Christie, Griggs, and Carter can be found in the field studies of Christie and Raleigh,<sup>(140)</sup> Riley,<sup>(141)</sup> and Hara.<sup>(151)</sup> While exceptions to their findings and support for the acute bisector equals  $\sigma_1$  hypothesis can be found in the work of Hansen and Borg (Ref. 120, Fig. 5(d)) and in Naha,<sup>(149)</sup> it is the writer's opinion that a unique solution will be forthcoming from a study of the sense of shear along the lamellae\*\* in slightly and moderately deformed

---

\* The preceding two paragraphs were written by Dr. J. M. Christie at the request of the author.

\*\* See Ref. 146, p. 10-89 n.

rocks in which the tectonic history is simple and interfering problems of recrystallization and preferred orientations of  $c_v$  are minimal.

### Recrystallization

General. Recrystallization of a given mineral species in a polycrystalline aggregate can occur below the melting temperature by solution and redeposition and/or solid diffusion. There is a large literature on the subject, especially in metallurgy, ceramic engineering, and glass technology.<sup>(94,152-158)</sup> Of concern here is the fact that the petrofabric literature abounds with descriptions of preferred crystallographic orientations of crystals, which for textural reasons can not be explained on the basis of cataclastic or gliding flow. That is, there is no visual evidence of grain breakage or intragranular gliding. Presumably these orientations have resulted from recrystallization during deformation (the paratectonic or syntectonic recrystallization of Sander<sup>(1)</sup>), i.e., under conditions of nonhydrostatic stress. Most of them have been interpreted only kinematically by means of the symmetry argument. The same crystallographic orientations, however, might be amenable to dynamic analysis if one understood the relationships between the orientations of the recrystallized grains and the principal stresses. Significant contributions to the problem have been made through thermodynamic and experimental investigations. Initial results are encouraging and suggest the potential usefulness of these approaches.<sup>(159)</sup>

Thermodynamic Approach. The thermodynamic principles of the behavior of elastically strained solids under nonhydrostatic stress in contact with fluids were laid down by Gibbs.<sup>(160)</sup> Significant departures from the Gibbs treatment were given by Goranson,<sup>(161-163)</sup> Verhoogen,<sup>(164)</sup> and MacDonald.<sup>(165)</sup> Kamb<sup>(166)</sup> has reviewed these in detail and finds that all are essentially identical with respect to prediction of the most stable crystal orientation. Kamb<sup>(167)</sup> believes that only the Gibbs theory is valid and applies it to the simplest possible model of the recrystallization process. Recently, Kamb<sup>(168)</sup> has demonstrated experimentally the validity of the Gibbs approach

and the inadequacy of all other theories so far advanced. It is instructive to compare the MacDonald and the Gibbs-Kamb approaches and the crystal orientations they predict.

MacDonald<sup>(165)</sup> assumed that the most stable orientation for a mineral would be the one for which the potential energy of the external forces plus the potential energy of strain was minimized. If the deformation is isothermal and obeys a linear elastic stress-strain law, then the most stable orientation will be the one in which the Helmholtz free energy is a maximum. This neglects any permanent strain energy, and the nature of the path from the initial to final states of the mineral, i.e., the final orientation, is supposed to be independent of the orienting mechanisms.

Brace,<sup>(169)</sup> using MacDonald's prediction, calculated the most stable orientations for calcite, high and low quartz, and ice for a uniaxial stress. His results show that the following crystallographic planes should be nearly normal to the load axis:  $\{10\bar{1}1\}$  in ice and calcite,  $\{10\bar{1}2\}$  in high quartz, and  $\{02\bar{2}1\}$  in low quartz. Their respective  $c_v$  will then tend to lie along small circles or girdles of specific half-angle about the unique stress axis (Fig. 47). Brace also examined the equilibrium orientation in a stress field of three different, nonzero, principal stresses. He found that the position of most stable orientation is a function of the confining pressure as well as the stress difference. Accordingly, different orientation patterns of grains might occur in rocks for which the stress difference was similar but the depth of burial different.

Very different results have been obtained by Kamb<sup>(167)</sup> from the Gibbs theory. He considers that the orientation of a mineral depends only on the stress deviators and is therefore independent of changes in hydrostatic pressure. When recrystallization takes place by solution and redeposition, the most stable orientation of the crystal is that which minimizes the chemical potential across the plane normal to the greatest principal pressure. Accordingly, the axis of least elastic modulus (e.g., the  $c_v$  of calcite) tends to align itself parallel to the greatest principal stress axis (axes), and the axis of greatest elastic modulus (e.g., the  $c_v$  of quartz) tends to become

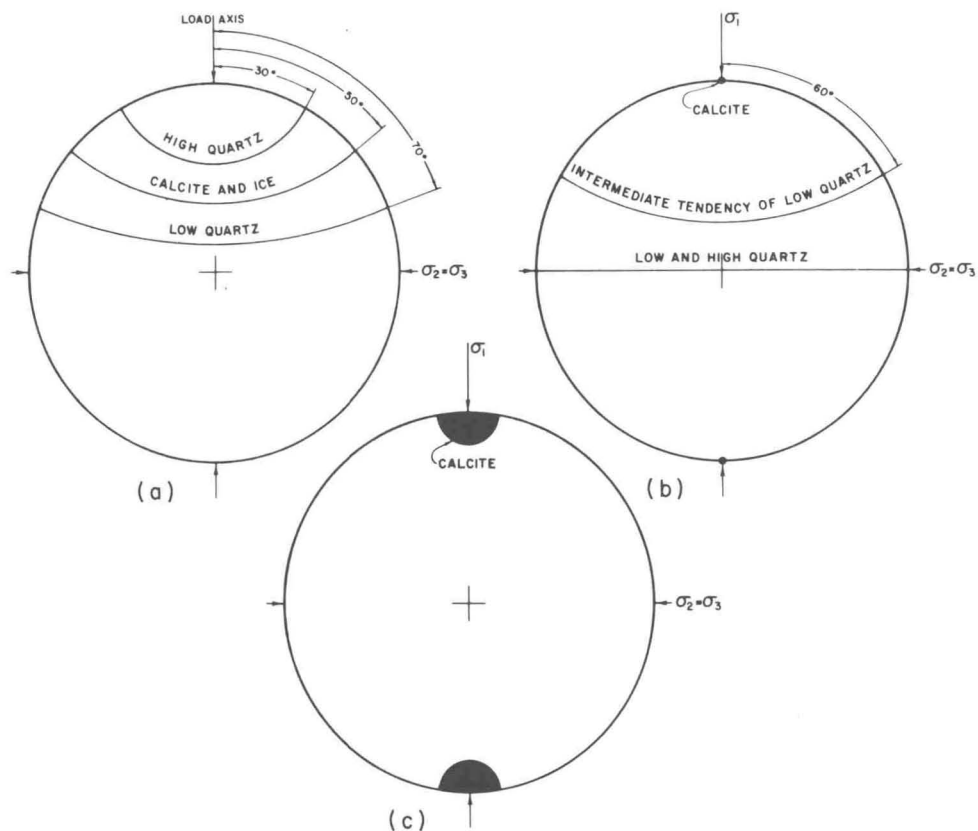


Fig. 47—Stereograms showing the predicted (a and b) and the experimentally determined (c) orientations of  $c_v$  in minerals recrystallized under a uniaxial state of stress (stereographic projection). (a) Orientations of  $c_v$  predicted by MacDonald<sup>(165)</sup> and calculated by Brace (Ref. 169, Fig. 4) for calcite, ice, high and low quartz. (b) Orientations of quartz and calcite  $c_v$  predicted by Kamb<sup>(167)</sup> for recrystallization in the presence of a fluid phase. (c) Orientation of calcite  $c_v$  produced in experiments as a result of syntectonic, dry recrystallization.

normal to  $\sigma_1$  (Fig. 47(b)). Moreover, low quartz is considered by Kamb to be unique among the common hexagonal and rhombohedral minerals in that the theory predicts "intermediate" orientation positions. For the case  $\sigma_1 > \sigma_2 = \sigma_3$ , the  $c_v$  will tend to lie along a small girdle at about 60 degrees to  $\sigma_1$ ; and for  $\sigma_1 = \sigma_2 > \sigma_3$ , the  $c_v$  will tend to develop a small girdle at about 29 degrees to  $\sigma_3$ . Kamb also extends Gibbs' theory to predict orientations under conditions of dry recrystallization. He finds that if the initial grain shapes are equant, the most stable orientation for most hexagonal or rhombohedral crystals is such that their axes of least elastic modulus tend to lie normal to

the unique stress axis (whether tensional or compressional). This orientation is directly opposite to that predicted for recrystallization by solution and redeposition. On the other hand, if the dry grains are initially much flattened normal to the load axis, the orientations would be reversed, and therefore identical wet or dry. If Kamb's view is correct, one must know the mechanism of recrystallization before applying his theory.

Although the thermodynamic approach holds great promise, the predictions of MacDonald and Kamb differ widely. Furthermore, they are based on infinitesimal strain. At present, they cannot be applied to geologic problems.

Experimental Approach. A most important experimental result has been the dry recrystallization of calcite and quartz under simulated geological conditions, since previously most geologists had seemed to regard the agency of solutions as necessary for metamorphic recrystallization.\* Syntectonic recrystallization occurs during the course of triaxial compression or extension tests, i.e., during deformation. Annealing recrystallization (familiar in metallurgy) occurs when an aggregate is first deformed at low temperature (cold-worked) and then held at an elevated temperature to accelerate the process. Presumably there is a critical temperature below which annealing recrystallization does not take place regardless of the duration of heating.<sup>(171)</sup> This temperature decreases as the initial strain is increased. Syntectonic recrystallization appears to occur not only above some critical temperature, but also below some temperature above which strain energy is annealed out faster than it can be stored.

Syntectonic recrystallization of calcite was first observed in specimens of Yule marble deformed at 300°C and at 5-kb confining pressure.<sup>(108)</sup> The evidence is intergranular flow and development of textures closely resembling those of naturally deformed marble. In specimens deformed at 400° and 500°C<sup>(110)</sup> the evidence is augmented by the development of small lobes and lensoid streaks in which new optic axes, differing from those of the host grains, tend to parallel the

---

\* See Refs. 43, 108, 110, 143, and 170.

direction of maximum principal stress in both compression and extension regardless of the orientation of the host crystals. Syntectonic recrystallization reaches a maximum at 600°C (Fig. 48) in short-time tests (strain rate about  $10^{-4}$  per second).<sup>(43)</sup> At lower strain rates the maximum seems to occur at a lower temperature, since the phenomenon is common in specimens deformed at 350° to 500°C and at  $10^{-7}$  sec<sup>-1</sup>.<sup>(170)</sup> In these, recrystallization may be the major mechanism of steady-state flow. What is important here is that the recrystallized grains are always strongly oriented with their  $c_v$  aligned parallel to the axis of maximum principal compressive stress (Fig. 47(c)), a result which agrees with the Gibbs-Kamb<sup>(168)</sup> prediction (but in the presence of solutions).

Annealing recrystallization of calcite crystals and aggregates has also been produced experimentally.<sup>(172)</sup> The critical temperature of annealing of Yule marble is about 500°C, and the annealing time (15-120 min) did not influence the recrystallization. In contrast to the syntectonic process, the annealing tends to produce a random orientation, although traces of the inherited fabric of the original material remain. An interesting exception was noted in specimens of powdered Yule marble (fragments 1 to 2  $\mu$ ) that were compressed between steel pistons at 1000°C for 30 min. After this treatment the material consists of groundmass, nearly uniform grains 10 to 20  $\mu$  in diameter, and porphyroblasts, about 0.2 mm in diameter. The  $c_v$  of the porphyroblasts tend to parallel the axis of compression, i.e., tend to lie normal to the piston faces (Fig. 49).

Crystallographic Orientations as Criteria for Dynamic Interpretations. The experimental fact that syntectonically recrystallized calcite crystals are oriented with their  $c_v$  parallel to the greatest principal compressive stress serves as a working hypothesis for the dynamic interpretation of natural calcite fabrics.

In calcite marbles  $c_v$  characteristically lie at high angles to the major foliation plane (e.g., Yule marble, Fig. 50).\*

---

\*For those marbles in which the grains are not highly elongated, one can reasonably be sure that the  $c_v$  subfabric has resulted from

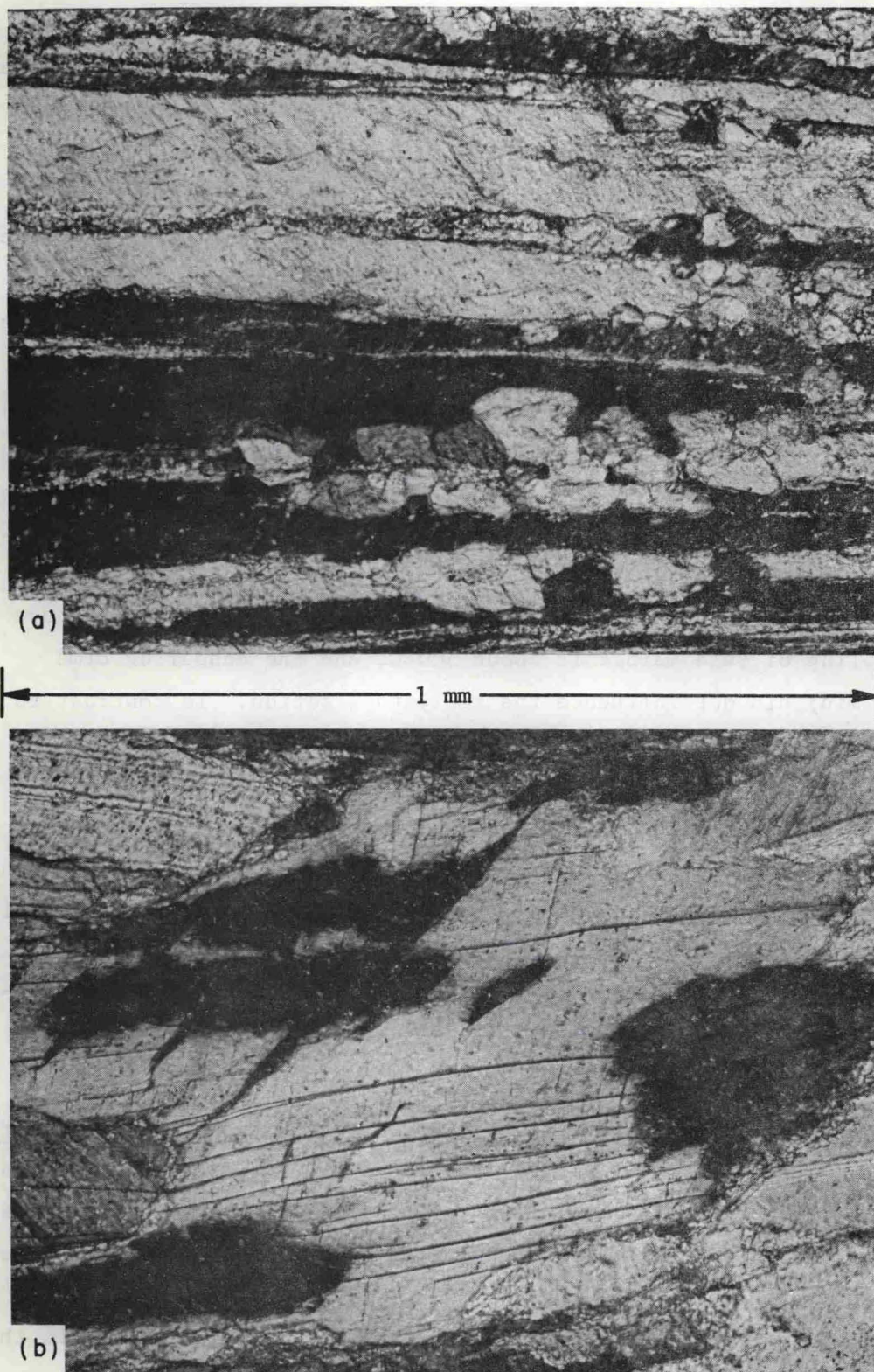


Fig. 48—Photomicrographs of Yule marble showing effects of syntectonic recrystallization (from Griggs, Turner, and Heard, Ref. 43, Plate 12). (a) New grains developed in marginal clusters in specimen locally elongated 590 per cent at 3-kb confining pressure and 600°C. Crossed Nicols. (b) New grains (dark) developed at three centers in single host crystal in specimen elongated 50 per cent at 3-kb confining pressure and 600°C. Crossed Nicols.

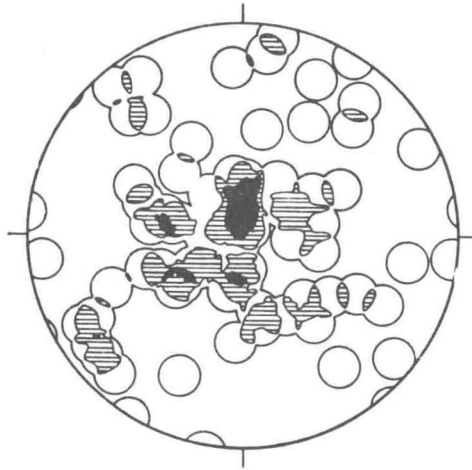


Fig. 49—Diagram illustrating orientation of calcite  $c_v$  in 72 porphyroblasts that resulted from the annealing recrystallization of powdered Yule marble. Contours are at 1.3, 2.7, and 5.5 per cent per 1 per cent area. Plane of the diagram is oriented normal to the axis of compression.

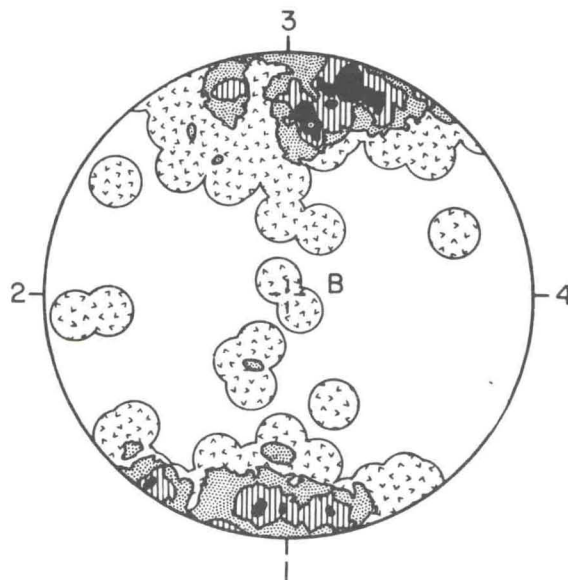


Fig. 50—Diagram showing orientation of 100 calcite  $c_v$  in Yule marble (from Handin, Higgs, and O'Brien, Ref. 175, Fig. 12). Contours are at 1, 3, 5, and 7 per cent per 1 per cent area. The foliation plane is parallel to the 2-B-4 plane.

hypothesis, the greatest principal compressive stress during the latest stages of recrystallization should be oriented nearly normal to the foliation. An interesting example is afforded by marble fabrics in five specimens from a recumbent fold in the Mojave Desert of southern California.<sup>(116)</sup> In three of these (Nos. 278, 161, and 70) the grains are nearly equant, and there is little evidence of postcrystallization strain. The other two specimens (Nos. 298 and 72) are conspicuously deformed and markedly elongated (average dimensional ratio is 1:2:7 with long and intermediate grain diameters in or near the plane of the foliation). Despite these textural differences the  $c_v$  maxima in all five specimens are similarly oriented at high angles to the foliation (Fig. 51). Weiss (Ref. 116, p. 77) concluded that "the preferred orientation of  $c_v$  in the calcite marbles dates from the main deformation, and the direction of maximum concentration in each specimen is thought to coincide with the axis of maximum compressive stress immediately before cessation of movements." This statement seems to recognize the ability of calcite grains to become reoriented by gliding flow. Although the textures of specimens Nos. 298 and 72 suggest that this

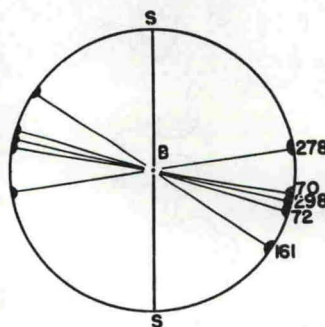


Fig. 51—Synoptic diagram showing the orientation of calcite  $c_v$  maxima in relation to the foliation (SS) in five marbles from southern California (from Weiss, Ref. 116, Fig. 27).

recrystallization rather than from mechanical reorientation of the grains by gliding flow. A nearly similar  $c_v$  subfabric can be produced by complete twinning and external rotation of grains. This, however, produces markedly elongated grains, remanent internally rotated lamellae, and a tendency for the  $c_v$  to lie along small circles rather than in a distinct maximum (Ref. 43, p. 91).

might be so, the equant grains in the other three specimens suggest that the orienting mechanism is the recrystallization. Weiss may have been dealing with a situation in which the effects of recrystallization and of gliding flow have both produced essentially the same  $c_v$  subfabric.

One could cite examples in which recrystallized grains have their  $c_v$  distributed in nearly complete girdles, which are related to  $\sigma_1 > \sigma_2 = \sigma_3$  or  $\sigma_1 = \sigma_2 > \sigma_3$  states of stress, but the technique should now be clear. It is important to point out, however, that if preferred orientations of calcite  $c_v$  arise from recrystallization under nonhydrostatic conditions, then nearly random patterns would probably imply recrystallization under essentially hydrostatic pressures. Although published accounts of random calcite  $c_v$  subfabrics are rare, random orientations are in fact common in recrystallized sedimentary rocks. (59,120,173) In undeformed rocks this might be evidence of an essentially hydrostatic state of stress due to simple overburden pressure.

#### Summary and Conclusions

Petrofabrics is the study of fabric elements that may range in size over 15 orders of magnitude from the crystal lattices to mountain ranges. It consists of a descriptive phase in which fabric elements are recognized, measured, and illustrated, and an interpretive phase in which the rock fabric serves as a basis of inference to the kinematic or dynamic aspects of the deformation. The kinematic approach, based on the symmetry argument of Sander,<sup>(1)</sup> provides no knowledge of the state of stress. The dynamic approach utilizes fabric elements to derive the orientations and relative magnitudes of the principal stresses in the rocks at the time of deformation. It is based on an understanding of the mechanisms of rock deformation gained largely through experiments.

The current physical understanding of fracturing and faulting, gliding flow, rotation, and recrystallization and of the corresponding fabric elements often enables one to determine the principal stress

directions in rocks at the time of deformation. A review of the literature shows that laboratory observations on the fabric elements are compatible with those from the field and illustrates the types of dynamic interpretations that can be made from the fabric data.

Faults, shear fractures, and extension fractures are viewed as phenomena that are independent of scale (down to the microscopic field, i.e.,  $>0.01$  mm) and that exhibit predictable orientations to the principal stresses in the rock at the time of failure. In naturally deformed rocks, fractures and faults are distinguished and identified primarily from their combined orientation pattern. Derivation of the principal stress directions follows from the genetic relationships--extension fractures are normal to the least principal stress, and faults and shear fractures are inclined at less than 45 degrees to the greatest principal compressive stress. Studies of microfractures in individual grains of folded sandstones and of fracture and fault systems in the Ouachita Mountains and Central Plains of Oklahoma and in the Great Basin of the western United States demonstrate the dynamic interpretations of these elements and emphasize that the elements are independent of scale. Consistent fracture-fault trends over large portions of the earth's crust suggest that the stress pattern is homogeneous on a regional scale.

Intracrystalline gliding involves mechanical twinning and translation parallel to a definite gliding plane along a fixed direction with or without restricted sense of shear. As gliding flow is essentially independent of normal stress, the most favorable state of stress for gliding is that which gives the maximum shear stress along the gliding line (in the proper sense). That is, the greatest and least principal stresses are each oriented at 45 degrees to both the gliding plane and direction so as to yield the known sense of shear. Accordingly, if the gliding systems are known, the principal stresses in each crystal can be derived from the gliding evidence (e.g., twin lamellae or internally rotated lamellae). From laboratory experience it is reasonable to suppose that the stress orientation pattern determined from many grains will correspond to the orientation of the principal stresses in the rock at the time of deformation. The dynamic

interpretations based on calcite and dolomite twin lamellae and on phenomena of internal rotation give the most reliable and meaningful results when studied in slightly and moderately deformed rocks.

Experimental kink banding in biotite crystals provides another criterion for dynamic inferences. In biotite the kink band boundaries are initially oriented at high angles to the greatest principal compressive stress.

In experimentally deformed quartz crystals and sands, deformation lamellae which resemble the natural counterparts lie only in planes of high resolved shear stress. This laboratory observation is valid in the field as well where the angle between the deformation lamellae and the greatest principal stress is evidently less than 45 degrees. Principal stress directions derived from the quartz deformation lamellae on this basis agree well with those located from extension fractures and calcite twin lamellae.

Experimental syntectonic recrystallization of dry calcite suggests that in the most stable orientation the  $c_v$  tend to parallel the greatest principal compressive stress. This agrees with the Gibbs-Kamb<sup>(167)</sup> thermodynamic prediction for recrystallization in the presence of solutions, but the theory is still controversial. Application of the experimental results to marbles implies that the greatest principal stress is characteristically oriented at high angles to the observed foliation during recrystallization. The random calcite  $c_v$  subfabrics common in recrystallized sedimentary rocks may be evidence that the state of stress due to simple overburden pressure is nearly hydrostatic.

It has been emphasized repeatedly that some petrofabric techniques serve to map the principal stresses in rocks at the time of their deformation. Future research will have to determine the relationship, if any, between these stresses and the present state of stress in the rocks.

#### Acknowledgments

Dr. D. V. Higgs and Dr. J. W. Handin of the Shell Development Company, through their stimulating and enthusiastic approach to rock

deformation, are largely responsible for my interest in petrofabrics. Thanks are due these gentlemen and Mr. D. W. Stearns and Dr. D. J. Atkinson, also with the Shell Development Company, for many helpful discussions and critical review of the manuscript.

## REFERENCES

1. Sander, B., Gefügekunde der Gesteine, Springer, Wien, 1930.
2. Turner, F. J., "Mineralogical and Structural Evolution of the Metamorphic Rocks," Geol. Soc. Am. Mem. 30, 1948.
3. Handin, J. W., and R. V. Hager, Jr., "Experimental Deformation of Sedimentary Rocks under Confining Pressure: Tests at Room Temperature on Dry Samples," Bull. Am. Assoc. Petrol. Geologists, Vol. 41, 1957, pp. 1-50.
4. Paterson, M. S., and L. E. Weiss, "Symmetry Concepts in the Structural Analysis of Deformed Rocks," Bull. Geol. Soc. Am., Vol. 72, 1961, pp. 841-882.
5. Turner, F. J., "Lineation, Symmetry, and Internal Movement in Monoclinic Tectonite Fabrics," Bull. Geol. Soc. Am., Vol. 68, 1957, pp. 1-17.
6. Sander, B., "Über Zusammenhänge zwischen Teilbewegung und Gefüge in Gesteinen," Mineral. Petrog. Mitt., Vol. 30, 1911, pp. 281-315.
7. Sander, B., Einführung in die Gefügekunde der geologischen Körper, 1, Springer, Wien, 1948.
8. Sander, B., Einführung in die Gefügekunde der geologischen Körper, 2, Springer, Wien, 1950.
9. Schmidt, W., "Gefügesymmetrie und Tektonik," Jahrb. Geol. Bundesanstalt, Vol. 76, Part 1, 1926, pp. 407-430.
10. Schmidt, W., Tektonik und Verformungslehre, Bornträger, Berlin, 1932.
11. Knopf, E. B., and F. E. Ingerson, "Structural Petrology," Geol. Soc. Am. Mem. 6, 1938.
12. Turner, F. J., and J. Verhoogen, Igneous and Metamorphic Petrology, McGraw-Hill Book Company, Inc., New York, 1951.

13. Turner, F. J., and L. E. Weiss, Structural Analysis of Metamorphic Tectonites, McGraw-Hill Book Company, Inc., New York, 1963.
14. Weiss, L. E., "Structural Analysis of the Basement System at Turoka, Kenya," Overseas Geological Surveys, Her Majesty's Stationery Office, London, 1959, pp. 1-65.
15. Krumbein, W. C., "Some Problems in Applying Statistics to Geology," Appl. Statist., Vol. 9, 1960, pp. 82-91.
16. Krumbein, W. C., "The 'Geological Population' as a Framework for Analyzing Numerical Data in Geology," Liverpool Manchester Geol. J., Vol. 2, 1960, pp. 341-368.
17. Chayes, F., Petrographic Modal Analysis, John Wiley & Sons, Inc., New York, 1956.
18. Fairbairn, H. W., Structural Petrology of Deformed Rocks, 2d ed., Addison-Wesley Publishing Company, Inc., Reading, Massachusetts, 1949.
19. Higgs, D. V., M. Friedman, and J. E. Gebhart, "Petrofabric Analysis by Means of the X-ray Diffractometer," in "Rock Deformation," Geol. Soc. Am. Mem. 79, 1960, pp. 275-292.
20. Gehlen, K. V., "Die röntgenographische und optische Gefügeanalyse von Erzen, insbesondere mit dem Zahlrohr-Texturgoniometer," Beitr. Mineral. Petrog., Vol. 7, 1960, pp. 340-388.
21. Kamb, W. G., "Refraction Corrections for Universal-stage Measurements, I. Uniaxial Crystals," Am. Mineralogist, Vol. 47, 1962, pp. 227-245.
22. Phillips, F. C., The Use of the Stereographic Projection in Structural Geology, Edward Arnold, Ltd., London, 1954.
23. Higgs, D. V., and G. Tunell, Angular Relations of Lines and Planes, with Application to Geological Problems, Wm. C. Brown Co., Dubuque, Iowa, 1959.
24. Lambert, J. H., "Anmerkungen und Zusätze zur Entwerfung der Land- und Himmelscharten," Ostwald's Klassiker der Exakten Wissenschaften, Nr. 54, Wilhelm Engelmann, Leipzig.
25. Schmidt, W., "Gefügestatistik," Mineral. Petrog. Mitt., Vol. 38, 1925, pp. 392-423.
26. Mellis, O., "Gefügediagramme in Stereographischer Projektion," Z. Mineral. Petrog. Mitt., Vol. 53, 1942, pp. 330-353.

27. Flinn, D., "On Tests of Significance of Preferred Orientation in Three-dimensional Fabric Diagrams," J. Geol., Vol. 66, 1958, pp. 526-539.
28. Kamb, W. B., "Ice Petrofabric Observations from Blue Glacier, Washington, in Relation to Theory and Experiment," J. Geophys. Res., Vol. 64, 1959, pp. 1891-1909.
29. Pincus, H. J., "The Analysis of Aggregates of Orientation Data in the Earth Sciences," J. Geol., Vol. 61, 1953, pp. 482-509.
30. Spencer, E. W., "Geologic Evolution of the Beartooth Mountains, Montana and Wyoming, Part 2, Fracture Patterns," Bull. Geol. Soc. Am., Vol. 70, 1959, pp. 467-508.
31. Orowan, E., "Fracture and Strength of Solids," Phys. Soc. London Report Prog. in Phys., Vol. 12, 1949, pp. 185-232.
32. Handin, J. W., "An Application of High Pressure in Geophysics: Experimental Rock Deformation," Trans. ASME, Vol. 75, 1953, pp. 315-324.
33. Griggs, D. T., and J. W. Handin, "Observations on Fracture and a Hypothesis of Earthquakes," in "Rock Deformation," Geol. Soc. Am. Mem. 79, 1960, pp. 347-364.
34. Brace, William F., "Brittle Fracture of Rocks," these Proceedings, pp. 111-174.
35. Handin, J. W., and R. V. Hager, Jr., "Experimental Deformation of Sedimentary Rocks under Confining Pressure: Tests at High Temperature," Bull. Am. Assoc. Petrol. Geologists, Vol. 42, 1958, pp. 2892-2934.
36. Handin, J. W., R. V. Hager, Jr., M. Friedman, and J. N. Feather, "Experimental Deformation of Sedimentary Rocks under Confining Pressure, Part III--Tests on Fluid-saturated Samples," Bull. Am. Assoc. Petrol. Geologists, Vol. 47, 1963, pp. 717-755.
37. Daubrée, A., "Application de la Méthode Experimentale a l'Étude des Déformations et des Cassures Terrestres," Bull. Soc. Geol. France, 1878 à 1879, pp. 108-141.
38. Kármán, Th. von, "Festigkeitsversuche unter allseitigem Druck," Z. Ver. Deutsch. Ingenieure, Vol. 55, 1911, pp. 1749-1757.

39. Ros, H. C., and A. Eichinger, "Experimental Attempt To Solve the Problem of Failure in Materials--Non-metallic Materials," Zurich Federal Materials Testing Lab., Report 28, 1928, Trans. in U.S. Bur. Reclamation Tech., Memoir 635.
40. Prandtl, L., and F. Rinne, in Plasticity, ed. by A. Nádai, McGraw-Hill Book Company, Inc., New York, 1931.
41. Griggs, D. T., "Deformation of Rocks under High Confining Pressure," J. Geol., Vol. 44, 1936, pp. 541-577.
42. Griggs, D. T., and J. F. Bell, "Experiments Bearing on the Orientation of Quartz in Deformed Rocks," Bull. Geol. Soc. Am., Vol. 49, 1938, pp. 1723-1746.
43. Griggs, D. T., F. J. Turner, and H. C. Heard, "Deformation of Rocks at 500° to 800°C.," in "Rock Deformation," Geol. Soc. Am. Mem. 79, 1960, pp. 39-104.
44. Balsley, J. R., "Deformation of Marble under Tension at High Pressure," Trans. Am. Geophys. Union, Part 2, 1941, pp. 519-525.
45. Jones, V., "Tensile and Triaxial Compression Tests of Rock Cores from the Passageway to Penstock Tunnel N-4 at Boulder Dam," U.S. Bur. Reclamation, Basic Structural Research Report SP-6, 1946, pp. 1-9.
46. Goguel, J., Introduction à l'Étude Mécanique des Déformations de l'Ecorce Terrestre, Imprimerie Nationale, Paris, 1948.
47. McHenry, D., "The Effect of Uplift Pressure on the Shearing Strength of Concrete," Intern. Congr. on Large Dams, 1948, pp. 1-31.
48. Bridgman, P. W., Studies in Large Plastic Flow and Fracture, McGraw-Hill Book Company, Inc., New York, 1952.
49. Balmer, G. G., "A Revised Method of Interpretation of Triaxial Compression Tests for the Determination of Shearing Strength," U.S. Bur. Reclamation, Basic Structural Research Report SP-9, 1946, pp. 1-20.
50. Balmer, G. G., "Physical Properties of Some Typical Foundations Rocks," U.S. Bur. Reclamation, Concrete Lab. Report SP-39, 1953, pp. 1-15.
51. Robertson, E. C., "Experimental Study of the Strength of Rocks," Bull. Geol. Soc. Am., Vol. 66, 1955, pp. 1275-1314.

52. Handin, J. W., and H. W. Fairbairn, "Experimental Deformation of Hasmark Dolomite," Bull. Geol. Soc. Am., Vol. 66, 1955, pp. 1257-1273.
53. Informal communication from J. W. Handin and I. Y. Borg, Shell Development Co., Houston, Texas, 1962.
54. Handin, J. W., "Experimental Deformation of Rocks and Minerals," Quart. Colo. School Mines, Vol. 52, No. 3, 1957, pp. 75-98.
55. Higgs, D. V., and J. W. Handin, "Experimental Deformation of Dolomite Single Crystals," Bull. Geol. Soc. Am., Vol. 70, 1959, pp. 245-277.
56. Robinson, L. H., Jr., "Effects of Pore and Confining Pressures on Failure Characteristics of Sedimentary Rocks," Quart. Colo. School Mines, Vol. 54, 1959, pp. 177-199.
57. Heard, H. C., "Transition from Brittle Fracture to Ductile Flow in Solenhofen Limestone as a Function of Temperature, Confining Pressure, and Interstitial Fluid Pressure," in "Rock Deformation," Geol. Soc. Am. Mem. 79, 1960, pp. 193-226.
58. Borg, I., M. Friedman, J. Handin, and D. V. Higgs, "Experimental Deformation of St. Peter Sand: A Study of Cataclastic Flow," in "Rock Deformation," Geol. Soc. Am. Mem. 79, 1960, pp. 133-191.
59. Friedman, M., "Petrofabric Analysis of Experimentally Deformed Calcite-cemented Sandstones," J. Geol., Vol. 71, 1963, pp. 12-37.
60. Serdengecti, S., and G. D. Boozer, "The Effect of Strain Rate and Temperature on the Behavior of Rocks Subjected to Triaxial Compression," Proceedings of the Fourth Symposium on Rock Mechanics, Pennsylvania State University, 1961, pp. 83-97.
61. Heard, H. C., "The Effect of Large Changes in Strain Rate in the Experimental Deformation of Rocks," Ph.D. thesis, University of California at Los Angeles, 1962.
62. Jaeger, J. C., "Shear Failure of Anisotropic Rocks," Geol. Mag., Vol. 97, 1960, pp. 65-72.
63. Donath, F. A., "Experimental Study of Shear Failure in Anisotropic Rocks," Bull. Geol. Soc. Am., Vol. 72, 1961, pp. 985-990.
64. Donath, Fred A., "Strength Variation and Deformational Behavior in Anisotropic Rock," these Proceedings, pp. 281-297.

65. Hubbert, M. K., "Mechanical Basis for Certain Familiar Geologic Structures," Bull. Geol. Soc. Am., Vol. 62, 1951, pp. 355-372.
66. Sax, H. G. J., "De Tectoniek van het Carboon in het Zuid-Limburgsche Mijng gebied," Mededel. Geol. Sticht., Ser. C-I-I, No. 3, 1946, pp. 1-77.
67. Leith, C. K., Structural Geology, 1st ed., Henry Holt and Co., New York, 1913.
68. Anderson, E. M., The Dynamics of Faulting, Oliver and Boyd, London, 1951.
69. Muehlberger, W. R., "Conjugate Joint Sets of Small Dihedral Angle," J. Geol., Vol. 69, 1961, pp. 211-219.
70. Woodworth, J. B., "Some Features of Joints," Science, Vol. 2, 1895, pp. 903-904.
71. Woodworth, J. B., "On the Fracture System of Joints, with Remarks on Certain Great Fractures," Proc. Boston Soc. Nat. History, Vol. 27, 1896, pp. 163-184.
72. Dale, T. N., and H. E. Gregory, "The Granites of Connecticut," U.S. Geol. Surv., Bull. No. 484, 1911, pp. 1-137.
73. Sheldon, P. G., "Some Observations and Experiments on Joint Planes," J. Geol., Vol. 20, 1912, pp. 53-79, 164-190.
74. Parker, J. M., III, "Regional Systematic Jointing in Slightly Deformed Sedimentary Rocks," Bull. Geol. Soc. Am., Vol. 53, 1942, pp. 381-408.
75. Raggat, H. G., "Markings on Joint Surfaces in Angelsea Member of Demon's Bluff Formation, Angelsea, Victoria," Bull. Am. Assoc. Petrol. Geologists, Vol. 38, 1954, pp. 1808-1810.
76. Hodgson, R. A., "Regional Study of Jointing in Comb-Ridge-Navajo Mountain Area, Arizona and Utah," Bull. Am. Assoc. Petrol. Geologists, Vol. 45, 1961, pp. 1-38.
77. Hodgson, R. A., "Classification of Structures on Joint Surfaces," Am. J. Sci., Vol. 259, 1961, pp. 493-502.
78. Roberts, J. C., "Feather-fracture, and the Mechanics of Rock-jointing," Am. J. Sci., Vol. 259, 1961, pp. 481-492.
79. Bonham, L. C., "Structural Petrology of the Pico Anticline, Los Angeles County, California," J. Sediment. Petrol., Vol. 27, 1957, pp. 251-264.

80. De Sitter, L. U., Structural Geology, McGraw-Hill Book Company, Inc., New York, 1956.
81. Schmidt, R. G., Joint Patterns in Relation to Regional and Local Structures in the Central Foothills Belt of the Rocky Mountains of Alberta, Ph.D. thesis, University of Cincinnati, 1957, Doctoral Dissertation Series, Pub. No. 23,242.
82. Cloos, H., Einführung in die Geologie, Gebrüder Bornträger, Berlin, 1936.
83. Dawson-Grove, G. E., "Analysis of Minor Structures near Ardmore, County Waterford, Eire," Quart. J. Geol. Soc. London, Vol. 111, 1955, pp. 1-22.
84. Price, N. J., "Mechanics of Jointing in Rocks," Geol. Mag., Vol. 96, 1959, pp. 149-167.
85. Harris, J. F., G. L. Taylor, and J. L. Walper, "Relation of Deformational Fractures in Sedimentary Rocks to Regional and Local Structure," Bull. Am. Assoc. Petrol. Geologists, Vol. 44, 1960, pp. 1853-1873.
86. Donath, F. A., "Analysis of Basin-range Structure, South-central Oregon," Bull. Geol. Soc. Am., Vol. 73, 1962, pp. 1-16.
87. Melton, F. A., "A Reconnaissance of the Joint Systems in the Ouachita Mountains and Central Plains of Oklahoma," J. Geol., Vol. 37, 1929, pp. 729, 746.
88. Nevin, C. M., Principles of Structural Geology, 4th ed., John Wiley & Sons, Inc., New York, 1949.
89. Hills, E. S., Outlines of Structural Geology, 3d ed., Methuen and Co., Ltd., London, 1953.
90. Billings, M. P., Structural Geology, Prentice-Hall, Inc., Englewood Cliffs, New Jersey, 1954.
91. Informal communication from F. B. Conger, Shell Oil Company, Los Angeles, California, 1961.
92. Reusch, E., "Über eine besondere Gattung von Durchgängen im Steinsalz und Kalkspath," Poggendorffs Ann. Physik., Vol. 132, 1867, pp. 441-451.
93. Schmid, E., and W. Boas, Plasticity in Crystals, F. A. Hughes and Co., Ltd., London, 1950.

94. Barrett, C. S., The Structure of Metals, McGraw-Hill Book Company, Inc., New York, 1952.
95. Turner, F. J., D. T. Griggs, and H. Heard, "Experimental Deformation of Calcite Crystals," Bull. Geol. Soc. Am., Vol. 65, 1954, pp. 883-934.
96. Handin, J. W., "Strength and Ductility," in Handbook of Physical Constants, 2d ed., Geological Society of America (in preparation).
97. Bell, J. F., "Morphology of Mechanical Twinning in Crystals," Am. Mineralogist, Vol. 26, 1941, pp. 247-261.
98. Pabst, A., "Transformation of Indices in Twin Gliding," Bull. Geol. Soc. Am., Vol. 66, 1955, pp. 897-912.
99. Cahn, R. W., "Twinned Crystals," Advan. Phys., Vol. 3, 1954, pp. 363-445.
100. Hall, E. D., Twinning and Diffusionless Transformations in Metals, Butterworth & Co. (Publishers), Ltd., London, 1954.
101. Brewster, D., "On a New Cleavage in Calcareous Spar, with a Notice of a Method of Detecting Secondary Cleavages in Minerals," Edin. J. Sci., Vol. 9, 1826, pp. 311-314.
102. Knopf, E. B., "Fabric Changes in Yule Marble after Deformation in Compression," Am. J. Sci., Vol. 247, 1949, pp. 433-461, 537-569.
103. Turner, F. J., "Preferred Orientation of Calcite in Yule Marble," Am. J. Sci., Vol. 247, 1949, pp. 593-621.
104. Griggs, D. T., and W. B. Miller, "Deformation of Yule Marble, Part I--Compression and Extension Experiments on Dry Yule Marble at 10,000 Atmospheres Confining Pressure, Room Temperature," Bull. Geol. Soc. Am., Vol. 62, 1951, pp. 853-862.
105. Handin, J. W., and D. T. Griggs, "Deformation of Yule Marble, Part II--Predicted Fabric Changes," Bull. Geol. Soc. Am., Vol. 62, 1951, pp. 863-885.
106. Turner, F. J., and C. S. Ch'ih, "Deformation of Yule Marble, Part III--Observed Fabric Changes," Bull. Geol. Soc. Am., Vol. 62, 1951, pp. 887-905.
107. Griggs, D. T., F. J. Turner, I. Borg, and J. Sosoka, "Deformation of Yule Marble, Part IV--Effects at 150°C," Bull. Geol. Soc. Am., Vol. 62, 1951, pp. 1386-1406.

108. Griggs, D. T., F. J. Turner, I. Borg, and J. Sosoka, "Deformation of Yule Marble, Part V--Effects at 300°C," Bull. Geol. Soc. Am., Vol. 64, 1953, pp. 1327-1342.
109. Borg, I., and F. J. Turner, "Deformation of Yule Marble, Part VI--Identity and Significance of Deformation Lamellae and Partings in Calcite Grains," Bull. Geol. Soc. Am., Vol. 64, 1953, pp. 1343-1352.
110. Turner, F. J., D. T. Griggs, R. H. Clark, and R. H. Dixon, "Deformation of Yule Marble, Part VII--Development of Oriental Fabrics at 300° to 500°C," Bull. Geol. Soc. Am., Vol. 67, 1956, pp. 1259-1294.
111. Turner, F. J., "Nature and Dynamic Interpretation of Deformation Lamellae in Calcite of Three Marbles," Am. J. Sci., Vol. 251, 1953, pp. 276-298.
112. Friedman, M., and F. B. Conger, "Dynamic Interpretation of Calcite Twin Lamellae in a Naturally Deformed Fossil," J. Geol., Vol. 71, 1963.
113. McIntyre, D. B., and F. J. Turner, "Petrofabric Analysis of Marbles from Mid-Strathspey and Strathavon," Geol. Mag., Vol. 90, 1953, pp. 225-240.
114. Gilmour, P., and M. Carman, "Petrofabric Analysis of the Loch Tay Limestone from Strachur, Argyll," Geol. Mag., Vol. 91, 1954, pp. 41-60.
115. Clark, R. H., "A Study of Calcite Twinning in the Strathavon Marble, Banffshire," Geol. Mag., Vol. 91, 1954, pp. 121-128.
116. Weiss, L. W., "A Study of Tectonic Style," Univ. Calif. (Berkeley) Publ. Geol. Sci., Vol. 30, 1954, pp. 1-102.
117. Turner, F. J., "'Compression' and 'Tension' Axes Deduced from {011̄2} Twinning in Calcite," J. Geophys. Res., Vol. 67, 1962, p. 1660.
118. Nickelsen, R. P., and G. W. Gross, "Petrofabric Study of Conestoga Limestone from Hanover, Pennsylvania," Am. J. Sci., Vol. 257, 1959, pp. 276-286.
119. Conel, J. E., "Studies of the Development of Fabrics in Naturally Deformed Limestones," Ph.D. thesis, California Institute of Technology, 1962.

120. Hansen, E., and I. Y. Borg, "The Dynamic Significance of Deformation Lamellae in Quartz of a Calcite-cemented Sandstone," Am. J. Sci., Vol. 260, 1962, pp. 321-336.
121. Nissen, H. U., "Dynamic and Kinematic Analysis of Deformed Crinoid Stems in a Quartz Graywacke," J. Geol., Vol. 71, 1963.
122. Johnsen, A., "Biegungen und Translationen," Neues Jahrb. Mineral. Geol. Palaeont., Teil II, 1902, pp. 133-153.
123. Turner, F. J., D. T. Griggs, H. Heard, and L. W. Weiss, "Plastic Deformation of Dolomite Rock at 380°C," Am. J. Sci., Vol. 252, 1954, pp. 477-488.
124. Crampton, C. B., "Structural Petrology of Cambro-Ordovician Limestones of the North-west Highlands of Scotland," Am. J. Sci., Vol. 256, 1958, pp. 145-158.
125. Christie, J. M., "Dynamic Interpretation of the Fabric of a Dolomite from the Moine Thrust-zone in Northwest Scotland," Am. J. Sci., Vol. 256, 1958, pp. 159-170.
126. Orowan, E., "A Type of Plastic Deformation New in Metals," Nature, Vol. 149, 1942, pp. 643-644.
127. Crussard, Ch., "Les Deformation des Cristaux Metalliques," Bull. Soc. Franc. Mineral., Vol. 68, 1945, pp. 187-197.
128. Hess, J. B., and C. S. Barrett, "The Structure and Nature of Kink Bands in Zinc," Trans. AIME, Vol. 185, 1949, pp. 599-606.
129. Washburn, J., and E. R. Parker, "Kinking in Zinc Single Crystal Tension Specimens," J. Metals, Vol. 4, 1952, pp. 1076-1078.
130. Ingerson, E., and O. Tuttle, "Relations of Lamellae and Crystallography of Quartz," Trans. Am. Geophys. Union, Vol. 26, 1945, pp. 95-105.
131. Kalkowsky, E., "Die Gneissformation des Eulengebirges," Habilitationschrift, Leipzig, 1878.
132. Boehm, A., "Über Gesteine des Wechsels," Mineral. Petrog. Mitt., Vol. 5, 1883, p. 204.
133. Judd, J. W., "The Development of a Lamellar Structure in Quartz Crystals," Mineral. Mag., Vol. 36, 1888, pp. 1-8.
134. Becke, F., "Petrographische Studien am Tonalit der Rieserferner," Mineral. Petrog. Mitt., Vol. 13, 1892, p. 447.

135. Mügge, O., "Der Quarzporphyr der Bruchhäuser-Steine in Westfalen," Neues Jahrb. Mineral., Vol. 10, 1896, p. 757.
136. Hietanen, A., "Petrology of the Finnish Quartzites," Bull. Comm. Geol. Finlande, No. 122, 1938, pp. 1-118.
137. Fairbairn, H. W., "Correlation of Quartz Deformation with Its Crystal Structure," Am. Mineralogist, Vol. 24, 1939, pp. 351-368.
138. Fairbairn, H. W., "Deformation Lamellae in Quartz from the Ajibik Formation," Bull. Geol. Soc. Am., Vol. 52, 1941, pp. 1265-1278.
139. Brace, W. F., "Quartzite Pebble Deformation in Central Vermont," Am. J. Sci., Vol. 253, 1955, pp. 129-145.
140. Christie, J. M., and C. B. Raleigh, "The Origin of Deformation Lamellae in Quartz," Am. J. Sci., Vol. 257, 1959, pp. 385-407.
141. Riley, N. A., "Structural Petrology of the Baraboo Quartzite," J. Geol., Vol. 55, 1947, pp. 453-475.
142. Bailey, S. W., R. A. Bell, and C. J. Peng, "Plastic Deformation of Quartz in Nature," Bull. Geol. Soc. Am., Vol. 69, 1958, pp. 1443-1466.
143. Carter, N. L., J. M. Christie, and D. T. Griggs, "Experimentally Produced Deformation Lamellae and Other Structures in Quartz Sand," J. Geophys. Res., Vol. 66, 1961, pp. 2518-2519.
144. Christie, J. M., N. L. Carter, and D. T. Griggs, "Plastic Deformation of Single Crystals of Quartz," J. Geophys. Res., Vol. 67, 1962, pp. 3549-3550.
145. Christie, J. M., D. T. Griggs, and N. L. Carter, "Experimental Evidence of Basal Slip in Quartz," J. Geol., Vol. 72, 1964 (in press).
146. Carter, N. L., J. M. Christie, and D. T. Griggs, "Experimental Deformation and Recrystallization of Quartz," J. Geol., Vol. 72, 1964 (in press).
147. Mackie, J. B., "Petrofabric Analyses of Two Quartz-Piedmontite-Schists from Northwest Otago," Trans. Roy. Soc. New Zealand, Vol. 76, 1947, pp. 362-368.
148. Preston, J., "Quartz Lamellae in Some Finnish Quartzites," Bull. Comm. Geol. Finlande, Vol. 180, 1958, pp. 65-78.
149. Naha, K., "Time of Formation and Kinematic Significance of Deformation Lamellae in Quartz," J. Geol., Vol. 67, 1959, pp. 120-124.

150. Hara, I., "Dynamic Interpretation of the Simple Type of Calcite and Quartz Fabrics in the Naturally Deformed Calcite Quartz Vein," J. Sci. Hiroshima Univ., Ser. C., Vol. 4, 1961, pp. 35-53.
151. Hara, I., "Petrofabric Study of the Lamellar Structures in Quartz," J. Sci. Hiroshima Univ., Ser. C., Vol. 4, 1961, pp. 55-70.
152. Buckley, H. E., Crystal Growth, John Wiley & Sons, Inc., New York, 1951.
153. Smoluchowski, R. (ed.), Phase Transformations in Solids, John Wiley & Sons, Inc., New York, 1951.
154. Shockley, W. (ed.), Imperfections in Nearly Perfect Crystals, John Wiley & Sons, Inc., New York, 1952.
155. Cottrell, A. H., Dislocations and Plastic Flow in Crystals, Clarendon Press, Oxford, 1953.
156. Read, W. T., Jr., Dislocations in Crystals, McGraw-Hill Book Company, Inc., New York, 1953.
157. Fisher, J. C. (ed.), Dislocations and Mechanical Properties of Crystals, John Wiley & Sons, Inc., New York, 1957.
158. Creep and Recovery, American Society for Metals, Cleveland, Ohio, 1957.
159. Voll, G., "New Work on Petrofabrics," Liverpool Manchester Geol. J., Vol. 2, 1960, pp. 503-567.
160. Gibbs, J. W., "On the Equilibrium of Heterogeneous Substances," in Collected Works of J. Willard Gibbs, Yale University Press, New Haven, Connecticut, 1906.
161. Goranson, R. W., "Thermodynamic Relations in Multicomponent Systems," Carnegie Institution of Washington, Pub. No. 408, 1930, pp. 1-329.
162. Goranson, R. W., "'Flow' in Stressed Solids: An Interpretation," Bull. Geol. Soc. Am., Vol. 51, 1940, pp. 1023-1033.
163. Goranson, R. W., "Physics of Stressed Solids," J. Chem. Phys., Vol. 8, 1940, pp. 323-334.
164. Verhoogen, J., "The Chemical Potential of a Stressed Solid," Trans. Am. Geophys. Union, Vol. 32, 1951, pp. 251-258.
165. MacDonald, G. J. F., "Orientation of Anisotropic Minerals in a Stress Field," in "Rock Deformation," Geol. Soc. Am. Mem. 79, 1960, pp. 1-8.

166. Kamb, W. B., "The Thermodynamic Theory of Nonhydrostatically Stressed Solids," J. Geophys. Res., Vol. 66, 1961, pp. 259-271.
167. Kamb, W. B., "Theory of Preferred Crystal Orientation Developed by Crystallization under Stress," J. Geol., Vol. 67, 1959, pp. 153-170.
168. Kamb, W. B., "An Experimental Test of Theories of Nonhydrostatic Thermodynamics," abstract, J. Geophys. Res., Vol. 67, 1962, p. 1642.
169. Brace, W. F., "Orientation of Anisotropic Minerals in a Stress Field (Discussion)," in "Rock Deformation," Geol. Soc. Am. Mem. 79, 1960, pp. 9-20.
170. Heard, H. C., "The Effect of Large Changes in Strain Rate in the Experimental Deformation of Yule Marble," J. Geol., Vol. 71, 1963, pp. 162-195.
171. Buerger, M. J., and E. Washken, "Metamorphism of Minerals," Am. Mineralogist, Vol. 32, 1947, pp. 296-308.
172. Griggs, D. T., M. S. Paterson, H. C. Heard, and F. J. Turner, "Annealing Recrystallization in Calcite Crystals and Aggregates," in "Rock Deformation," Geol. Soc. Am. Mem. 79, 1960, pp. 21-37.
173. Sander, B., Contributions to the Study of Depositional Fabrics, trans. by E. B. Knopf, American Association of Petroleum Geologists, Tulsa, Oklahoma, 1951.
174. Christie, J. M., H. C. Heard, and P. N. La Mori, "Experimental Deformation of Quartz Single Crystals at 27-30 Kb Confining Pressure and 24°C," abstract, Bull. Geol. Soc. Am., Vol. 71, 1960, p. 1842.
175. Handin, J. W., D. V. Higgs, and J. K. O'Brien, "Torsion of Yule Marble under Confining Pressure," in "Rock Deformation," Geol. Soc. Am. Mem. 79, 1960, pp. 245-274.
176. Paterson, M. S., and L. E. Weiss, "Experimental Folding in Rocks," Nature, Vol. 195, 1962, pp. 1046-1048.
177. Turner, F. J., "Rotation of the Crystal Lattice in Kink Bands, Deformation Bands, and Twin Lamellae of Strained Crystals," Proc. Natl. Acad. Sci. U.S.A., Vol. 48, 1962, pp. 955-963.

## DISCUSSION

D. COATES (Canada):

Can you suggest a definition and description of joints so that they can be identified on a rock face? It is often difficult to distinguish a joint plane from a plane which has been formed by blasting. Some material property aside from bedding provides a preferential surface for such breaking.

M. FRIEDMAN (in reply):

Certain trivial cases can easily be recognized. For example, there is little doubt about the origin of fractures that radiate from blast holes or of fractures that are filled with natural vein material. However, consider two situations where such obvious features are not developed. In the first, let us assume it is possible to move away from the blasted face to some structurally similar location where only the natural fractures can be observed. In the second, we will assume it is impossible to observe an unblasted exposure.

In the former situation, it is possible to map the natural fracture geometry, the average spacing for each of the fracture sets, and any markings that might exist on the natural fracture surfaces (e.g., plumose or conchoidal structures) in the region unaffected by blasting. These can then be traced back into the blasted area and compared with the observed fracture array. At the blasted face, one could then detect the development of new fracture sets (recognized by their geometry or perhaps by the presence or absence of surface markings) or changes in the spacing between natural fracture sets.

In the second situation, where one cannot move away from the blasted area, my first inclination is to say that one could not differentiate between the natural and the induced fractures. After all, they are fractures in rock, and the only difference between them is the energy source used to initiate them. However, if you can measure the residual strain gradient away from the fracture surfaces you may find that the gradients associated with paleo-fractures are different from those adjacent to induced fracture surfaces. The nature of this difference, if any, would have to be determined under controlled conditions. As far as

I am aware, the measurement of such gradients has not been attempted, but it should be possible by use of resistance foil gages, photostress methods, or X-ray diffractometry.

R. P. TRUMP (USA):

I have a question for Dr. Friedman. In your talk on the fold, you show a rather high amplitude fold having the neutral axis within the fold. If this fold is developed by thrusting or buckling, the neutral axis is not contained in the fold in the early stages of the process. Now, the question is, do you believe that your correlation with the neutral axis means that what you are seeing is a late stage deformation after the wave length has already been determined and, in turn, that the lateral pressure was relatively low at the time of initial fold development?

M. FRIEDMAN (in reply):

I do not think this question can be answered from study of the fractures alone. However, in the course of studying fractures on folds we have also investigated the deformed calcite in limestones. In many cases the same orientations for the principal stresses are derived from the calcite twin lamellae as from the fracture geometry. As the critical resolved shear stress to initiate twin gliding in calcite is low (less than 100 bars), I visualize the calcite as beginning to deform rather early in the development of the fold. Accordingly, as both the calcite and the fractures reflect the same principal stress orientations, I conclude that some fractures also were initiated early in the folding history.